# ANALYSIS OF SOLAR RADIO BURSTS TYPE II AND III USING MULTIPLE INSTRUMENTS OBSERVATIONS

AHMAD NAJWAN ZULKIPLEE

FACULTY OF SCIENCE UNIVERSITI MALAYA KUALA LUMPUR

2024

# ANALYSIS OF SOLAR RADIO BURSTS TYPE II AND III USING MULTIPLE INSTRUMENTS OBSERVATIONS

### AHMAD NAJWAN ZULKIPLEE

# THESIS SUBMITTED IN FULFILMENT OF THE REQUIREMENTS FOR THE DEGREE OF MASTER OF SCIENCE

FACULTY OF SCIENCE UNIVERSITI MALAYA KUALA LUMPUR

2024

# UNIVERSITI MALAYA ORIGINAL LITERARY WORK DECLARATION

Name of Candidate: AHMAD NAJWAN ZULKIPLEE	
Matric No: S2030854/1	
Name of Degree: MASTER OF SCIENCE	
Title of Thesis:	
ANALYSIS OF SOLAR RADIO BURSTS TYPE II AND III USING MULTIPI	LE.
INSTRUMENT OBSERVATIONS	
Field of Study: EXPERIMENTAL PHYSICS	
I do solemnly and sincerely declare that:	
<ol> <li>I am the sole author/writer of this Work;</li> <li>This Work is original;</li> <li>Any use of any work in which copyright exists was done by way of fair dea and for permitted purposes and any excerpt or extract from, or reference to reproduction of any copyright work has been disclosed expressly and sufficient and the title of the Work and its authorship have been acknowledged in this Work.</li> <li>I do not have any actual knowledge nor do I ought reasonably to know that making of this work constitutes an infringement of any copyright work;</li> <li>I hereby assign all and every rights in the copyright to this Work to the Universal Malaya ("UM"), who henceforth shall be owner of the copyright in this Work that any reproduction or use in any form or by any means whatsoever is prohibit without the written consent of UM having been first had and obtained;</li> <li>I am fully aware that if in the course of making this Work, I have infringed copyright whether intentionally or otherwise, I may be subject to legal action any other action as may be determined by UM.</li> </ol>	o or ently York; t the ersitic and oited any
Candidate's Signature Date:	
Subscribed and solemnly declared before,  Witness's Signature  Date:	

Name:

Designation:

# ANALYSIS OF SOLAR RADIO BURSTS TYPE II AND III USING MULTIPLE INSTRUMENTS OBSERVATIONS

#### **ABSTRACT**

Solar radio activity is one of the elements that can be harvested to obtain knowledge of our solar system in the field of radio astronomy. Using the Compound Astronomical Low-Frequency Low-cost Instrument for Spectroscopy and Transportable Observatory (CALLISTO) as one of the mediums in capturing the radio emission coming from the Sun, the studied of the solar radio bursts dynamics can be extensively analyzed which is the primary object for this work. This work emphasizes the use of multiple solar radio instruments used for capturing the emission of solar radio bursts other than CALLISTO such as Nancay Radioheliograph (NRH) and Half-wave Dipole Antenna (HWDA). The purpose of using these multiple instruments will benefit in the exploration of the unique features such as band splitting and 'herringbone' that existed within the solar radio bursts emission which are still lowly studied. The brightness temperature and degree of circular polarization of the solar radio bursts emission has been determined to propose an early finding of the emission mechanism of these unique features. Previous studies have proof that the solar radio bursts phenomena have a strong relation with solar activities such as solar flares and coronal mass ejections (CMEs) but the effect of the latter activities in a large-scale manner is still limited. This work has presented the influence of it toward the formation of solar radio bursts activities with the use of instrument from Space Weather Prediction Centre by National Oceanic and Atmospheric Administration (SWPC/NOAA), Geostationary Operational Environmental Satellite (GOES), and the Solar and Heliospheric Observatory mission's instrument which is the Large Angle and Spectrometric Coronagraph (SOHO/LASCO). Through these multiple observations, it was found that strong solar flares and CMEs do play a role in generating multiple solar radio bursts. Lastly, with the knowledge of the solar radio bursts unique features and its relationship with strong solar flares and CMEs, determination of suitable candidate of solar radio burst type II with clear appearances of band splitting has been performed across the year of 2017. This candidate will be useful for future detection of the HWDA that is currently undergoing major improvement for its next version of upgraded HWDA (uHWDA). In summary, the result of this work clearly shown that radio emission of 'herringbone' features is being generated through the fundamental plasma mechanism, large scale of solar flares and CMEs activities resulted in formation of multiple bursts of different types simultaneously and solar radio burst event on 23<sup>rd</sup> July 2016 would be the best candidate to be observed using the newly developed uHWDA.

Keywords: Radio Astronomy, Solar Radio Burst, Solar Flares, Coronal Mass Ejections (CMEs), Emission Mechanism, Solar Radio Instrumentation.

# ANALISIS LETUSAN RADIO SURIA JENIS II DAN III MENGGUNAKAN PENELITIAN PELBAGAI INSTRUMEN

#### **ABSTRAK**

Aktiviti radio suria adalah salah satu elemen yang boleh dikaji untuk memperoleh pengetahuan tentang sistem suria melalui penyelidikan bidang astronomi radio. Dengan menggunakan alat Compound Astronomical Low-Frequency Low-cost Instrument for Spectroscopy and Transportable Observatory (CALLISTO) sebagai salah satu medium untuk mengesan pelepasan radio yang datang dari Matahari, dinamik letusan radio suria boleh dianalisis secara mendalam yang merupakan objek utama untuk kajian ini. Kajian ini menekankan penggunaan pelbagai instrumen radio selain CALLISTO seperti Nancay Radioheliograph (NRH) dan Half-wave Dipole Antenna (HWDA). Tujuan penggunaan pelbagai instrumen ini adalah untuk melakukan penelitian secara mendalam ciri-ciri unik seperti pemisahan jalur dan 'herringbone' yang wujud dalam letusan radio suria yang masih kurang dikaji. Suhu kecerahan dan darjah polarisasi bulatan oleh pelepasan letusan radio suria telah ditentukan untuk mencadangkan penemuan awal mekanisma pancaran letusan radio suria yang mempunyai ciri-ciri unik ini. Kajian terdahulu membuktikan bahawa fenomena pelepasan letusan radio suria mempunyai hubungan yang kuat dengan aktiviti suria seperti suar suria dan pemancutan jisim korona (CME). Akan tetapi, kesan aktiviti tersebut dalam skala besar masih terhad. Kajian ini telah membentangkan bukti pengaruhnya terhadap pembentukan aktiviti letusan radio suria dengan menggunakan instrumen dari Pusat Ramalan Cuaca Angkasa oleh *National Oceanic and Atmospheric Administration* (SWPC/NOAA), Satelit Operasi Persekitaran Geostasionari (GOES), dan instrument bagi misi Observatori Suria dan Heliosphera yang dikenali sebagai Large Angle and Spectrometric Coronagraph (SOHO/LASCO). Melalui kepelbagaian pemerhatian ini, didapati bahawa suar suria yang kuat dan CME memainkan peranan dalam menghasilkan letusan radio suria yang pelbagai. Akhir sekali, dengan menggunakan pengetahuan tentang ciri-ciri unik letusan radio suria dan hubungannya dengan suar suria yang kuat dan CME, penentuan calon yang sesuai untuk jenis letusan radio suria berkelas II dengan ciri-ciri pemisahan jalur yang jelas telah dilakukan sepanjang tahun 2017. Pemilihan calon ini membantu dalam pemerhatian menggunakan HWDA yang bakal dilakukan pada masa depan oleh kerana alat ini sedang menjalani pengubahsuaian ke versi terkini yang dikenali sebagai uHWDA. Secara keseluruhannya, hasil kajian ini dengan jelas menunjukkan bahawa pelepasan radio berciri 'herringbone' dihasilkan melalui mekanisma plasma asas, aktiviti suar suria dan CME dalam skala besar mengakibatkan pembentukan letusan radio suria pelbagai jenis secara serentak, dan aktiviti letusan radio suria pada 23 Julai 2016 akan menjadi calon terbaik untuk diperhatikan menggunakan uHWDA yang sedang dibangunkan.

Kata Kunci: Astronomi Radio, Letusan Radio Suria, Suar Suria, Pemancutan Jisim Korona (CMEs), Mekanisma Pancaran, Instrumentasi Radio Suria

#### **ACKNOWLEDGEMENTS**

First and foremost, I would like to take this opportunity to express my deepest gratitude to my supervisor, Prof. Dr. Zamri Zainal Abidin for all his unwavering support, motivational words, guidance and positive criticisms throughout the period of my master's degree. His dedication and expertise in shaping the direction of my research and academic growth has provided me a platform for me to grow my career for my future especially with this branch of work of mine.

I would like to extend my appreciation to my family for their encouragement and understanding. I am truly grateful for having such a family that always supports these big dreams of mine. I will never forget their endless love and continuous support throughout this journey. Their belief in my potential has always been the pillar of my strength.

Also, I want to give tremendous thanks to my collaborators and fellow researchers from Yunnan Astronomical Observatory (YNAO) especially to Prof Liu Yu and Dr Dong Liang who constantly teach me about solar radio astronomy and instrumentations, enriching the depth of my understandings for my research. Their expertise and experiences truly made this effort memorable. I acknowledged the ministry of Science, Technology and Innovation (MOSTI) Technology Development Fund 1 grant (TDF07221598) for providing me with the graduate research assistant funding and I thank them for this contribution towards the completion of my thesis.

Lastly, I would like to thank all members of the Radio Cosmology Research Laboratory, especially Mohd Shazwan Mohd Radzi as well as all the lecturers and students of the lab who have been directly or indirectly involved with this work. All of them have been such a great help since the day that I was introduced to the lab.

## TABLE OF CONTENTS

ABSTRA	.CT	ji
ABSTRA	.K	ν
ACKNO	WLEDGEMENTS	vii
TABLE (	OF CONTENTS	viii
LIST OF	FIGURES	<b>x</b> i
LIST OF	TABLES	xiv
	SYMBOL AND ABBREVIATIONS	
LIST OF	APPENDICES	xix
СНАРТЕ	ER 1: INTRODUCTION	
1.1	Research Background	1
1.1.1	Solar Atmosphere	2
1.1.2	Solar Radio Burst	4
1.1.3	Solar Flares	5
1.1.4	Coronal Mass Ejections (CMEs)	6
1.2	Problem Statement	6
1.3	Research Objectives	8
1.4	Significant of Research	9
1.5	Research Questions	9
СНАРТЕ	ER 2: LITERATURE REVIEW	10
2.1	Sun's Corona: The Source of Intense Solar Activities	10
2.2	Solar Astronomy and Their Associated Solar Activities	11
2.3	Space Weather: Investigating the Sun-Earth Relationship	13
2.4	Magnetic Field Reconnection	14
2.5	Solar Radio Bursts	15
2.6	Solar Radio Bursts Type II and Type III	16
СНАРТЕ	ER 3: METHODOLOGY	18
3.1 Transpo	Compound Astronomical Low-frequency Low-cost Instrument for Spectroscopy and ortable Observatory (CALLISTO)	
3.1.1	CALLISTO Spectrogram	21
3.1.2	CALLISTO FIT Data	22
3.1.3	CALLISTO Data Processes	23

3.1.	4 Wave Speed Calculation	24
3.2	Space Weather Prediction Centre (SWPC)	25
3.3	Large Angle and Spectrometric Coronagraph (LASCO)	26
3.4	Nancay Radio Heliograph (NRH)	27
3.4.	1 NRH Data Processing.	28
3.4.	2 NRH Data Analysis	30
3.5	Half-wave Dipole Antenna Array (HWDA)	30
3.5.		
3.5		
3.6	Correlated Theories and Calculations	
3.6.	1 Plasma Frequency	34
СНАРТ	ER 4: RESULTS AND DISCUSSIONS	35
<b>4.1</b> Featur	Summarizing Radiation Mechanism That Contribute to the Formation of Unique res in Solar Radio Bursts	35
4.1.		
4.1.		
4.1.		
4.1.	4 Radiation Mechanism of 'Herringbone' Bursts	47
4.2	Analyzing Influence of Solar Activities Towards Formation of Solar Radio Bursts	49
4.2.	1 CALLISTO Spectrogram	50
4.2	2 Frequency Drift Determination	54
4.2	3 Active Region	56
4.2	4 Solar Radio Bursts and Solar Flares Relation	58
4.2.	5 Solar Radio Bursts and Coronal Mass Ejections Relation	63
<b>4.3</b> Upgra	Identification of Solar Radio Bursts Candidate with Band-splitting to be Detected U ded Half-wave Dipole Antenna (uHWDA)	_
4.3.	1 Solar Radio Bursts Type II	66
4.3.	2 Investigation on the Solar Radio Burst Event on 23 <sup>rd</sup> July 2016	68
4.3.	3 Upgraded vs First Version HWDA Array	78
СНАРТ	ER 5: CONCLUSION	80
<b>5.1</b> in Sol	Identifying Radiation Mechanism That Contribute to the Formation of Unique Featuar Radio Bursts	
5.2	Influence of Solar Events with Extreme Eruptions Towards Solar Radio Bursts Acti 81	vities
<b>5.3</b> Half-v	Identification of Solar Radio Bursts Features Candidate to be Detected Using Upgravave Dipole Antenna (uHWDA)	

REFERENCES	85
LIST OF PUBLICATIONS AND CONFERENCES	93
APPENDIX A	94

## LIST OF FIGURES

Figure 3.1	:	Flowchart of the research.	19
Figure 3.2	:	Raw e-CALLISTO Spectrogram from HUMAIN Station.	22
Figure 3.3	:	CALLISTO spectrogram data plotted in RAPP FITS Viewer software.	23
Figure 3.4	:	Schematic diagram for wave speed calculation.	24
Figure 3.5	:	Replotting spectrogram of event 3 <sup>rd</sup> November 2010 obtained from the NRH raw data and performing background subtraction to remove unwanted radio signals using SSW-IDL software.	29
Figure 3.6	:	(a) HWDA array; (b) Single-antenna sky-viewed; (c)3-D side view. (Pauzi et al., 2020)	31
Figure 3.7	:	Schematic block diagram of HWDA receivers. (Pauzi et al., 2020)	32
Figure 4.1	:	Spectrograms displaying the dynamic spectra of the solar radio burst event captured at 12:00:00 to 12:30:00 UT (top and bottom) on 3 <sup>rd</sup> November 2010 obtained from station BLEN7M (200-800 MHz).	37
Figure 4.2	:	Spectrogram displaying the dynamic spectra of the solar radio burst event captured at 12:00:00 to 12:30:00 UT (top and bottom) on 3 <sup>rd</sup> November 2010 obtained from station HUMAIN (50-350 MHz).	38
Figure 4.3	:	Dynamic spectrum of the Type II solar radio bursts showing presence of 'herringbones' feature on 3 <sup>rd</sup> November 2010. The spectrogram shown is a combined spectrum from BLEN7M (180-600 MHz) and HUMAIN (150-180 MHz).	39
Figure 4.4	:	Overplotted spectrum with NRH radio frequencies at 10 frequencies during the 'herringbones'. The contours are 95% of	42

the maximum value	. From 12:15:15	UT to 12:17:15	UT, the radio
source of each frequ	iency remains sta	ationary.	

Figure 4.5	:	Brightness temperature of NRH frequencies from 12:15:00 UT to 12:20:00 UT on 3 <sup>rd</sup> November 2010.	45
Figure 4.6	:	Degree of polarization (q) of NRH frequencies 12:15:15 UT to 12:18:05 UT.	46
Figure 4.7	:	Spectrograms (top and bottom) showing solar radio bursts captured on 6 <sup>th</sup> September 2017 for a period from 11:55 UT until 12:25 UT.	51
Figure 4.8	:	Re-plotted and combined spectrogram of the multiple solar radio burst event from 11:55 - 12:25 UT using SSW-IDL software.	52
Figure 4.9	:	Spectrogram plotted for the multiple burst event captured on 6 <sup>th</sup> September 2017 using RAPP FITS Java Viewer.	53
Figure 4.10	:	Sunspot region in white light (left) and Hydrogen Alpha (right) from SDO/HMI.	56
Figure 4.11	:	Magnetogram of AR 2673 from HMI. The colors represent the polarity of the magnetic field. Yellow-red region indicates negative polarity while Blue-Green region indicates positive polarity.	58
Figure 4.12	:	GOES-14 X-ray data on 6 <sup>th</sup> September 2017.	60
Figure 4.13	:	GOES-14 electron flux on 6 <sup>th</sup> September 2017.	61
Figure 4.14	:	GOES-13 proton flux on 6 <sup>th</sup> September 2017.	61
Figure 4.15	:	C2 coronagraph image on 6 <sup>th</sup> September 2017.	64

Figure 4.16	:	STEREO SECCHI COR1 A coronagraph image on 6 <sup>th</sup> September 2017.	64
Figure 4.17	:	C2 AIA image on 6 <sup>th</sup> September 2017.	65
Figure 4.18	:	CMEs height variation from $5^{th} - 7^{th}$ September 2017.	66
Figure 4.19	:	e-CALLISTO observations (top and bottom) at 05:15 – 05:45 UTC from BLENSW 01 Observatory for event 23 <sup>rd</sup> July 2016.	69
Figure 4.20	:	e-CALLISTO observations (top and bottom) at 05:15 – 05:45 UTC from BLENSW 02 Observatory for event 23 <sup>rd</sup> July 2016.	70
Figure 4.21	:	Event images (top and bottom) zoomed into smaller frequency range using RAPP FITS Viewer software.	71
Figure 4.22	:	C2 Telescope data obtained from CDAW catalog and GOES X-rays data for event 23 <sup>rd</sup> July 2016.	73
Figure 4.23	:	GOES X-ray Flux 3-day data obtained from SWPC archive.	73
Figure 4.24	:	Active region of the Sun on 23 <sup>rd</sup> July 2016 at 05:17 UTC.	75
Figure 4.25	:	Active region of the Sun on 23 <sup>rd</sup> July 2016 at 05:22 UTC.	76
Figure 4.26	:	First version of HWDA antenna array (left); Antenna of uHWDA array obtained from YNAO confidential report (right).	78

## LIST OF TABLES

Table 4.1	:	Solar radio bursts event details obtained from NOAA for 3 <sup>rd</sup> November 2010.	40
Table 4.2	:	Characteristics of various radiation mechanisms (Liu et al. 2018) and observed events. TB refers to the brightness temperature and q refers to degree of circular polarization. The observational parameters of the Type II 'herringbones' on 3 <sup>rd</sup> November 2010 are also listed for comparison.	47
Table 4.3	:	Solar radio bursts details obtained from NOAA data archive for event on 6 <sup>th</sup> September 2017.	54
Table 4.4	:	List of solar flares on 6 <sup>th</sup> September 2017.	59
Table 4.5	:	CME features information captured on 6 <sup>th</sup> September 2017.	65
Table 4.6	:	Event data of 23 <sup>rd</sup> July 2016 adapted from NOAA data archive.	72
Table 4.7	:	Information of CMEs occurring on the 23 <sup>rd</sup> July 2016 at 05:24 UTC.	77

#### LIST OF SYMBOL AND ABBREVIATIONS

 $\omega_p$  : angular frequency

 $k_B$ : Boltzmann constant

 $T_B$ : brightness temperature

q : degree of circular polarization

*e* : electron particle

f: Frequency of radiation

 $I_f$ : intensity of the radiation at frequency f

 $I_{\lambda}$ : intensity of the radiation at wavelength  $\lambda$ 

 $m_e$ : mass of electron

 $f_o$ : observed frequency

 $\varepsilon_0$ : permittivity constant

n : plasma density

 $f_p$ : plasma frequency

c : speed of light

v : Speed

I: Stokes I component

V: Stokes V component

 $\lambda$  : wavelength of the radiation

**AR** : Active Region

**BLEN7M**: Blein Observatory

**TB** : Brightness Temperature

CALLISTO: Compound Astronomical Low-cost Low-frequency Instrument for

Spectroscopy and Transportable Spectrometers

**CDAW** : Coordinated Data Analysis Workshop

UTC : Coordinated Universal Time

CME : Coronal Mass Ejections

**EM** : Electromagnetic

FITS : Flexible Image Transport System

GOES : Geostationary Operational Environmental Satellite

**GPS** : Global Positioning System

HMI : Helioseismic Magnetic Imager

**LASCO** : Large Angle and Spectrometric Coronagraph

**MHD** : Magnetohydrodynamics

NRH : Nançay Radio Heliograph

NASA : National Aeronautics and Space Administration

NOAA : National Oceanic and Atmospheric Administration

**RAPP** : Radio Astronomy Plasma Physics

**RFI** : Radio Frequency Interference

**SOHO** : Solar and Heliospheric Observatory

**SDO** : Solar Dynamics Observatory

**SEP** : Solar Energetic Particles

**SPE** : Solar Proton Event

**SXI** : Solar X-ray Imager

**SSW-IDL** : SolarSoftWare Interactive Data Language

**SWPC** : Space Weather Prediction Centre

**TEC** : Total Electron Content

UM : Universiti Malaya

**uHWDA** : Upgraded Half-wave Dipole Antenna

**VLBI** : Very Long Baseline Interferometry

YNAO : Yunnan Astronomical Observatory

## LIST OF APPENDICES

**Appendix A**: Pipeline codes for extracting NRH images and background 94 noise subtraction.

#### **CHAPTER 1: INTRODUCTION**

#### 1.1 Research Background

Radio astronomy is a branch of astronomy that involves the observation of celestial bodies by analyzing their radio wave emissions. This specialized field of study provides crucial insights into the universe evolution by examining these radio frequency energies. The electromagnetic (EM) waves are energy propagated through space, with the simplest models being oscillating electric charges, and they exist in a continuous spectrum extending from radio waves to X-rays and gamma rays (Alpen, 1997). These radio emissions can be observed for further analyzation with the help of constructed technologies that converted these analog signals into digital data.

Solar astronomy has been one of the major studies in understanding more about the solar system. Technological advancements have been made to facilitate the study of solar astronomy. There have been a lot of technologies developed mainly focusing on the Sun as the main interest in understanding more about the solar system and its effect toward the planets revolving it. These technologies include radio telescopes or radio antennas, enable researchers to do detailed studies to have a better understanding of the Sun and its own nature.

Developed radio antennas such as the dipole antenna, Yagi-Uda antenna, and even the parabolic or dish antenna have been tested and built across the globe by various levels of generations of humanity to conduct this study. Each of these designs has its own unique benefits in obtaining the readings of the radio signals including in which the frequency ranges they are targeted to observe and obtain their collection of data. Each frequency range that the

radio antennas focus on has different sets of readings which explain the nature of the science of the subjects differently. These frequencies data are a valuable tool for scientists and researchers to gain insights into the dynamics of the Sun, including their temperature and the magnetic field surrounding them. It also can help in understanding the activities that happen within outer space subjects such as the activities that happen on the surface of the Sun such as the solar flares and sunspots.

Sun is the closest star that happens to be within the Earth's solar system. The Sun itself has been playing an important role as the source of having the day and night on the Earth. Researchers study the Sun's dynamic nature to understand its impact on the solar system and human population. These studies have been ongoing for a long time and aim to solve the mysteries surrounding the Sun's activities and their effects on Earth. The Sun's atmosphere and surface are host to a wide range of phenomena, including solar flares, coronal mass ejections (CMEs), high-speed solar wind, solar energetic particles, and solar radio bursts (Kolarski et al., 2022). Each of these events exhibits unique characteristics and effects that can be studied through the collection and analysis of data obtained from radio signals detected by radio telescopes and antennas (Al Banna, 2023).

#### 1.1.1 Solar Atmosphere

The Sun has three distinct atmospheric layers which are the photosphere, the chromosphere, and the corona. The photosphere is the lowest region of the Sun's atmosphere (Hoven, 1989). The Sun emits radiation that passes in an upwards direction through the mechanism of absorption and reemission process. This enables the radiation to be released and escape out of the Sun where the fraction of this radiation content decreases as the depth of the Sun's surface increases. Sunspots are dark patches that appear on the surface of the

Sun, often caused by a momentary disruption in the convection beneath the photosphere due to an intense magnetic field. These spots typically form in clusters, with a dark nucleus called an umbra surrounded by a penumbra. Despite their striking appearance, sunspots are temporary phenomena. While the spot itself fades, the magnetic field that created it may persist for a longer period of time (Kundu, 1965). Solar activities are typically linked to magnetically active sunspot groupings. A significant discovery was made by Appleton and Hey in February 1946, who found that solar flares were the cause of intense radio emission during their observations of a large sunspot group (Kundu, 1965).

The outermost layer of the Sun's atmosphere is known as the corona, which can be observed during a solar eclipse or with the use of a coronagraph. A significant feature of the hot corona is prominence, which appears as bright arches in contrast to the dark expanse of space. Conversely, it appears as a dark filament when compared to the surface of the Sun. Prominence is characterized by a bright arch that rises and aligns along the magnetic lines of sunspot pairs. (Hoven, 1989). These arches are created when cool gas condenses along magnetic lines. Prominences or filaments on the Sun's surface ascend and vanish into space due to sudden changes in the magnetic field, which may be linked to the emergence of sunspots. Loop prominences in particular are often linked with significant solar flares (Kundu, 1965). CMEs has been established as one of the main solar events that occur in the Sun where this event can be demonstrates as an activity of ejection of solar energetic particles to the space. While there are suggestions that Active Regions (ARs) may be responsible for CMEs, the link between the two phenomena remains under investigation (Chen et al., 2011).

#### 1.1.2 Solar Radio Burst

Solar radio bursts have been known since 1942, yet they remained a puzzle mystery for scientists up till now. The discovery of radio waves from the Milky Way dates to 1932, when K.G. Jansky made the first observation (Kundu, 1965). Since then, researchers have started to shift their perspectives and have been studying radio phenomena occurring within the Milky Way. Many military-developed radio techniques, receivers, and antennas have been adapted and refined for the purpose of analyzing solar and cosmic radio emissions.

Solar radio burst is an event in which the Sun project radio energy into the interstellar medium. It is a transient enhancement of solar radio emissions due to energies of accelerated electrons is greater than the quiet corona thermal energy (Klein et al., 2018). Solar radio bursts exhibit five primary types: Solar Radio Burst Type I, Solar Radio Burst Type II, Solar Radio Burst Type III, Solar Radio Burst Type IV, and Solar Radio Burst Type V. Observing these bursts is made possible through the use of a spectrogram, a three-dimensional plot that displays the radio emissions of the solar radio burst in color contours to demonstrates its intensity. The frequency of the solar radio burst emission is represented on the vertical axis, while the time of the formation of solar radio burst is shown on the horizontal axis. These spectrograms can be obtained with *Compound Astronomical Low-cost Low-frequency Instrument for Spectroscopy and Transportable Spectrometers* (CALLISTO) technology.

Solar Radio Burst Type I, referred to as a noise storm, is characterized by a lengthy sequence of narrow and short bands that can last for several hours. Meanwhile, Solar Radio Burst Type II appears in the spectrogram as a slow drift burst (Monstein, 2011). The name is derived from its low frequency drift, which refers to the change in frequency that occurs over a specific duration of time. In this investigation the unit is megahertz per second (MHzs<sup>-1</sup>).

The spectrogram of Solar Radio Burst Type II presents a unique tick-marked shape (Monstein, 2011). Solar Radio Burst Type III, also known as fast drift, is characterized by its rapid frequency drift (Monstein, 2011). Typically, this type of burst lasts anywhere from a few seconds to several minutes and appears in groups. Flare accelerated electron beams that propagate through the corona at high velocity are responsible for this type of burst (Monstein, 2011). Solar Radio Burst Type IV is a wide-ranging continuum spectrum that generally precedes Solar Radio Burst Type I. On the other hand, Solar Radio Burst Type V is a brief continuum that appears as a flag attached to the lower frequency of Solar Radio Burst Type III (Monstein, 2011).

#### **1.1.3** Solar Flares

Solar flares are abrupt explosions that occur in intricate sunspot clusters where these outbursts result from the sudden change in magnetic fields (Hoven, 1989). Solar flares have a tendency to reemerge in a similar active region (AR) or become more luminous at the chromospheric structure. Solar flares can take various forms, exhibit different levels of brightness, and emit diverse spectra. At the peak of brightness, a solar flare will go through a "flash" phase that triggers fast buildup of the flare border. This expansion can be considered to be caused by hydrodynamic disturbances which can impact a remote filament located on the surface of the Sun. Flares and sub flares have short lifespan (Kundu, 1965). Flares are distinct phenomena compared to CME. They can be divided into confined ones and eruptive ones (Chen et al., 2011). Solar Flare is an astronomical occurrence in which the sun emits energy and electromagnetic radiation into the interstellar spaces (Pekünlü, 1999). The magnitude of these flares can be classified into three categories: C-class, M-class, and X-class (Marusek, 2007). Solar Flares and CME can excite plasma oscillation which can emit at radio wavelengths (Zucca et al., 2012). This type of event is called Solar Radio Burst. The

solar flare can be studied using X-ray flux provided by Geostationary Operational Environmental Satellite (GOES).

#### **1.1.4** Coronal Mass Ejections (CMEs)

Coronal Mass Ejection is a current event discovered in space studies in the early 1970s. It took nearly two decades for scientists to realize the importance of the event (Gopalswamy, 2016). The CME itself is a mystery. They are known as major natural hazard as it causes large solar energetic particles (SEP) and huge geomagnetic storm (Gopalswamy, 2016). CME is a phenomenon that occurs on the Sun's surface. It is a massive explosion of plasma and magnetic field that is ejected from the corona, the outermost layer of the Sun's atmosphere. CMEs are often associated with solar flares. When a CME is directed towards the Earth, it can cause a variety of effects. The solar energetic particles released during a CME can pose a risk to astronauts and satellites in space, while the geomagnetic storms that follow are able to disrupt power grids and communication systems on Earth.

#### **1.2** Problem Statement

Solar radio bursts are sudden bursts of radio waves originating from the Sun's atmosphere, which can last from a fraction of a second to several hours (Hanslmeier & Messerotti, 1999). These bursts are typically associated with solar flares, coronal mass ejections, and shocks, which generate intense electromagnetic and particle radiation that can impact the Earth's atmosphere and space environment (Gopalswamy, 2016). Solar radio bursts can be classified into several types, depending on their frequency and duration (Wijesekera et al., 2018) The most common types are Type I, II, III, IV and V bursts. The radio bursts are detected by radio telescopes, which can measure their frequency, intensity, and duration. Studying solar radio bursts provides valuable insights into the dynamics of the Sun's atmosphere and the processes

that drive space weather. Radio observations can be used to probe the structure and properties of the solar corona and to monitor the activity of the Sun. Additionally, solar radio bursts can have significant impacts on technological infrastructure and human health, highlighting the importance of understanding and predicting their occurrence.

One of the types of solar radio burst is the solar radio burst type II which has its own unique characteristics in which it appears to have frequency band splitting and herringbone structures (Chen et al., 2023). Recently, the mysteries of these unique features within type II solar radio bursts have caught significant interest and raised a lot of questions around the solar research communities. There have been various proofs recorded by various researchers across the globe in which they witness this phenomenon. These proofs have been presented by various scientists throughout their findings from their research papers which have been published for quite a few years (Ramesh et al., 2023). However, thorough studies of the solar radio bursts type II on its unique features still been lowly made and the understanding of these phenomenon remains a mystery. This lack of exploration for these phenomena is the driving force of this study to be made on.

This study has also been made to investigate the formation of these unique characteristics of solar radio bursts with solar events such as solar flares and coronal mass ejections (CMEs). A detailed report of these activities will give a significant insight on its effect toward the Earth's atmosphere, magnetic field, and the communication technologies system developed across the Earth. This study will also use a newly designed radio antenna which is known as the Upgraded Half-wave Dipole Antenna (uHWDA) to capture the radio signals from the solar and make thorough study on the dynamics of the solar radio bursts type II specifically within the range of 55-65 MHz to enhance the observation of the band-splitting feature. This

will test the capability of these newly designed radio antennas and provide room for improvements for the instruments which will help in advancing the technologies specially used for the solar radio communities.

#### 1.3 Research Objectives

- 1. To determine the radiation mechanism in the formation of the 'herringbones' features in solar radio bursts type II using brightness temperature and degree of polarization.
- 2. To investigate the influence of solar activities toward formation of solar radio bursts by studying solar flares energetic particles flux and coronal mass ejections (CMEs) characteristics.
- 3. To identify suitable solar radio burst candidate with comprehensible appearance of band-splitting that can be detected through upgraded Half-wave Dipole Antenna (uHWDA) array.

Through this work, several solar radio bursts data have been observed for the years 2010, 2016 and 2017 in e-CALLISTO database to find suitable events with appearances that show high clarity based on each of the objectives studied. As a result, only events of 3<sup>rd</sup> November 2010, 23<sup>rd</sup> July 2016 and 6<sup>th</sup> September 2017 are chosen to fit the goals of the observations. A clear structure of the solar radio bursts events would increase the chances of understanding its formation mechanism, its relationship with major solar events and a deeper analyzation of the unique features can be performed. All of this information is crucial in finding the plasma behavior and its energetic particles that cause the formation of the solar radio bursts itself. This also can benefit this work for further analysis by looking at different perspectives

of observing it such as learning the magnetic field environment during these particular solar activities and improving the current radio instruments. In summary, this work will analyze the radiation mechanisms of the solar radio burst by interpreting its brightness temperature and degree of circular polarization, investigating the influence of solar activities that drive the formation of the solar radio burst, and finding the candidates of solar radio bursts that can be studied using future constructed uHWDA for the purpose of studying the bursts band-splitting features.

#### **1.4** Significant of Research

Observation of solar radio bursts activities have been widely recorded through multiple publications across the world. However, the lack of information of its dynamic is still not well understood. Using multiple radio instruments to observe the solar radio bursts, solar flares, and coronal mass ejections (CMEs), this would provide a more detailed explanation of this phenomena's dynamic and increase the chances of providing alternatives of reducing the risk of its effect toward our Earth technologies.

#### 1.5 Research Questions

The following research questions need to be addressed:

- 1. What is the possible mechanism for the formation of 'herringbones' feature in solar radio bursts type II?
- 2. What is the effect of solar activities of solar flares and CMEs on the formation of solar radio bursts?
- 3. What is the suitable solar radio bursts candidate that can be observed using the upgraded Half-wave Dipole Antenna (uHWDA)?

#### **CHAPTER 2: LITERATURE REVIEW**

#### **2.1** Sun's Corona: The Source of Intense Solar Activities

The Sun is a dynamic object that is constantly undergoing a wide range of activities on its surface and in its atmosphere. It is the closest star to the Earth and is the most important source of energy for our planet. It is a colossal, spherical mass of gas composed primarily of hydrogen and helium, exhibiting a complex internal structure divided into several distinct layers. The Sun is a complex and dynamic object with each layer playing a critical role in its structure and behavior. The innermost layer of the Sun is the core which is where nuclear fusion takes place. This is where hydrogen atoms are fused together to form helium, releasing energy in the process (Kundu, 1965).

The energy produced in the core is what powers the Sun and provides the energy that is capable to sustain life on the Earth. Surrounding the core is the radiative zone where the energy produced in the core is transferred outward by radiation (Vieira et al., 2022). Beyond the radiative zone is the convective zone, where energy is transferred outward by convection process in which hot gas rises and cooler gas sinks. The outermost layer of the Sun is the atmosphere which is divided into several layers. The lowest layer of the atmosphere is the photosphere which is the visible surface of the Sun. Above the photosphere is the chromosphere, and the outermost layer of the atmosphere is the corona, which is a tenuous, hot layer of gas that extends millions of kilometers into space (Fiorentini et al., 2004).

One of the biggest mysteries of the solar corona is its high temperature, which can reach several million degrees Kelvin (Pontieu et al., 2011). This contrasts with the Sun's surface which has a temperature of around 5,500 degrees Kelvin. Scientists are still trying to

understand what causes the corona to be so hot, and there are several theories involve including magnetic waves and magnetic reconnections. It houses many intense solar activities such as solar flares and coronal mass ejections (CMEs) (Zucca et al., 2012). These events are caused by the Sun's magnetic field, which becomes twisted and distorted over time. When the magnetic field becomes unstable, it can release vast amounts of energy in the form of flares and mass ejections, which can have significant impacts on the Earth's space environment. CMEs and solar flares can cause geomagnetic storms when they reach the Earth, leading to disruptions in power grids, satellite communications, and Global Positioning System (GPS) systems (Gopalswamy, 2016). Understanding the Sun and its layers is essential for predicting and mitigating the effects of solar activity on Earth.

#### 2.2 Solar Astronomy and Their Associated Solar Activities

Solar astronomy has been one of the important focuses in understanding more about the solar system. The study of the Sun itself and its properties, using a variety of techniques such as radio telescopes and spectroscopy able to interpret deep information such as its structure, behavior, and evolution of this subject of interest. As time passes, there have been a lot of technologies developed mainly pivoted in the study of the Sun including its environmental effects towards the Earth. These technologies include the building of telescopes or radio antennas to provide multiple data observations readily available for the community to harness every knowledge on the Sun and its nature.

One of the most important phenomena studied in solar astronomy is sunspots. Sunspots are dark, relatively cool regions on the surface of the Sun that are caused by magnetic variation activities. They are often associated with solar flares, coronal mass ejections, and other solar phenomena that can affect Earth's environment and technology (Chen et al.,

2011). Nowadays, researchers use a range of instruments and techniques to study sunspots and their associated phenomena. These instruments include ground-based telescopes, as well as space-based observatories specifically design to observe the Sun's activities in variety of wavelengths including visible light, ultraviolet and X-ray radiation (Hamidi et al., 2014). A few examples that are worth mentioning are the Solar Dynamics Observatory (SDO) by the National Aeronautics and Space Administration (NASA) and the Solar and Heliospheric Observatory (SOHO).

Explosive solar phenomena such as solar flares and CMEs are mainly caused by the magnetic activities happening on the Sun (Kontar et al., 2017). Solar flares are generated when magnetic field lines around the sunspots experienced volatile tangles causing a sudden eruptive burst of energy (Chen et al., 2011). These flares can emit intense radiation in the form of electromagnetic waves and high-energy particles (Marusek, 2007). Solar flares can occur in any active region of the Sun and can last from a few minutes to several hours. They are often associated with sunspots and can be detected by telescopes and satellites. CMEs are massive eruptions of plasma and magnetic fields from the Sun's corona. CMEs can contain up to a billion tons of material and travel at speeds of up to several million miles per hour. CMEs are triggered by a sudden and violent release of magnetic energy, which causes the plasma in the corona to be rapidly accelerated and ejected into space (Lara et al., 2020). When a CME impacts the Earth's magnetic field, it can cause geomagnetic storms that can disrupt communication systems and power grids (Gopalswamy, 2016).

#### **2.3** Space Weather: Investigating the Sun-Earth Relationship

The Sun's magnetic activities have a strong influence towards the space weather occurring near the Earth. The Sun is a highly dynamic object, with constantly changing magnetic fields and energy flows. These changes can lead to the formation of solar events (such as solar winds and solar flares) unpredictably occurred in every part of the Sun to release huge amounts of energy and charged particle into space in which some of them are directed towards the Earth (White, 2007). When these solar events impact Earth's magnetic field and upper atmosphere, they can produce a variety of effects collectively known as space weather. These effects include auroras, magnetic storms, radiation storms, and disturbances to communication and navigation systems. Invention of spacecrafts such as SDO and SOHO, and ground-based instruments like magnetometers and radio receivers measure the effects of solar activity on Earth's magnetic field and ionosphere.

Earth's geomagnetic field is a crucial part of our planet's space environment, providing a protective shield against the charged particles and radiation emitted by the Sun. However, this protective layer is not always stable, and its fluctuations can cause ionospheric disturbances. Geomagnetic fluctuations occur when there are changes in the magnetic field lines surrounding the Earth. These changes can be caused by a variety of factors, including the interactions between the solar wind and the Earth's magnetosphere (White et al., 2003). When these fluctuations are large enough, they can cause ionospheric disturbances that can affect the propagation of radio waves through the ionosphere.

Ionospheric disturbances can take several forms, including scintillation and Total Electron Content (TEC) variations. Scintillation occurs when radio waves passing through the ionosphere are distorted causing a loss of signal. TEC variations occur when the density of free electrons in the ionosphere changes, affecting the speed of radio waves passing through the Earth's ionosphere (Gulyaeva et al., 2021). Ionospheric disturbances can have significant effects on communications and navigation systems (Kumar & Kumar, 2014). For example, TEC variations can cause errors in GPS measurements, while scintillation can cause signal loss and interference. As a result, it is important to monitor and predict geomagnetic fluctuations and ionospheric disturbances to mitigate their effects on critical systems.

#### **2.4** Magnetic Field Reconnection

The Sun is one of the celestial objects that experiences complex magnetic field behavior. Due to its vast size and intricate structure, the Sun has a significant impact towards the surrounding planets, notably the Earth. The magnetic field of it can extend to a great distance surpassing all the planets within the solar system. It has been demonstrated that the changes in the Sun's magnetic field are primarily responsible for all the solar events mentioned earlier. One of the most appealing phenomena that occurs on the Sun is magnetic field reconnection.

Magnetic reconnection is a process that reconstructs the structures of magnetic field lines to break and reconnect causing the release of energy and dramatic changes to its surroundings (Li et al., 2021). Most of the time this phenomenon can be witnessed in the corona vicinity. Through this, the magnetic energy of the Sun that commonly incorporate multiple magnetic zones will undergoes conversion into kinetic energy and thermal energy, resulted in the acceleration of the Sun's particles changing the magnetic topology (Aegerter et al., 2020). The formation of various solar activities like solar flares, solar wind and solar radio bursts fully depend on the degree of the abrupt changes of these magnetic fields to its interaction with the plasma in the solar atmosphere.

The interaction mechanism known as magnetohydrodynamics (MHD) interprets the information of plasma's behavior under the influence of the magnetic field (Yalim et al., 2023). This data is important in studying the dynamics of plasma in magnetic field environments in solar atmosphere (Srivastava et al., 2021). MHD theory has been widely used to explain many observations of solar activities including sunspots, coronal mass ejections and solar flares. Together with magnetic reconnections, MHD is a key process that drives the energetic particles of the Sun within solar atmosphere to emit electromagnetic radiation in the radio wave range known as solar radio bursts (Vršnak & Lulić, 2000).

#### 2.5 Solar Radio Bursts

Solar activities such as CMEs and solar flares have a strong influence on the generation of these solar radio bursts. Through the process of magnetic reconnection, the magnetic field lines of the Sun will be forced to break and re-join in a lower energy configuration reconstructing the complex magnetic lines structures to a more stable one, resulting in the conversion of the magnetic energy into plasma kinetic energy (Ishikawa et al., 2021). Large amounts of high-energy electrons, ions, and atoms will undergo this energy conversion and accelerate along these magnetic field lines causing the initiation of the solar activities mentioned (Klein et al., 2018). Intense formation of these solar activities enables the solar radio bursts to form a few minutes later in random magnetic field structures.

Solar radio bursts are the elevation of the Sun's radio emission above its background radio radiation level in which it occurs in a brief period. Each of these solar radio bursts can be simply said to be categorized by their physical characteristics such as duration and their unique ranges of frequencies in which they commonly detected (Behlke, 2001). Typically, most of the observed solar radio bursts are usually seen in low frequency radio emission

below 1 GHz. Using current observation instruments such as the Compound Astronomical Low-frequency Low-cost Instrument for Spectroscopy and Transportable Observatory or CALLISTO, these bursts can be analyzed in the form of spectrogram data images to study each detail of the characteristics of the solar radio bursts (Monstein, 2013; Mohd et al., 2020).

Based on their attributes and possible origins, it is confirmed that five categories of solar radio bursts have been discovered (Behlke, 2001). Type I bursts are short-lived and have a frequency of around 100 MHz (Monstein, 2011), while Type II bursts are longer and have a lower frequency range of 20-80 MHz (White, 2007). Type III bursts are characterized by a rapid frequency drift and originate from the lower corona (Monstein, 2011), while Type IV bursts are associated with the eruption of a coronal mass ejection and have a broad frequency range (White, 2007), and solar radio burst Type V is a rare and less understood type of burst that is characterized by a continuum of radio emission, rather than a discrete burst of energy like other types of solar radio bursts (White, 2007). Through the spectrogram analysis, the primary information such as the frequency and observation period can be extracted as an early feature to identify the bursts type. However, confirming the specific categories of it needed further analysis involving the magnetic field environment and correlated solar activities.

### **2.6** Solar Radio Bursts Type II and Type III

Solar radio bursts Type II and Type III are the most commonly detected bursts. This can be found widely recorded in the database in e-CALLISTO and National Oceanic and Atmospheric Administration (NOAA) (Monstein, 2012; Wijesekera et al., 2018). Due to these, researchers have made quite remarkable progress in learning the dynamics and physics of the solar radio burst activities with variety of explanation and theories. The formation of

solar radio bursts is strongly related to other large scale solar activities such as solar flares and CMEs. It has been found that most of the solar radio bursts type II have close relation with CMEs (Cane & White, 1989; Cho et al., (2011); G. Chernov & V. Fomichev, 2021) while for solar radio bursts type III have correlation with the detected solar flares (Fainberg & Stone, 1970; Wijesekera et al., (2018); Thejappa et al., (2020)). This relation is important in providing the essential information for the space weather studies and creates an early warning system which could mitigate the issues occurring in the technologies within the Earth's atmosphere.

## **CHAPTER 3: METHODOLOGY**

For this work, the study involves the use of various low-frequency instrument to record and analyses the formation of solar activities across its environment. The research mainly focusses on acquiring information of solar radio bursts activities of its unique features and its relation to solar events such as CMEs and solar flares. This work will involve solely the data concerning solar radio bursts recorded in the years 2010, 2016, and 2017. This selection is attributed to the abundance of accessible references relevant to the analyzed events, which have been extensively researched and documented. The work can be briefly understood through the representation of the Figure 3.1 shown below:

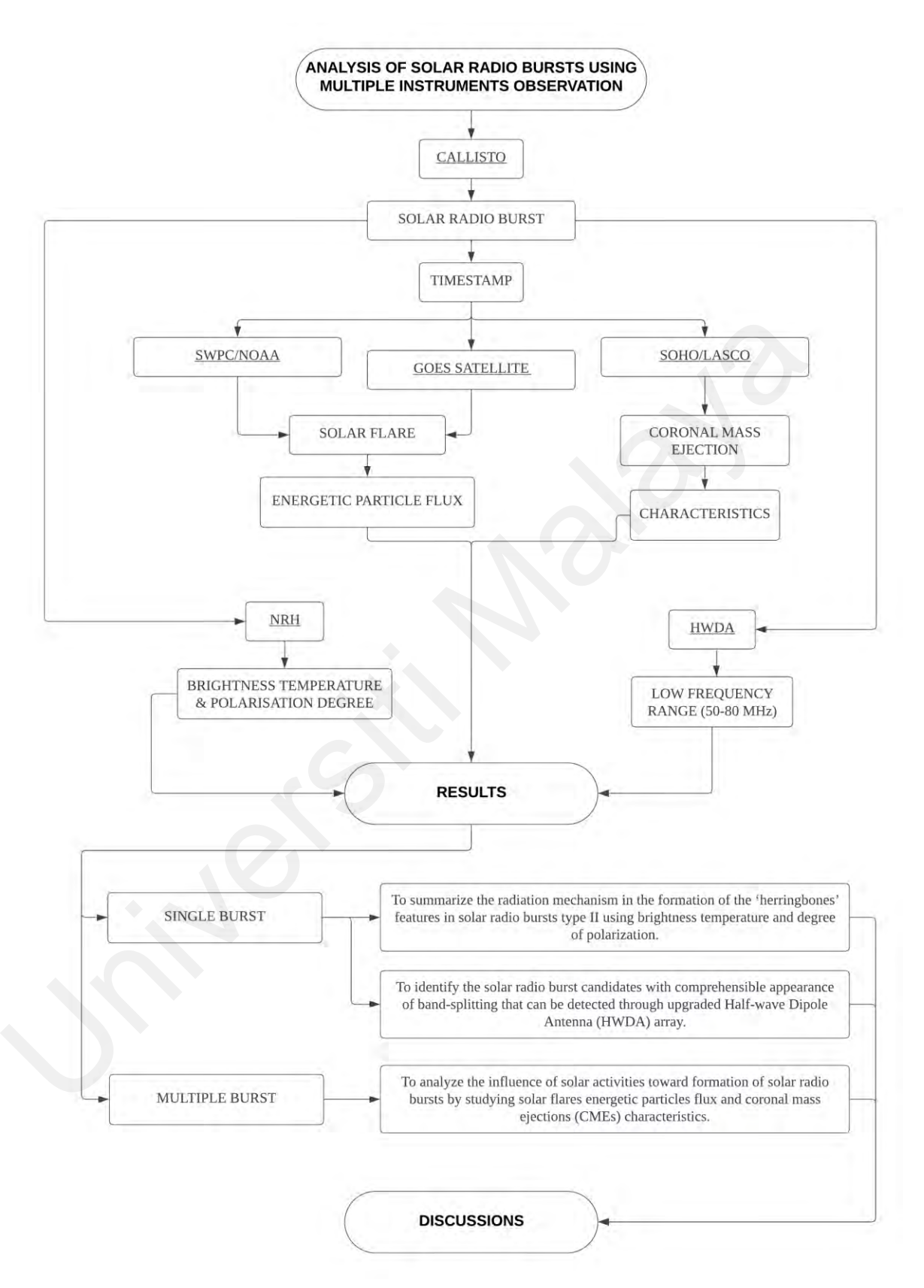


Figure 3.1: Flowchart of the research.

**3.1** Compound Astronomical Low-frequency Low-cost Instrument for Spectroscopy and Transportable Observatory (CALLISTO)

The Compound Astronomical Low-frequency Low-cost Instrument for Spectroscopy and Transportable Observatory or CALLISTO is a radio spectrometer network that aims to detect and analyze solar and space phenomena, with a specific focus on identifying solar radio bursts. This network is a joint venture between multiple institutions and observatories across the globe in creating a comprehensive solar observation station. Its data archive system known as e-CALLISTO is a catalogue accessible via the internet that offers daily spectrograph data for solar radio bursts. This database provides a thorough catalogue that records information including the type, the timestamp, and the period of each solar radio burst.

The establishment of this such catalogue provides the ability to differentiate between observed solar radio bursts and artificial radio interference, particularly radio frequency interference (RFI). Obscure solar radio bursts detected by an e-CALLISTO station are cross-checked against spectrograms from other stations to confirm their presence. Using the frequency range and duration of solar radio bursts in e-CALLISTO spectrograms, they are classified and assigned to their corresponding region of origin. The frequency range of solar radio bursts detected by e-CALLISTO spans from 45 MHz up to 870 MHz. This extensive bandwidth of the system enables the detection of various solar radio bursts, thus improving the comprehension of these solar activities.

## **3.1.1** CALLISTO Spectrogram

The publicly accessed database such as CALLISTO provides ready use data of spectrograms for identifying time frame of solar radio bursts, its patterns, and their correlation with established solar events. The e-CALLISTO catalogue is utilized for this purpose, which provides information and illustrations including RFI sources such as terrestrial lightning, radio transmission devices, and electrical appliances. Additionally, solar radio bursts are catalogued chronologically by date and time of confirmed events. For this study, the CALLISTO spectrogram served as the primary source of solar radio bursts observation data. The spectrogram provides valuable insights into the trend and characteristics of different types of solar radio bursts.

From the CALLISTO's data archive, spectrograms and fit files were extracted from the catalogue for the analysis of this study. The e-CALLISTO catalogue created by (Monstein, 2011) and his team was utilized to compare detected solar radio bursts spectrograms from an e-CALLISTO station with uncertain solar radio bursts against those from other stations to verify it. Users have the flexibility to choose their preferred date and time of the solar radio bursts event from the CALLISTO catalog. The detection period and frequency range captured from the e-CALLISTO are used to identify the regions responsible for generating the solar radio bursts. Figure 3.2 illustrates the raw spectrogram data acquired from the e-CALLISTO data catalogue.

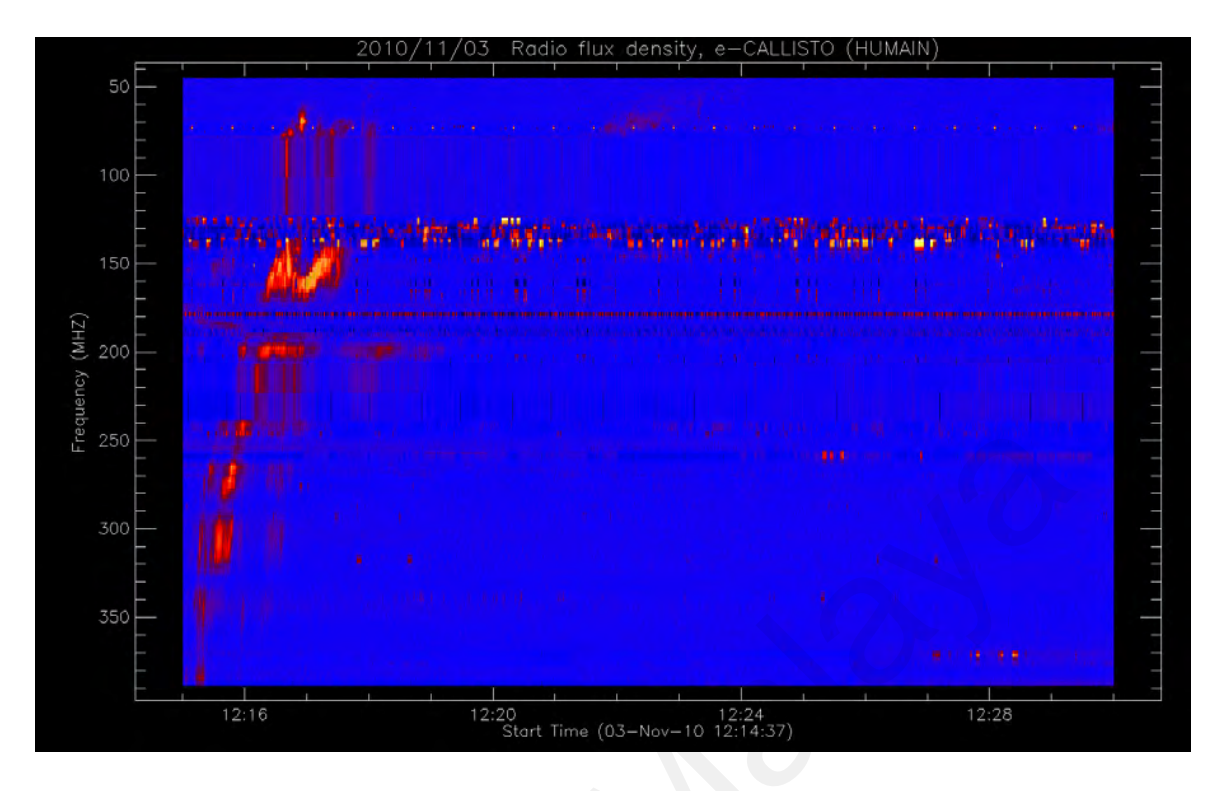


Figure 3.2: Raw e-CALLISTO Spectrogram from HUMAIN Station.

## **3.1.2** CALLISTO FIT Data

Apart from the spectrogram, e-CALLISTO also provides other types of data that can be customized to suits with the user's requirements. To view the data output from CALLISTO, users need to connect it to a computer via an interface cable and view it through a designated software. The majority of CALLISTO's output data are stored in the Flexible Image Transport System (FITS) file format. The e-CALLISTO website allows users to download the FITS files from its data archive. The Radio Astronomy Plasma Physics or RAPP FITS Viewer program is purposely used to generate the radio signal spectrogram image. For this research work, the details of the specific frequency and time in the spectrogram were obtained mainly using the FITS file in the RAPP FITS Viewer software. Figure 3.3 represents the spectrogram that was recorded in the RAPP FITS Viewer using the FITS file.

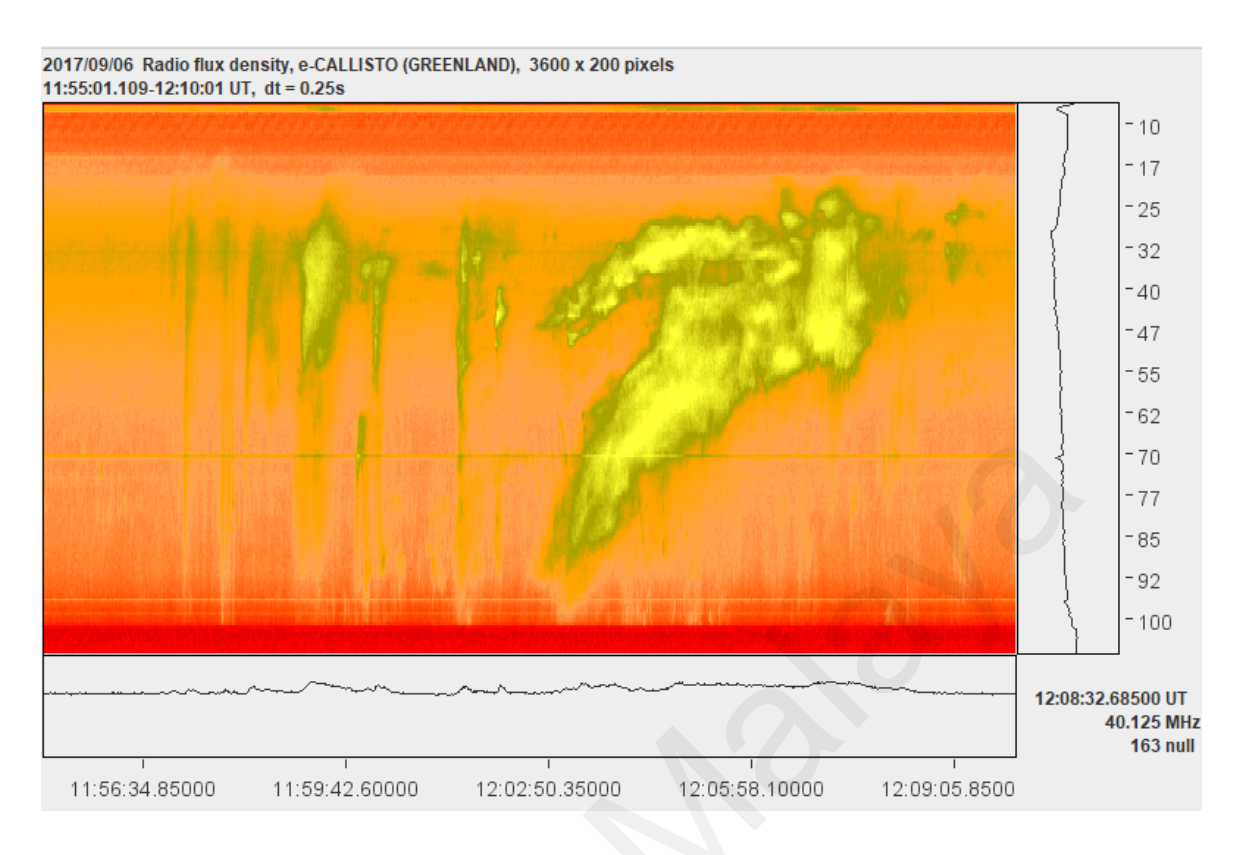


Figure 3.3: CALLISTO spectrogram data plotted in RAPP FITS Viewer software.

## 3.1.3 CALLISTO Data Processes

The spectrograms data of solar radio bursts analyzed in this study were taken and generated from e-CALLISTO archive. To improve the clarity of the trends in the detection of solar radio bursts, alternative software was used to record and plot the spectrogram images. The majority of the recorded spectrograms were undergoing a cleaning data process known as background subtraction to eliminate noise from the data. Even though the raw spectrograms data collected from each station are available in the catalogue, FITS file data were used primarily within the framework of this investigation. The FITS file contains essential parameters for spectrogram display such as time, frequency, and intensity, and it can be used in various programs for further data processing. To plot the spectrograms, SolarSoftWare Interactive Data Language (SSW-IDL) programming software was use where

all spectrograms were plotted using the same axis as the raw spectrograms with additional background subtraction to reduce noise from the signal detected. The SSW-IDL pipeline programming codes for performing the plotting and background subtraction can be referred to APPENDIX A.

## **3.1.4** Wave Speed Calculation

The e-CALLISTO website offers access to the source of the data collected from multiple observing stations, which were later utilized in the FITS calculations. The RAPP FITS Viewer software was used to obtain the precise frequency and time of the observed bursts ejections which were then taken to compute the wave speed. To calculate the shock wave speed, multiple frequencies and times data were used with the formula written below:

$$v = 3.5 \times 10^5 \left(\frac{\Delta f}{\Delta t f_o}\right) \left(\frac{1}{f_o}\right) \tag{3.1}$$

The schematic diagram shown in Figure 3.4 demonstrates the steps taken to acquire all the necessary parameters required for making the calculation.

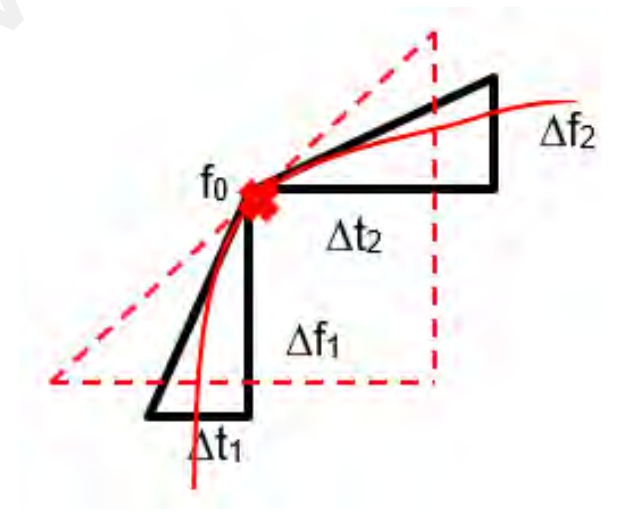


Figure 3.4: Schematic diagram for wave speed calculation.

### **3.2** Space Weather Prediction Centre (SWPC)

The Space Weather Prediction Centre (SWPC) is an official division under the National Oceanic and Atmospheric Administration (NOAA) that is responsible for forecasting and monitoring the evolution of space weather phenomena. Space weather refers to the state of surrounding in space that able to influence the technologies on the Earth, particularly satellites, communication systems and power grids. The SWPC has a diverse range of instruments and models at its disposal, enabling it to investigate space weather phenomena across a broad spectrum and accurately forecast their behavior. One of the instruments available in the SWPC which operated by NOAA is the Geostationary Operational Environmental Satellite (GOES) series. Operated since 1975, several number of GOES satellites have been launched since then until the current generation, GOES-18 (Darnel et al., 2022). One of the primary functions of the GOES satellites is to monitor various parameters, including the flux of high-energy particles, the strength of the Earth's magnetic field, and the intensity of solar radiation.

Three of the GOES satellites, which are the GOES-13, GOES-14 and GOES-15 have been used to verify the occurrence of solar radio bursts reported by e-CALLISTO with its relation to the major solar activities such as the solar flares. One of the most important observations of the GOES satellites is through the Solar X-ray Imager (SXI), which measures the intensity of solar X-rays. X-rays are radio emission produced by the Sun during solar flares, which are explosive events that release a tremendous amount of energy. GOES satellites also can provide data for proton and electron flux for the period of observation chosen. This data was recorded and compiled through the spaceweatherlive.com portal managed by the SWPC for the public use. The data on solar events is presented in tabular text file format, containing

vital information such as the class, start time, peak time, and end time of solar flares occurred throughout the day. One example of data provided to support various scientific fields is the solar flare X-ray spectrograms from NOAA/SWPC, which offer a spectrum of solar flares at five-minute intervals every day.

In this study, the solar radio bursts that are associated with the solar flare formation, especially during its peak, were then compared between the two catalogues: solar radio bursts by e-CALLISTO and solar flares by GOES satellites. The flare peak was selected due to its elevated electron density in comparison to the start and end of the solar flares. This highlights the possibility that solar flares may be a significant factor in the development of solar radio bursts. In order to determine the duration of each type of solar radio burst after a flare peak, mean and standard deviation were calculated using descriptive statistics. Throughout this work, only coordinated universal time (UTC) was used for this SPWC data to standardize the time unit for each observation involved.

## 3.3 Large Angle and Spectrometric Coronagraph (LASCO)

SOHO/LASCO refers to the Large Angle and Spectrometric Coronagraph (LASCO) equipment installed in the Solar and Heliospheric Observatory (SOHO) satellite. This equipment is capable of observing the Sun's corona, the outermost layer, and tracking coronal mass ejections during specific timeframes. This instrument specifically generates an artificial solar eclipse by using an occulting disk to block the direct light from the Sun, revealing the much fainter outer corona. One of the LASCO satellites captured the solar corona in radio white light aid in monitoring and tracking the evolution of the CMEs activities that can affect the Earth's magnetosphere and ionosphere.

Comprehending CMEs activities are very important in learning the relationship of the Sun and the Earth magnetic field. Detecting CMEs early and issuing warnings can significantly reduce their adverse impact on both space and ground stations from leading to temporary shutdowns of the operation of these man-made technologies. Acquiring data from coronagraph telescopes is accessible through websites such as "CDAW" and "Solarsoft". These data are represented in the form of images of the solar corona viewed in multiple observation wavelengths. However, for this research only C2 telescope will be focused more for used to get a visual of the corona layer of the Sun for further analysis of this study. The year-month matrix saved in the catalogue data gives the compilations of monthly CMEs that contain most of the information assembled of the measurements and compilation from online database.

# 3.4 Nancay Radio Heliograph (NRH)

The Nançay Radio Heliograph (NRH) is a radio interferometer located in France that is used to observe the Sun's radio emissions in the meter wavelength range. The NRH has the unique ability to produce two-dimensional images of the Sun at high temporal and spatial resolutions, which are crucial for studying the evolution of solar radio emissions and the magnetic field structure of the Sun's atmosphere. It is particularly useful for studying coronal mass ejections (CMEs), which are powerful eruptions of plasma and magnetic fields from the Sun. One of the key advantages of the NRH is its ability to image the Sun's corona, which is the outermost layer of the Sun's atmosphere that is visible during a total solar eclipse.

Through the NRH website, raw radio data can be downloaded which was later processed using the SolarSoftWare Interactive Data Language (SSW-IDL) to generate images and graphs containing useful information. The raw data contains important pieces of information

for this analysis, including the position of the brightness temperature with contours in relation to the Sun, the maximum brightness temperature, and the degree of polarization. Each of these is associated with one of ten unique frequencies that can be used, ranging from 150 MHz to 445 MHz. To be specific, these ten frequencies are 150, 173, 228, 270, 298, 327, 360, 406, 432 and 445 MHz.

## **3.4.1** NRH Data Processing

The raw images of solar radio bursts were generated by downloading and analyzing the data obtained from the NRH web portal. Multiple images were captured at 40-ms intervals, covering the duration of each solar radio burst event under investigation. The Nancay Radio Heliograph station recorded frequencies of 150 up to 445 MHz emitted by the Sun. Every image segment contains essential details such as duration of the observation, frequency, and the maximum brightness temperature (max TB) during that specific observation period. Due to the station being located in France and the Sun can only be observed during daylight hours, the instruments are restricted to daytime observations only. In addition to brightness temperature (TB), the degree of polarization was also measured and used to propose potential mechanisms for the generation of solar radio bursts.

The NRH captures images of the solar corona by observing the Sun for a period of seven hours daily, covering the frequency range of 150 MHz up to 445 MHz. This instrument is capable of detecting both the brightness temperature and the degree of circular polarization up to ten times within this frequency range. The spatial resolution of the instrument ranges from 0.3 to 6 arc minutes, and the temporal cadence is 5 ms where both depending on the observation frequency. With the use of SSW-IDL programming software, raw NRH data were extracted and processed to produce various types of images for in-depth analysis. These

images include radio source images, as well as visualizations of brightness temperature and polarization degree variations. In the Figure 3.5 is an example of processing the raw NRH data in SSW-IDL and performing the combination of different raw data and the data is further processed to undergo background subtraction to remove unwanted radio signals that might affected the real representation of the solar radio bursts activity coming from the Sun.

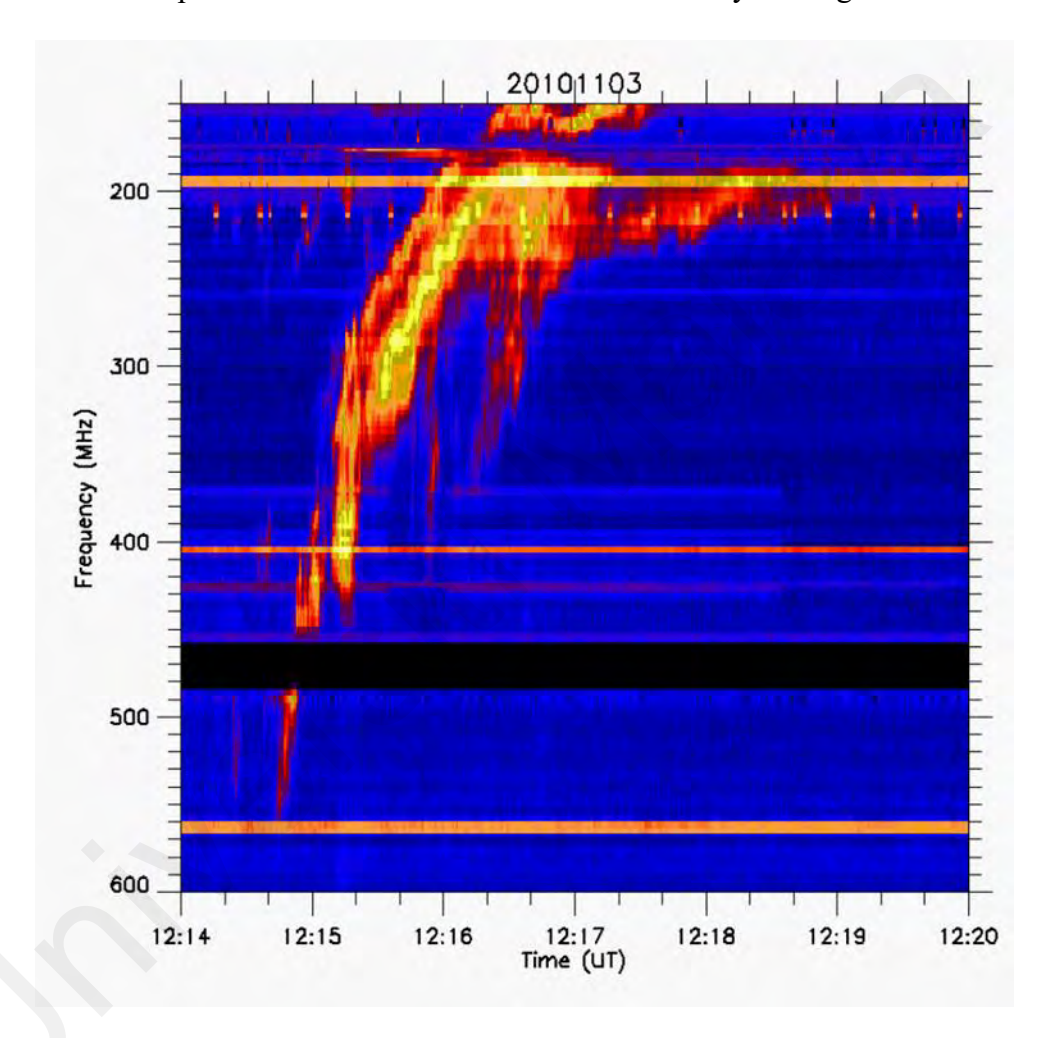


Figure 3.5: Replotting spectrogram of event 3<sup>rd</sup> November 2010 obtained from the NRH raw data and performing background subtraction to remove unwanted radio signals using SSW-IDL software.

### **3.4.2** NRH Data Analysis

The NRH data was utilized in the determination of parameters such as polarization degree and maximum brightness temperature. To access the data for specific events, users were required to input date and observation time according to their interest. The software produced graphs that displayed the degree polarization and maximum brightness temperatures for each event considered. The highest brightness temperature recorded at each time interval represents its highest value across all frequencies. Similarly, the degree of polarization also achieved its highest value for all previously mentioned frequencies. The images generated for radio sources exhibit distinct variations in brightness, temperature, and polarization during specific events, with a particular interest in the analysis interval. The images will later be then deeply studied to determine the mechanisms underlying the radio emissions of solar radio bursts. The primary focus of this study centers around the analysis of bursts type II and III events.

## 3.5 Half-wave Dipole Antenna Array (HWDA)

A research collaboration between the Universiti Malaya (UM) and Yunnan Astronomical Observatory (YNAO) in China has begun the process of establishing an antenna array known as the Half-wave Dipole Antenna (HWDA) installed at UM's observatory site. The main goal of this collaboration project is to create a Very Long Baseline Interferometry (VLBI) array between the YNAO and UM antennas, with current testing taking place at UM. Solar radio bursts observations are relevant for studying solar atmospheric events, as they resulted in electromagnetic and particle radiation that can impact the Earth (White, 2007). In general, the HWDA gets its name from the dipole antenna having a length that is equal to half-wavelength at the frequency of the operation. There are few advantages deploying this

antenna design such as it has more effective radiation due to its radiation pattern appear as Omni-directional, less-sensitive input impedance resulted in better maximum power transfer and better application for low-frequency antenna structure.

The arrangement of the HWDA array involves four twin-dipole antennas that are visually represented in Figure 3.5 (a). The antenna is designed to be twin dipole to operate as a dual oscillator with symmetrical broadband capabilities, and it is oriented orthogonally, as shown in Figure 3.5 (b). The two dipoles in each twin are placed in a configuration of an inverted V, which is illustrated in Figure 3.5 (c). The twin dipole antenna is constructed using dual HWDA antenna with operating frequency of 30-70 MHz, boasting a bandwidth of 40 MHz. These antennas are equipped with two receivers that have the capability of filtering the frequency to required radio signals from 55 to 65 MHz. The HWDA blades are arranged in either North-South or East-West orientation, spanning all four cardinal directions. The configuration guarantees that every complete HWDA system with twin dipole antennas can effectively receive signals from all directions. The technical specifications of the twin dipole antenna include a gain of 6 dBi and VSWR less than 3:1(Pauzi et al., 2020).

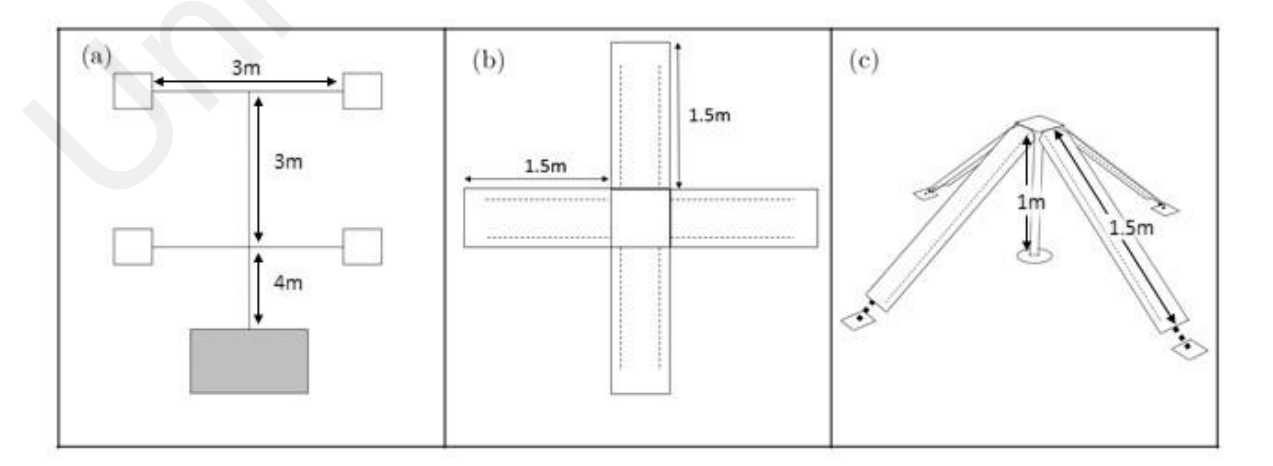


Figure 3.6: (a) HWDA array; (b) Single-antenna sky-viewed; (c)3-D side view. (Pauzi et al., 2020)

#### **3.5.1** HWDA Receivers

The HWDA array system is equipped with their own specifically engineered receivers. These receivers which are provided by YNAO are capable of sorting the signal to the required interest range of frequency through band-pass filtering. Upon filtering process, the signal exhibits a rapid increase in signal's strength until it reaches around 55 MHz, after which it is attenuated or suppressed at 65 MHz. Band-pass filters serve to eliminate undesired frequencies and allow only signals within a specified range to pass through (Kuphaldt, 2007). The receivers comprise of band-pass filters, monolithic amplifiers, and a correlator, with each input signal originating from one of the antenna blades. Figure 3.6 shows the complete schematic diagram of one of the receivers used in the HWDA array system.

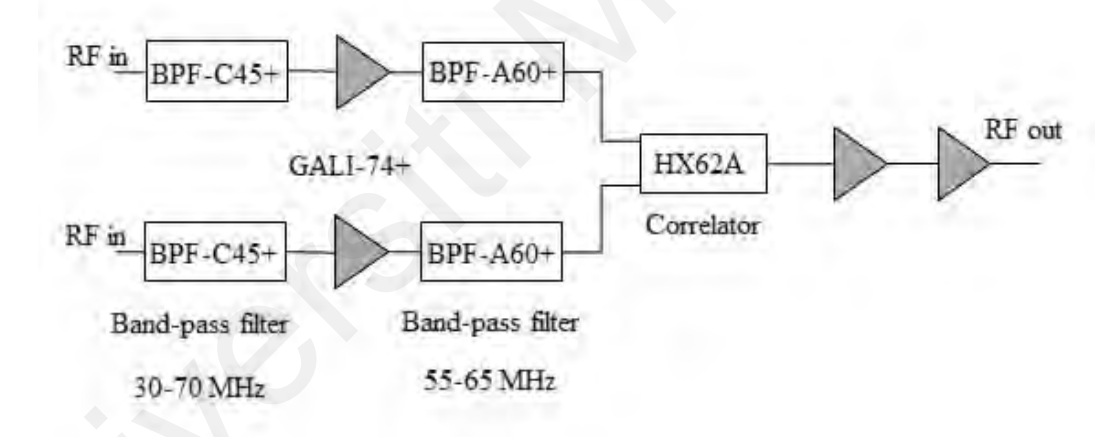


Figure 3.7: Schematic block diagram of HWDA receiver. (Pauzi et al., 2020)

Two types of band-pass filters used, namely BPF-C45+ and BPF-A60+, are utilized in the receiver's circuit to optimize sensitivity through double filtering. BPF-C45+ exhibits a response rate of frequencies between 30-70 MHz, while BPF-A60+ functions within a range of 55-65 MHz. GALI-74+ monolithic amplifiers are utilized to optimize filtered signals from being wasted. (Pauzi et al., 2020). The receiver uses an HX62A correlator to deduce both input signals (RF in) for each receiver. The receiver has an overall performance of band-pass

at 55 to 65 MHz with a total gain of 52 dB, a noise temperature of 320K, and a flatness of  $\pm 1$ dB (Pauzi et al., 2020).

#### **3.5.2** HWDA and CALLISTO

The Compound Astronomical Low-frequency Low-cost Instrument for Spectroscopy and Transportable Observatory (CALLISTO) system developed by Christian Monstein team and the Half-wave dipole antenna (HWDA) system which is builded by the China's Yunnan Astronomical Observatory (YNAO) share a lot of common features in terms of their structure and purpose. Both instruments apply similar concepts of antenna system of a half-wave dipole antenna which is a simple and efficient design that can be easily constructed and deployed. HWDA and CALLISTO have been closely used for solar radio emission monitoring, precisely the solar radio bursts with the correlated solar activities occurring on the Sun. Additionally, both equipment systems are transportable and can easily be used in remote places.

Although both systems share several similarities, there are still some parts of the instruments to be in difference. One of them is the observation frequencies covered by the system. CALLISTO provides a vast frequency range covering from 45 MHz to 870 MHz while HWDA only limited radio observation in the range between 30 MHz to 70 MHz. The CALLISTO system was developed specifically as a low-cost, portable instrument for monitoring solar radio emissions activities across a wide frequency range, while the HWDA system was developed as a more comprehensive system for studying the solar radio bursts unique features that only can be observe within a specific frequency band. For this research, both systems have been used together especially in verifying the detection of the solar radio bursts captured by the HWDA. With the CALLISTO being catalogue with large number of

ground stations, radio detection from HWDA have been cross-checked with all the stations under CALLISTO to identify the category of the solar radio bursts observed.

## **3.6** Correlated Theories and Calculations

# 3.6.1 Plasma Frequency

There is a close association between the observed frequency,  $f_o$  to the plasma frequency,  $f_p$  by using the following relation in which S = 2 indicate harmonic frequency while S = 1 indicate fundamental frequency (Gao et al., 2014).

$$f_o = Sf_p \tag{3.2}$$

The most crucial time-scale parameter in plasma physics is the plasma frequency. It is important to note that the plasma frequency pertains to the electron plasma frequency. Since:

$$\omega_p^2 = \frac{ne^2}{\varepsilon_0 m_e}$$
 ;  $f_p = \frac{\omega_p}{2\pi}$  (3.3)

where  $\omega_p$  is the angular frequency, n is the plasma density,  $\varepsilon_0$  is the permittivity constant, e is the electron particle,  $m_e$  is the mass of electron and  $f_p$  is the plasma frequency (Fitzpatrick, 2008). Thus, by calculating both equation in (3.3), where e is  $1.602 \times 10^{-19}$  C,  $\varepsilon_0$  is  $8.85 \times 10^{-12}$  Fm<sup>-1</sup>, and  $m_e$  is  $9.11 \times 10^{-31}$  kg, the equation can then be represented as:

$$f_p = 9 \times 10^{-3} \sqrt{n} \text{ (In MHz)}$$
 (3.4)

#### **CHAPTER 4: RESULTS AND DISCUSSIONS**

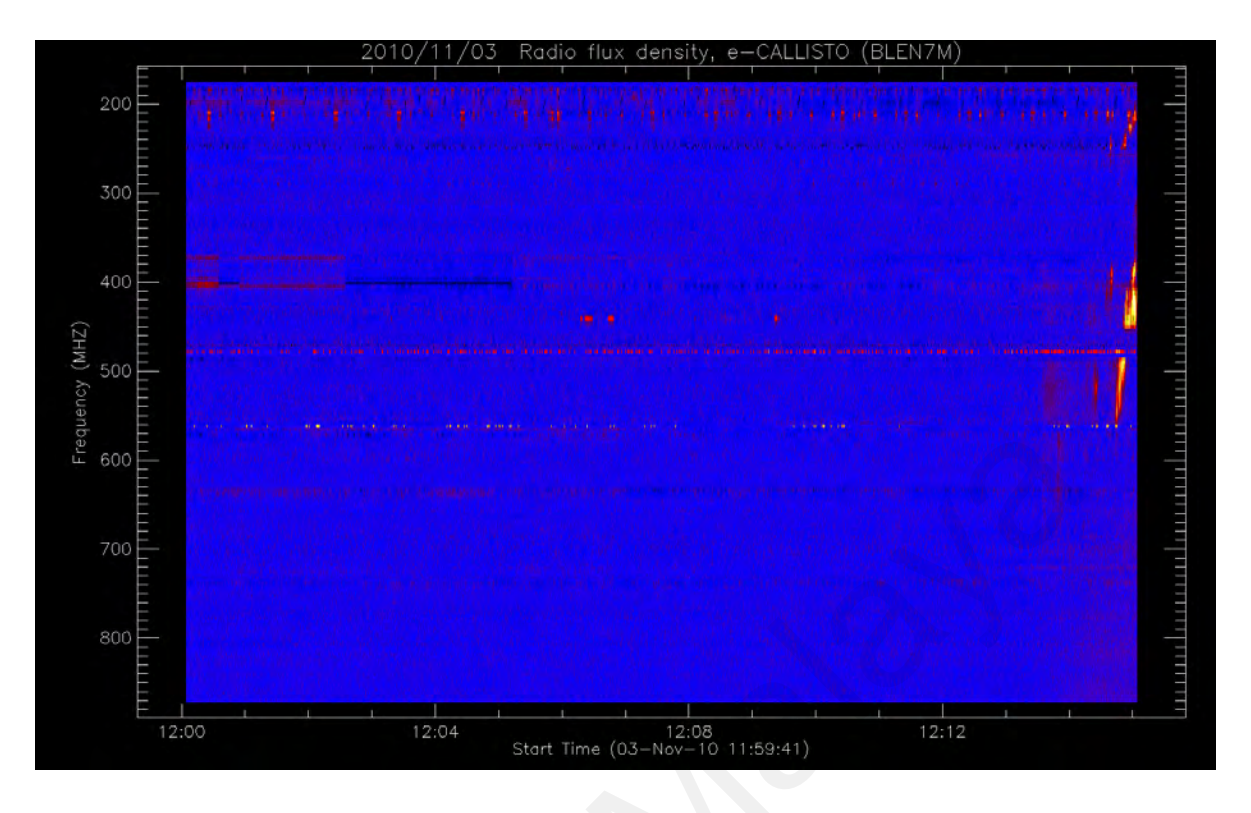
The study of solar radio bursts plays a significant role in comprehending solar activities and the Sun's magnetic field. However, the correlation between solar radio burst activities and other solar activities such as solar flares and CMEs is still not yet fully understood. By utilizing various instruments to observe solar radio bursts activities, it can enhance the understanding of the Sun's magnetic environment and how it contributes to the formation of solar activities within its atmosphere. This research will provide valuable insights into the relationship between solar radio bursts and solar activities, ultimately improving the understanding of solar astrophysics. This chapter will discuss the results on each of the research objectives accordingly.

**4.1** Summarizing Radiation Mechanism That Contribute to the Formation of Unique Features in Solar Radio Bursts

## **4.1.1** 'Herringbone' Features in Solar Radio Bursts Type II

The creation of Type II solar radio bursts is attributed to the presence of Magnetohydrodynamics (MHD) shock waves that occur alongside coronal mass ejections (CMEs) (Zucca et al., 2012). As noted by (Monstein, 2012), Type II bursts are characterized by narrow bands of intense radiation that gradually drift towards lower frequencies. This phenomenon usually occurs after major solar flares and can sometimes appear irregular. (White, 2007) quoted: "Type II bursts typically occur at around the time of the soft X-ray peak in a solar flare." Distinguishing between Type II and Type III solar radio bursts is a simple process. The frequency drift in Type II bursts is typically two orders of magnitude slower than the rapid drift of Type III bursts, hence the term "slow drift burst".

Although Type II bursts can be intricate and challenging to distinguish, they can occasionally display both fundamental and harmonic emission in frequency. Additionally, a rare feature known as "herringbones" has been discovered among Type II bursts (Monstein, 2012). This particular structure allows for the calculation of the velocity of the solar disturbance that generates slow drift bursts. This calculation is based on the frequency shift rate and should result in a velocity of approximately 1000 kms<sup>-1</sup>. This velocity is associated with superalfvenic shocks, similar to those found in solar flares and CMEs, that propagate through the solar corona (Monstein, 2012). Based on Figure 4.1 and 4.2, a solar radio burst showing an appearance of 'herringbones' feature was captured by the CALLISTO stations of Blein Observatory (BLEN7M) and HUMAIN on 3<sup>rd</sup> November 2010. Similar event has also been studied and being reported in previously published paper in (Zimovets et al., 2012) and (G. Chernov & V. Fomichev, 2021) where they studied on the formation of the solar radio burst type II is due to the piston shock wave being set off by the eruptive multitemperature plasmas. However, their studied do not explained much about the presence of the 'herringbone' feature and this work would be a great addition to the currently existed analysis that can give a better understanding on this solar radio burst event.



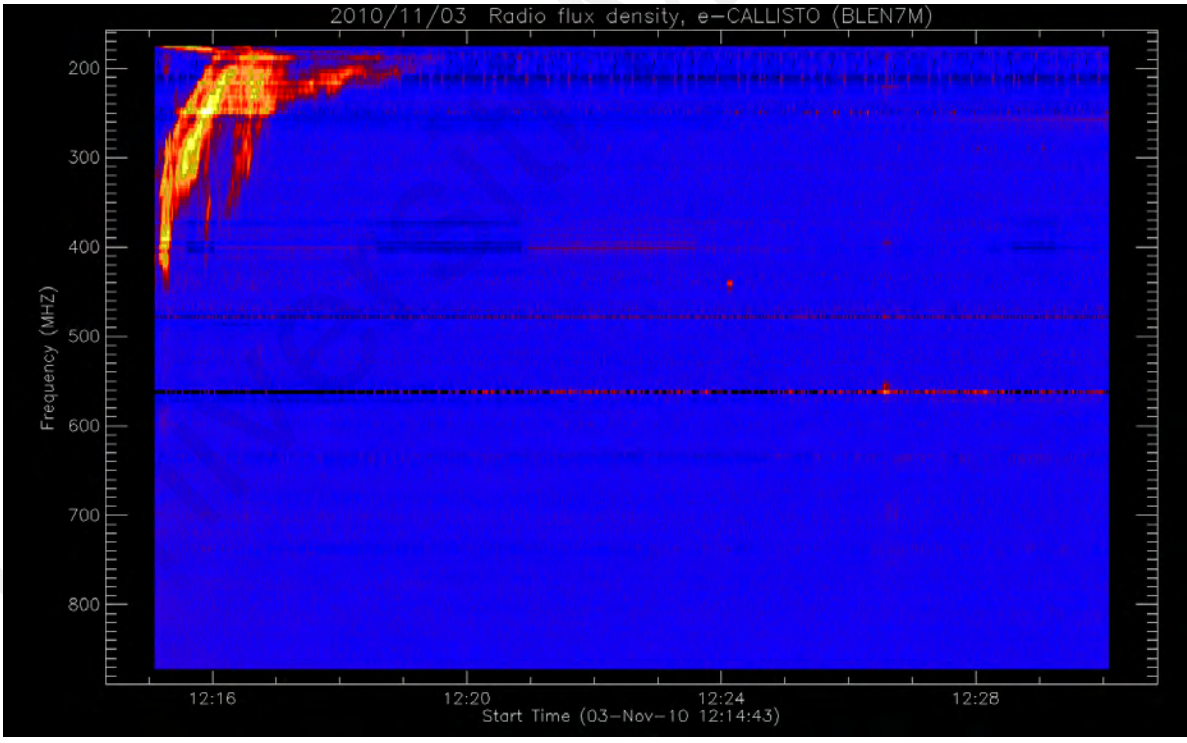


Figure 4.1: Spectrograms displaying the dynamic spectra of the solar radio burst event captured at 12:00:00 to 12:30:00 UT (top and bottom) on 3<sup>rd</sup> November 2010 obtained from station BLEN7M (200-800 MHz).

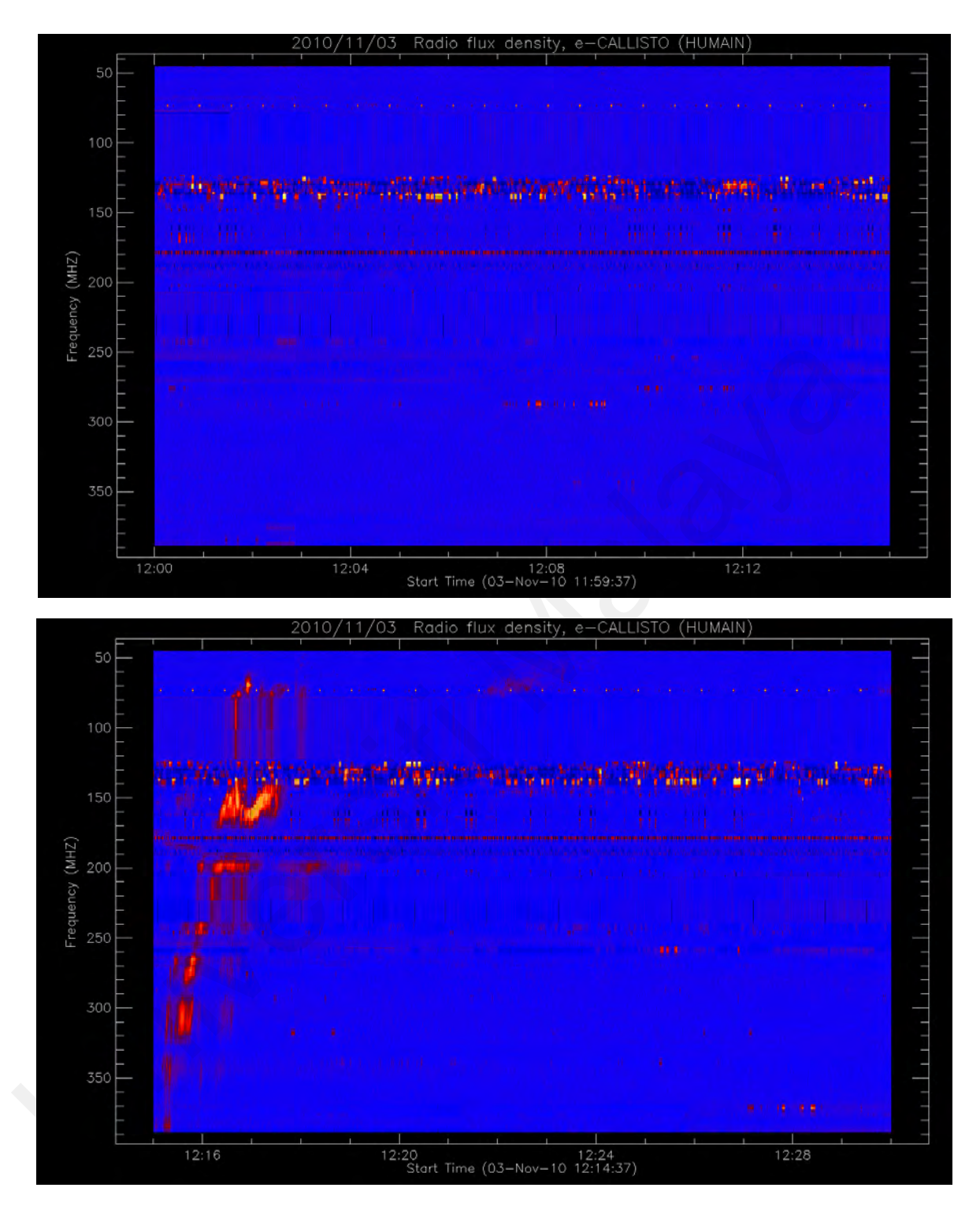


Figure 4.2: Spectrogram displaying the dynamic spectra of the solar radio burst event captured at 12:00:00 to 12:30:00 UT (top and bottom) on 3<sup>rd</sup> November 2010 obtained from station HUMAIN (50-350 MHz).

After filtering through all the observations from multiple stations, only the data taken from two different stations which are Bleien Observatory (BLEN7M) and HUMAIN Observatory will be used for these works where the observation of the event can be seen starting from 12:15:00 UT to 12:20:00 UT. These are due to only data taken from the two stations showing clear detection of the burst with presence of the 'herringbone' feature. These data were later then replotted and combined to form a complete dynamic spectrum that covers the whole frequency range of the detected solar radio burst event. By using SSW-IDL, the replotted spectrogram can be formed and is illustrated in the following Figure 4.3.

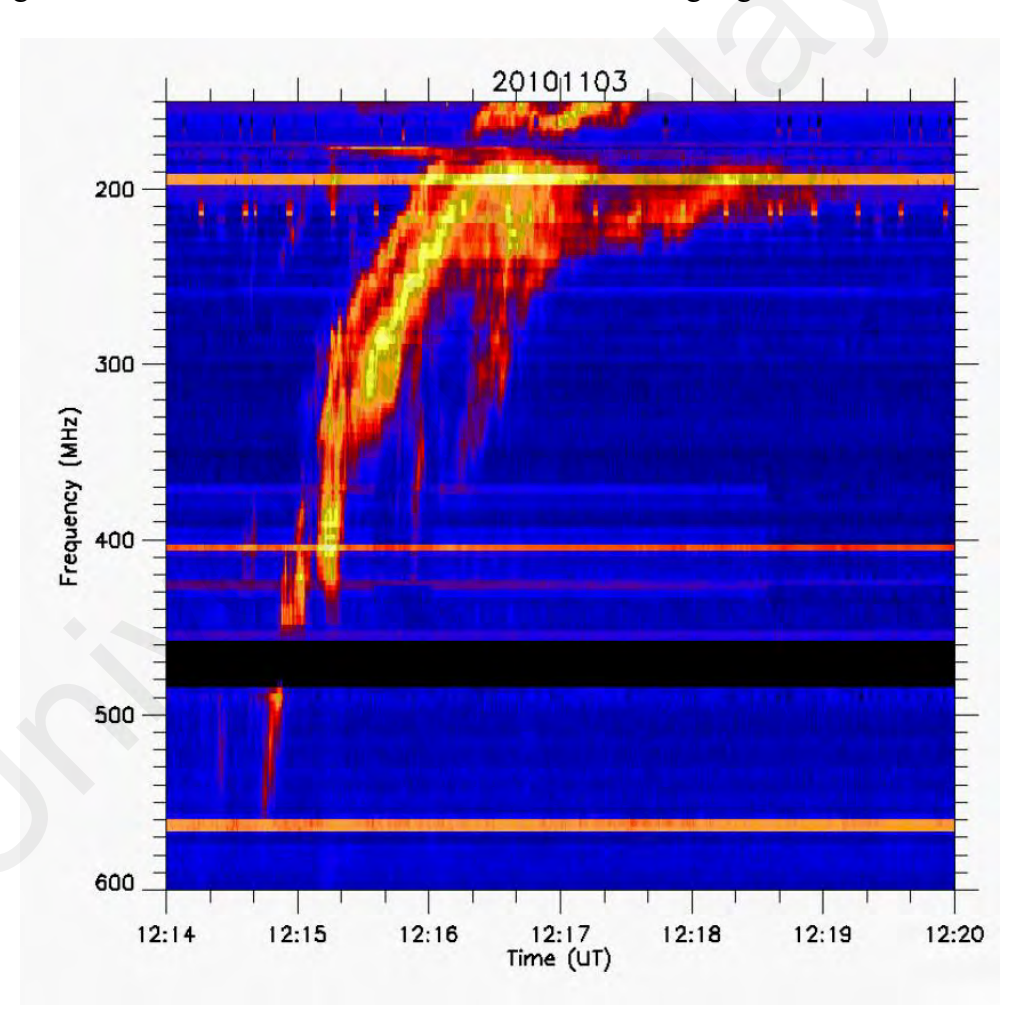


Figure 4.3: Dynamic spectrum of the Type II solar radio bursts showing presence of 'herringbones' feature on 3<sup>rd</sup> November 2010. The spectrogram shown is a combined spectrum from BLEN7M (180-600 MHz) and HUMAIN (150-180 MHz).

Based on the combined images, thorough structure of the 'herringbone' can be found where there is a significant drop in radio emission to lower frequency that depicted the 'herringbone' pattern. The rate of frequency change in 'herringbone' structure is much higher compared to the standard Type II bursts. The studied feature starts forming around 12:15:00 UT to 12:18:00 UT. As obtained from SWPC/NOAA, data dated 3<sup>rd</sup> November 2010 shown that a class C4.9 solar flare and a Type II solar radio bursts have been observed to confirm the detection for the event of this work. The detection of Type II solar bursts, characterized by distinct 'herringbone' structures, has also been confirmed by (Zimovets et al., 2012).

Table 4.1: Solar radio bursts event details obtained from NOAA for 3<sup>rd</sup> November 2010.

Flare	Flare	Flare	Flare Class	Details	Frequency
Begin	Peak Time	End Time			(MHz)
Time					
12:07 UT	12:21 UT	12:33 UT	C4.9	Type II	150-450
		(5)		(Herringbone)	

Table 4.1 demonstrates the details of the event information sourced from the NOAA database. Type II solar radio bursts commonly detected in the range of frequency from 200 MHz to 500 MHz. The frequency range of the burst detected for this event is found to be aligned within the previously recorded type II solar radio bursts. Before the formation of the type II solar radio bursts, a C4.9 class flare is observed to occur from 12:07:00 UT until 12:33:00 UT with its flare peaked at 12:21:00 UT. This might show that there might be an influence coming from the solar flare captured with the generation of the 'herringbone' feature in detected solar radio burst.

## **4.1.2** Multi-radio Sources Region of Solar Radio Bursts

For clarity and to have a general understanding of the sources region, data from the Nancay RadioHeliograph (NRH) were used. NRH can provide a variety of type of data including the animation of the data, brightness temperature, and data of degree of polarization up to ten frequencies within 150 MHz to 445 MHz. The time cadence is 5 ms, and the spatial resolution is 0.3 ~ 6 arcmin, depending on the observing frequency. Only the integrated 1-s data was utilized for the purpose of this work (Liu et al., 2018). Images of several wavelengths and multi-frequency of the NRH radio sources were carefully examined from 12:15:15 UT to 12:17:15 UT with 40-ms interval between the first and the next image. A contour of 95% of the maximum intensity is drawn also for all the NRH radio sources. All of these are shown in Figure 4.4. During the Type II solar radio burst event captured, it was found that the radio sources remain stationary. This radio source is consistent across all ten NRH frequencies, with radio sources lining up neatly from the lower flaring site to the higher corona.

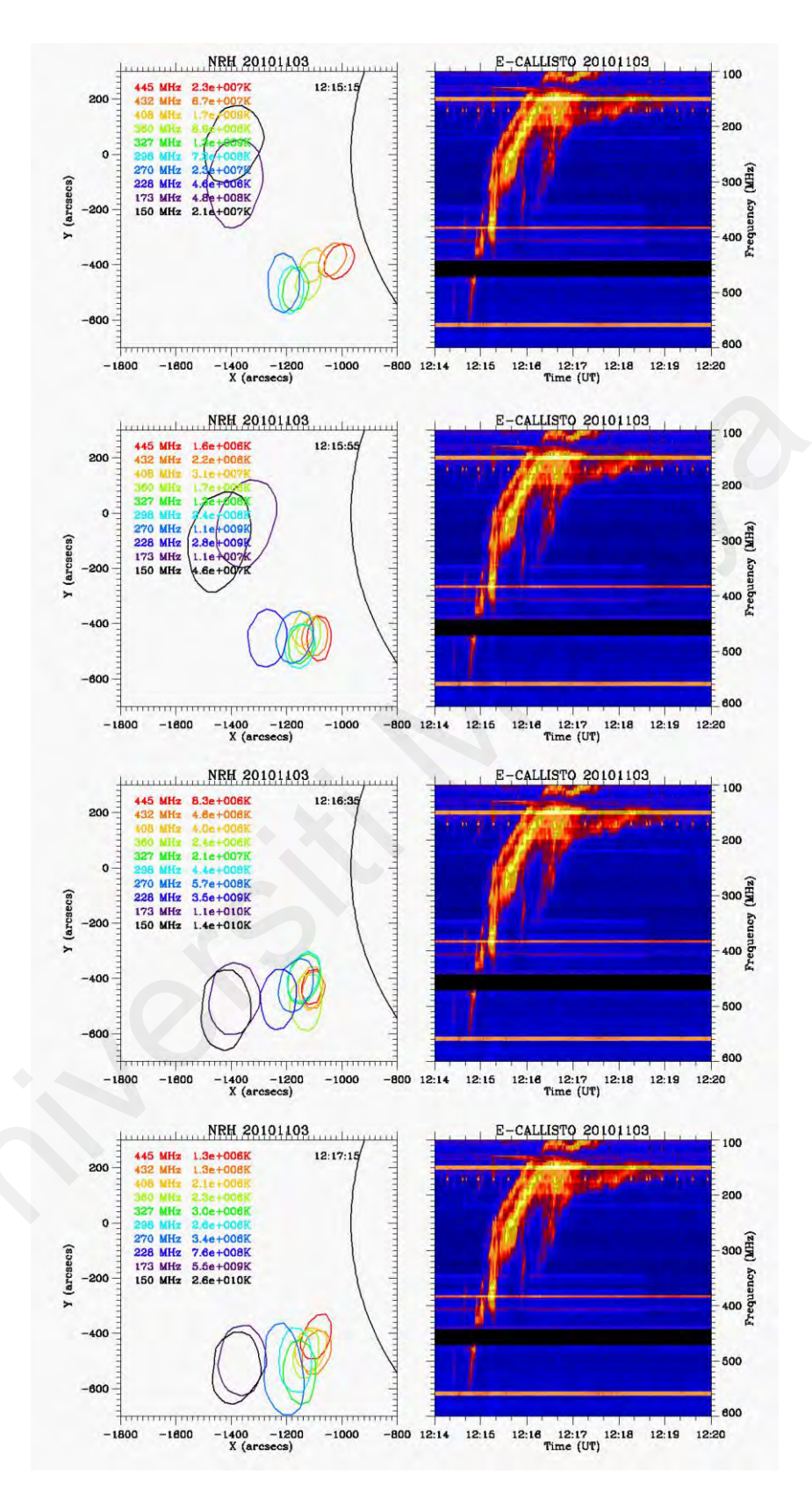


Figure 4.4: Overplotted spectrum with NRH radio frequencies at 10 frequencies during the 'herringbones'. The contours are 95% of the maximum value. From 12:15:15 UT to 12:17:15 UT, the radio source of each frequency remains stationary.

### **4.1.3** Analysis of the 'Herringbone' Structure

According to (Cane & White, 1989), "Not all Type II solar radio bursts have this 'herringbones.' Only those of intense Type II bursts have this feature". In the field of radio astronomy, brightness temperature (TB) is widely used as a measure of received intensity. The definition of brightness temperature can be derived from Plank's black body radiation law (Alley & Jentoft-Nilsen, 1999):

$$T_B \equiv \frac{c^2 I_f}{2f^2 k_B} = \frac{\lambda^2 I_\lambda}{2k_B} \tag{4.1}$$

 $(T_B \text{ is the brightness temperature; } c \text{ is the speed of light; } I_f \text{ is the intensity of the radiation at frequency } f; f \text{ is the frequency of the radiation; } k_B \text{ is the Boltzmann constant; } \lambda \text{ is the wavelength of the radiation; } I_{\lambda} \text{ is the intensity of the radiation at wavelength } \lambda). Hence, the formal definition of brightness temperature is the temperature at which a black body in thermal equilibrium with its surroundings would have to be in order to duplicate the observed intensity of an object at a frequency } f(\text{Alley & Jentoft-Nilsen, 1999}).$ 

An important property of electromagnetic wave propagation is the polarization of the electric field (E), which is defined by the orientation of the E vector as it varies in time. At each point during a polarization state, the electromagnetic field of the wave has a constant magnitude and is rotating at a constant rate in a plane perpendicular to the direction of the wave. In a circularly polarized wave, the electromagnetic wave can rotate in two possible directions such as right-handed (clockwise) and left-handed (counterclockwise) (Toh et al.,

2003). The degree of circular polarization (q) is defined by the Stokes V component over the Stokes I component as follow in Equation 5 (Liu et al., 2018):

$$q = \frac{V}{I} \tag{4.2}$$

Based on the event captured on 3<sup>rd</sup> Nov 2010, the maximum brightness temperatures (TBs) observed at NRH frequencies, and their time dependencies are plotted (Figure 4.5). An average TB of all pixels within the 95% maximum contour is presented in the same figure. Based on the extracted data, the maximum TBs at all frequencies are above 10<sup>8</sup> K. The maximum TB at 150 MHz even exceeds 10<sup>10</sup> K for several minutes. It was found that the decrease in frequency will result in better TB and vice versa (Liu et al., 2018). The rise of the frequencies TBs value at 12:15:00 UT marked the beginning of the 'herringbones' of the Type II solar radio burst in which its radio emission gradually increase to its peak value where it become the hottest whereas the drop of the low frequencies (228 MHz, 150 MHz) TBs at 12:18:00 UT marked the decrease of frequency spectrum and demonstrate the ending point of the 'herringbones' structure of the Type II solar radio burst.

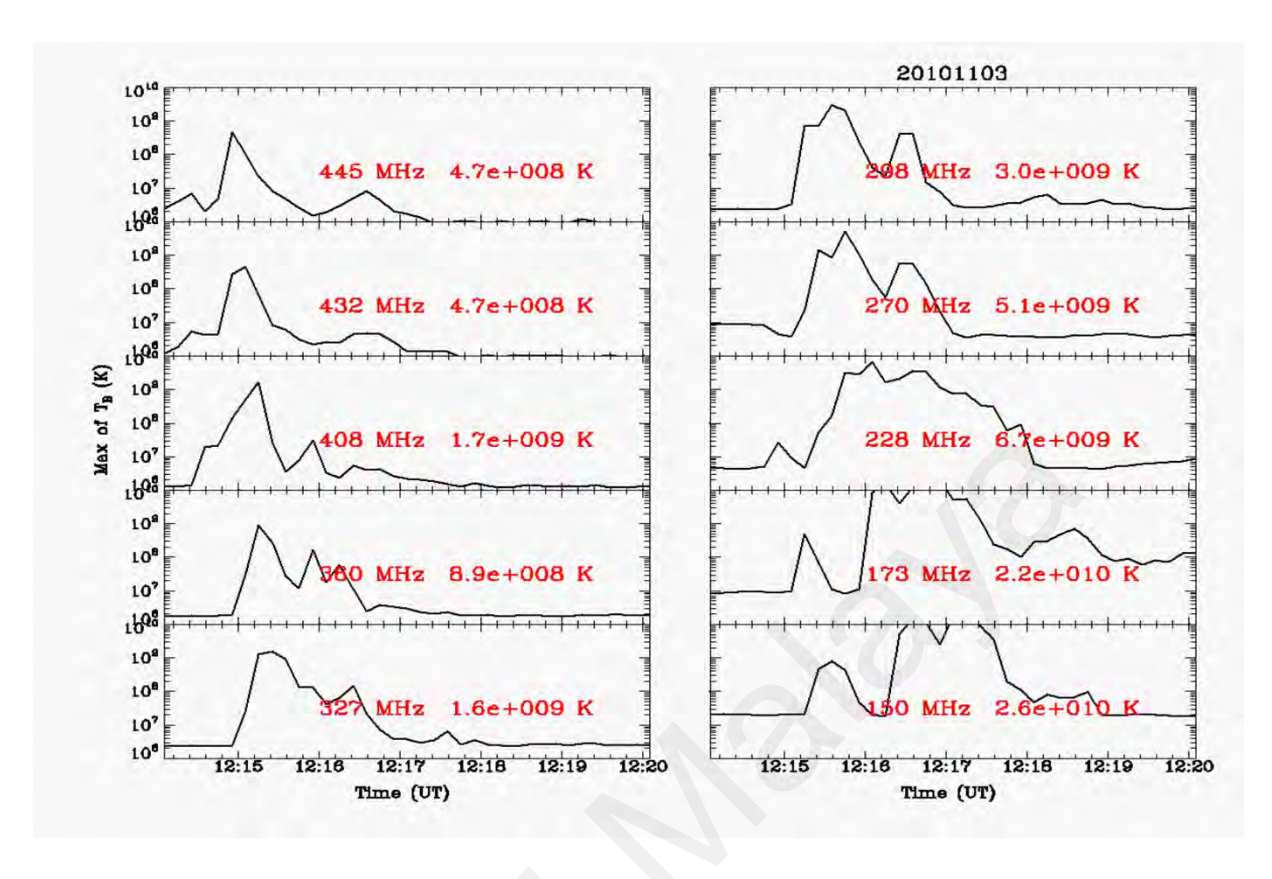


Figure 4.5: Brightness temperature of NRH frequencies from 12:15:00 UT to 12:20:00 UT on 3<sup>rd</sup> November 2010.

The time dependence of the degree of circular polarization (q) is also plotted and shown in (Figure 4.6). The average q of all pixels within the 95% maximum contour is used. Throughout the 'herringbones' of Type II solar radio burst, |q| remains steady at the values from as low as 1% to as high as 27% (1%  $\sim$  27%). At the same time, most of the q (445 MHz, 432 MHz, 408 MHz, 270 MHz, 228 MHz, 173 MHz, 150 MHz) are negative, which

indicated left-handed circular polarization based on the previous works (Liu et al., 2018; Vasanth et al., 2016; Vasanth et al., 2019).

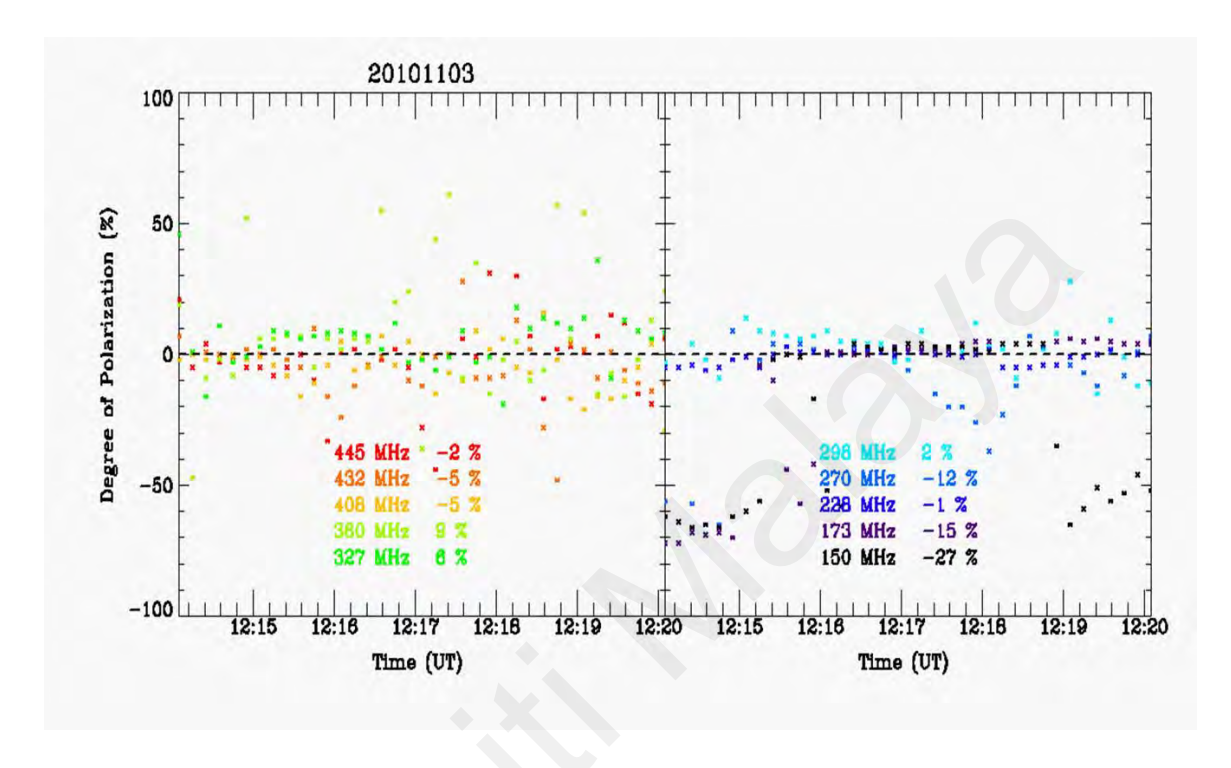


Figure 4.6: Degree of polarization (q) of NRH frequencies 12:15:15 UT to 12:18:05 UT.

## 4.1.4 Radiation Mechanism of 'Herringbone' Bursts

Table 4.2: Characteristics of various radiation mechanisms (Liu et al., 2018) and observed event. TB refers to the brightness temperature and q refers to degree of circular polarization. The observational parameters of the Type II 'herringbones' on  $3^{\rm rd}$  November 2010 are also listed for comparison.

5 November 2010 are also listed for comparison.						
Mechanism	ТВ	Polarization ( $ q $ )	Reference			
Cyclotron	< 10 <sup>9</sup> K	Any	(Dulk, 1985)			
Synchrotron	< 10 <sup>9</sup> K	0% (Linear)	(Dulk, 1985)			
Gyrosynchrotron	< 10 <sup>9</sup> K	Any	(Robinson, 1978)			
Fundamental Plasma	≥ 10° K	~ 100% ~ 0%	(Robinson, 1978)			
2 <sup>nd</sup> Harmonic Plasma	$\leq 10^{13} \text{ K}$	< 10%	(Melrose, 1975)			
ECM Emission	$\geq 10^{10} \mathrm{K}$	~ 100%	(Winglee, 1985)			
II HB of 03112010	$10^{10} { m K}$	1% ~ 27%	-			

From these two parameters of TBs and q obtained previously, the derivation of the radiation mechanism of this 'herringbone' feature can be analyzed. When interpreting 'herringbones' Type II solar radio bursts, there are four main radiation mechanisms that can be utilized (Table 4.2). When examining the solar radio burst event studied, the primary factors considered were the observational characteristics. From there, the appropriate mechanism was determined. Earlier research by (Dulk, 1985) has outlined the observational features of various solar radio bursts, including their underlying radiation mechanisms.

In this study, the focus is on the radiation mechanisms, with accentuation on important physical parameters such as brightness temperature and degree of circular polarization. The physical parameters of the  $3^{rd}$  November 2010 event are listed at the bottom row of the table. First, an important characteristic is the extremely high brightness temperature ( $\sim 10^{10}$  K).

This indicated that it must be either Fundamental Plasma or 2<sup>nd</sup> harmonic plasma or ECM emission. Second, the polarization degree is around 1% to 27%, which precluded that this originated from the 2<sup>nd</sup> harmonic plasma and the ECM emission.

The radiation mechanisms of the 'herringbones' bursts not necessarily be Fundamental plasma but can be 2<sup>nd</sup> harmonic plasma as well since this type of radiation mechanism is also a plasma radiation. (Cairns & Robinson, 1987) summarized that the maximum brightness temperature of the 'herringbones' bursts according to their radiation mechanism (Fundamental plasma or 2nd harmonic plasma) as follow:

$$1 \times 10^{10} \text{ K} < TB(f) < 6 \times 10^{11} \text{ K}$$
And
$$2 \times 10^{8} \text{ K} < TB(h) < 2 \times 10^{11} \text{ K}$$

where TB(f) is the maximum brightness temperature for Fundamental plasma and TB(h) is for  $2^{nd}$  harmonic plasma. It can be seen that the two maximum brightness temperatures show obvious differences in which TB(f) is at extremely high brightness temperature while TB(h) is at slightly lower brightness temperature than that of TB(f).

Based on data collected, the maximum brightness temperature of 'herringbones' of Type II solar radio burst on  $3^{rd}$  November 2010 is  $4.7 \times 10^8$  K  $< TB < 2.6 \times 10^{10}$  K. At first glance, this event seems to be following the radiation mechanism of the 2nd harmonic plasma. However, this is not enough to justify the type of radiation mechanism. Additional information is needed on the physical parameters as proposed by (Cairns & Robinson, 1987).

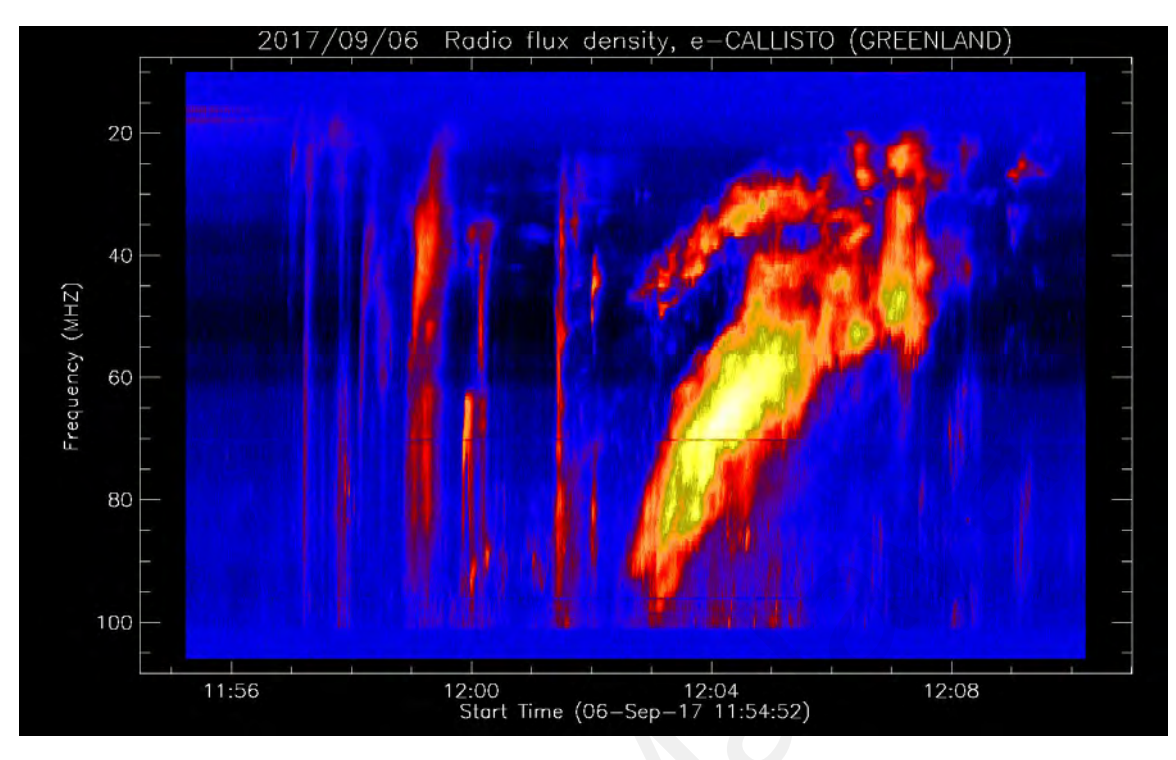
Polarization degree can provide the information that is required. According to a study by (Stewart, 1966), the circular polarization of 'herringbones' bursts ranged from less than 10% to more than 70%. This also coincide with the polarization degree of the studied event (1% ~ 27%). Then, it becomes more obvious that the radiation mechanism of the observed 'herringbones' follows the Fundamental plasma. By taking high TB and the polarization degree, the only feasible mechanism is the Fundamental plasma. This is consistent with earlier theoretical study by (Cairns & Robinson, 1987).

# 4.2 Analyzing Influence of Solar Activities Towards Formation of Solar Radio Bursts

The e-CALLISTO network provides wide coverage of observations. As of now, there have been more than 98 locations that this instrument has been installed and fully operated across the world including Switzerland, Australia, Egypt, South Korea, Russia, India, Kenya and Malaysia. All these observatories have been continuously working to provide the day-to-day data which can be publicly accessed through the official portal of e-CALLISTO. For this work, fruitful solar radio bursts event detected on 6th September 2017 are deeply analyzed by comparing with the correlated solar activities such as solar flares and coronal mass ejections (CMEs). This work adds a deeper analysis for this event by performing the analysis for the formation of the solar radio burst type II with its correspond CMEs compared to the previous studies made by (Y. Yasyukevich et al., 2018) and (M. Karlický & J. Rybák, 2020) which studied only on the correlation of the strongest flare form during that day which causes the formation of the solar radio burst type III. This result will give hints on how the solar flares and CMEs eruption can affect the formation of the solar radio burst itself.

## **4.2.1** CALLISTO Spectrogram

On 6<sup>th</sup> September 2017, CALLISTO spectrograms show that there is presence of multiple types of solar radio bursts detected on that particular day. The observed activity reveals to be a series of type III solar radio bursts and type II solar radio bursts. By referring to a similar event, different CALLISTO stations have been used to cross-check the detection of the occurrence of these bursts. However, detailed analysis of these bursts is done only using spectrogram data from Greenland station as it shows the most structure of the event. Figure 4.7 demonstrates the spectrogram of solar radio bursts event observed throughout the exact date. The spectrogram period was taken starting from 11:55 UT until 12:25 UT.



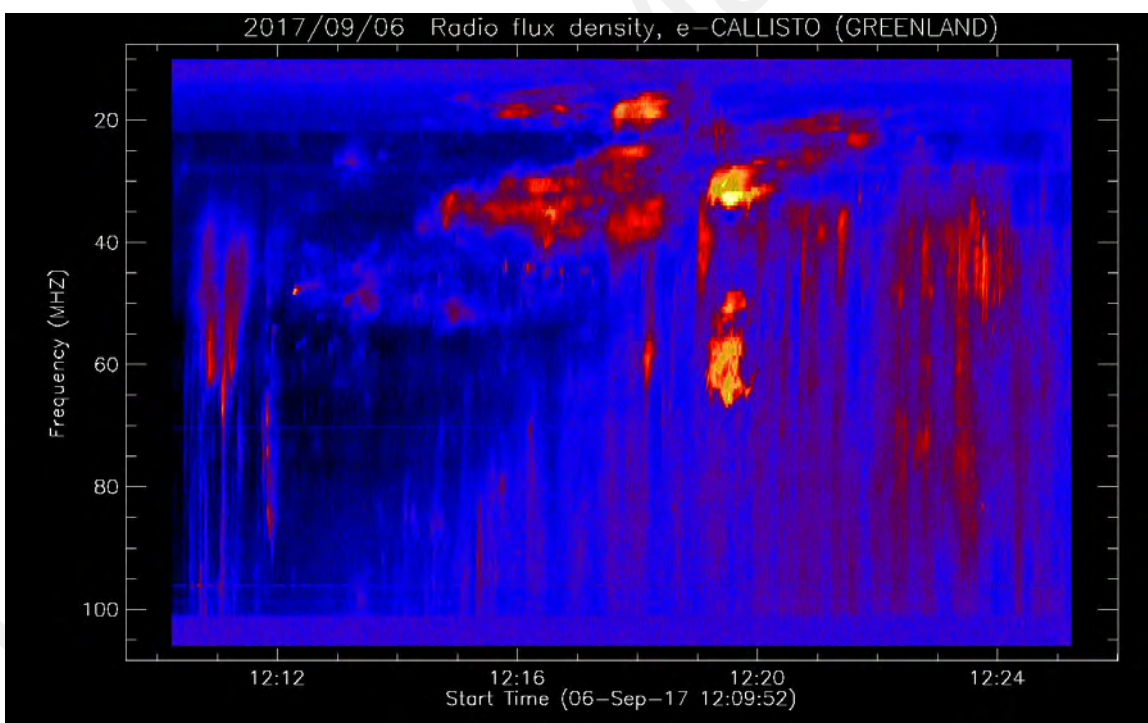


Figure 4.7: Spectrograms (top and bottom) showing solar radio bursts captured on  $6^{th}$  September 2017 for a period from 11:55 UT until 12:25 UT.

Referring to Figure 4.7 and using the SolarSoftWare Interactive Data Language (SSW-IDL), a spectrogram for event on 6<sup>th</sup> September 2017 has been re-plotted after processing it

through noise background subtractions as shown in Figure 4.8. This figure has been configured by referring to its original spectrogram images retrieved from the CALLISTO network to avoid loss of data for the whole observation period of the solar radio bursts event captured. Additional spectrogram also has been plotted as seen in Figure 4.9 to obtain the accurate time and frequency for each point of interest occurring throughout the event.

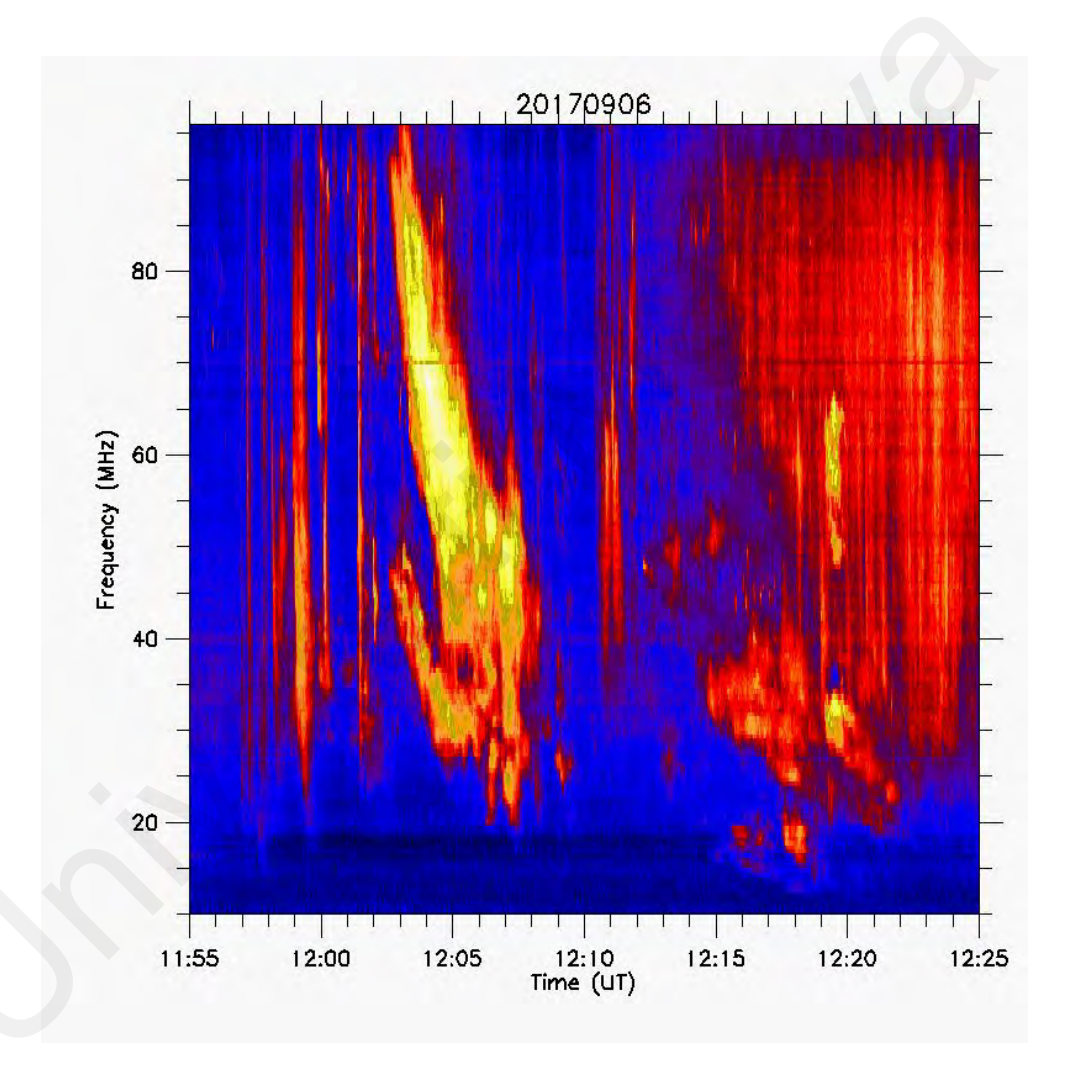


Figure 4.8: Re-plotted and combined spectrogram of the multiple solar radio burst event from 11:55 - 12:25 UT using SSW-IDL software.

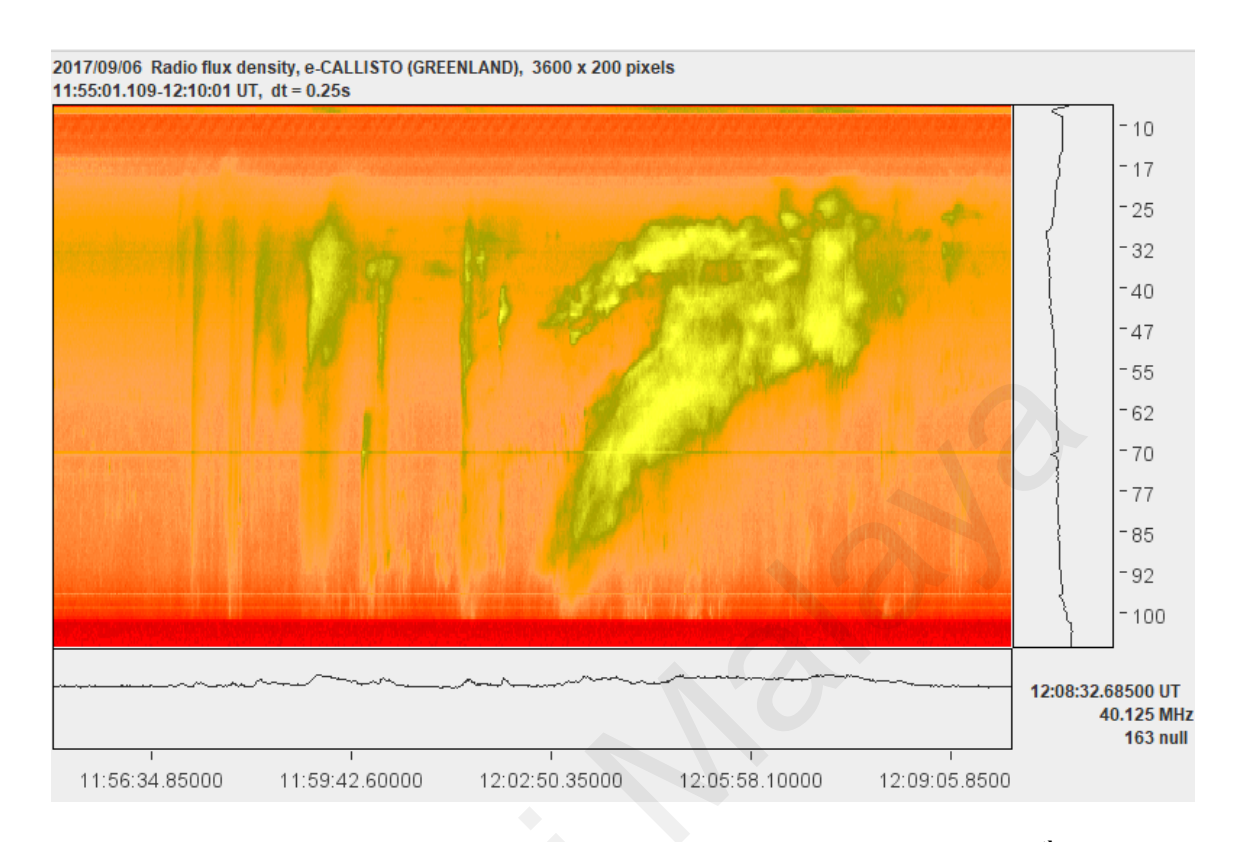


Figure 4.9: Spectrogram plotted for the multiple burst event captured on 6<sup>th</sup> September 2017 using RAPP FITS Java Viewer.

In Figure 4.8, the spectrogram shows that the series type III burst started from 11:56 UT to 12:02 UT. Then, one of the series of Type III bursts is detected simultaneously with type II burst starting from 12:02 UT. Both started at 12:02 UT and end at 12:08 UT for type III while end at 12:21 UT for type II. More specifically, NOAA mentioned that the burst only occurred at frequency of 25 MHz – 81 MHz. The studied observations are found to be supported by (Gergely et al., 1984) where the starting frequencies of the type III burst is around 55 MHz, and the type II burst is around 70 MHz which also happened to be within the same range. From NOAA data shown in Table 4.3, it also shows the simultaneous occurrence of these two types of bursts. Both were generated over a period of 10 minutes or more.

Table 4.3: Solar radio bursts details obtained from NOAA data archive for event on 6<sup>th</sup> September 2017.

Begin Time	End Time	Observatory	Frequency	Details	Active
			(MHz)		Region
12:02 UT	12:08 UT	Sagamore	25-61	Series of	2673
				Type III	
12:02 UT	12:21 UT	San Vito	25-81	Type II	2673

## **4.2.2** Frequency Drift Determination

In this event, two frequency drift have been determined for both types of solar radio bursts. The RAPP viewer for CALLISTO software was used to get exact value for the frequency and time. Figure 4.9 also shows the spectrogram for the event that has been plotted using RAPP FITS Java Viewer (RAPP viewer) of CALLISTO. From the plotted spectrogram, the exact value for frequency and time for the spectrogram can be obtained. From the value obtained in the RAPP viewer for CALLISTO, frequency drift obtained for the simultaneous type II and type III bursts are 0.204 MHzs<sup>-1</sup> and 9.4 MHzs<sup>-1</sup> respectively. Based on the plasma hypothesis made by (Wild, 1950) the frequency drift of type III solar radio burst is produced due to the outward motion of a disturbance, which in this case the exciter, which it causes the plasma waves to have decreasing frequency as it travels through the Sun's corona along a path of decreasing electron density (Fainberg & Stone, 1970). There is some suggestion that type III having higher frequency drift is due to involvement of the burst with the fast downward reconnection out flows from the reconnection. As time pass, the slow motion of flare loop (76 kms<sup>-1</sup>) may decelerate the fast flow and caused the drift rate to be decreased. (Huang et al., 2007). One of the characteristics for solar radio bursts type III are

the fast drift of frequency from high to low that attributes the decreasing of electron plasma frequency (Lin et al., 1981).

Drift rates at higher frequencies commonly have rapid speed because the density scale heights lower in the atmosphere are smaller, and a disruption at constant speed will therefore cause a higher frequency drift rate. For solar radio bursts type III remarkably labelled as fast-drift bursts have consistently the fastest drift rates of bursts at metric wavelengths. The exciter speeds tend to be in the order of one—tenth of the speed of light, and accordingly the only plausible drivers for solar radio bursts type III are beams of electrons having energies up to tens of keV. Such beams of electrons have long been known to be very efficient initiators of electrostatic Langmuir waves via the bump—in—tail instability. They can be seen to start at densities corresponding to the very low corona (frequencies up to several GHz) and propagate through its frequency range all the way up to 1 AU, where their electrons can be detected in—situ by spacecraft in the solar wind (Thejappa et al., 2020).

From the frequency drift value obtained, the series of Type III bursts can be seen to have much faster frequency drift which occurred in shorter period time as spike bursts in spectrogram. Both type solar radio bursts type II and III are highly correlated with fast-electron and emission being at plasma frequency. The frequency drift rate of the burst is related to the shock's velocity. The slow drift rate determines the lifespan for the solar radio bursts Type II (Batubara et al., 2017).

## **4.2.3** Active Region

Table 4.3 shows the details of both types of solar radio bursts on 6<sup>th</sup> September 2017. From the NOAA data archive shown, it seems that both bursts from the event originated from the same active region which is AR 2673. To obtain the image of the AR 2673, Solar Dynamics Observatory (SDO) data were chosen to be equipped with white light filter and hydrogen alpha filter as seen in Figure 4.10.

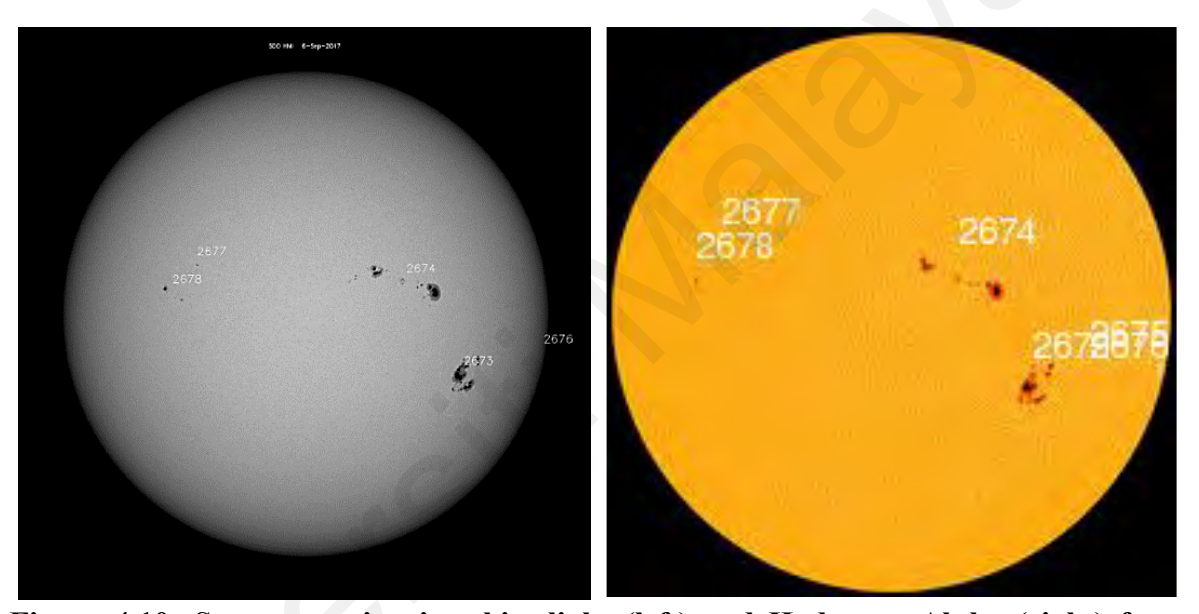


Figure 4.10: Sunspot region in white light (left) and Hydrogen Alpha (right) from SDO/HMI.

The two visuals in Figure 4.10 displayed the appearance of the sunspots during this selected event. It shows that there were many distinct active regions that appeared on that day. For this work, the active region of AR 2673 was selected as the multiple solar radio bursts event occurred within this specific active region. This visualization is useful to highlight the variations in the appearance of solar phenomena, such as sunspots and active regions depending on the wavelengths of light being observed. On the day of 6<sup>th</sup> September 2017, AR 2673 was found to cause the formation of four powerful eruptions of class X solar

flares. The strongest solar flare that occurred throughout that day was the solar flare X9.3 of solar cycle 24. Later on the date of  $7^{th} - 8^{th}$  September 2017, a significant geomagnetic storm of class G4 occurred which was initiated by the same strong solar flare class X9.3 and CMEs event on  $6^{th}$  September 2017. This event caused a considerable difference in the horizontal geomagnetic field as reported by (Anuar et al., 2018) indicating magnetic reconnection due to solar wind from North to South. These findings align with (Tassev et al., 2017) who documented the alarming geomagnetic storm that occurred during the same period.

Corollary, the maximum solar wind speed with values of 880 kms <sup>-1</sup> and high dynamic pressure obtained during the geomagnetic storm event possibly was led by the occurrence of strongest solar flares and CMEs event on that observed day. The geomagnetic storm event also caused a reduction in the H component value at the three chosen magnetometers, particularly at DAW station as noted by (Zafar et al., 2021). Through this work analysis, it is revealed that this event originated from the same active region as the solar eruptions which is consistent with the findings reported by previous studies such as (Stewart & Sheridan, 1970; Robinson & Sheridan, 1982; Gergely et al., (1984); Shanmugaraju et al., (2005); Cho et al., (2011); Ma & Chen, 2020). The magnetogram of AR 2673 as seen in Figure 4.11 displayed the polarity distribution of this active region. The magnetogram of it was extracted from the Helioseismic Magnetic Imager (HMI).

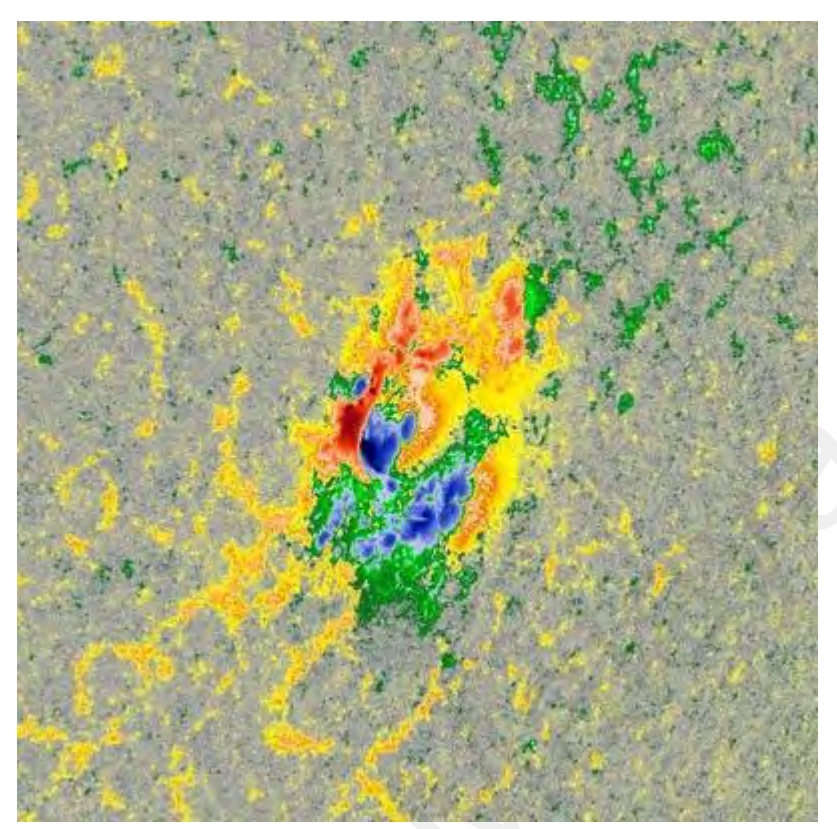


Figure 4.11: Magnetogram of AR 2673 from HMI. The colors represent the polarity of the magnetic field. Yellow-red region indicates negative polarity while Blue-Green region indicates positive polarity.

## 4.2.4 Solar Radio Bursts and Solar Flares Relation

Obtained from SWPC/NOAA archive data, a list of solar flares occurring on 6<sup>th</sup> September 2017 was shown in Table 4.4. All the listed solar flares take place in the same active region AR 2673. By referring to Table 4.4, it can be seen that flare X9.3 is the strongest (reaches X class level) of the solar flare detected on that day. The flare begins to form at 11:53 UT until 12:10 UT and it reaches its peak at around 12:02 UT.

Table 4.4: List of solar flares on 6<sup>th</sup> September 2017.

Tuble 1.11. Elist of solut fluites on a September 2017.					
Region	Class	Start Time	Peak Time	End Time	
2673	C1.6	06:17 UT	06:22 UT	06:29 UT	
2673	C2.7	07:29 UT	07:34 UT	07:48 UT	
2673	X2.2	08:57 UT	09:10 UT	09:17 UT	
2673	X9.3	11:53 UT	12:02 UT	12:10 UT	
2673	M2.5	15:51 UT	15:56 UT	16:03 UT	
2673	M1.4	19:21 UT	19:30 UT	19:35 UT	
2673	M1.2	23:33 UT	23:39 UT	23:44 UT	

The formation of the multiple bursts of series of the solar radio bursts Type III and type II solar radio burst seems to be closely related with the strongest solar flare event. The peak time of this flare is found to be at the same observed time of the detected multiple bursts. This X9.3 solar flare occurs in the impulsive phase, which is more intense at meter wavelengths and may have a continuum which is usually associated with a single flare or flare-like events that excited through the lower solar corona. During the flare, strong series of solar radio bursts Type III is observed over a broad frequency range. The correlation of solar radio bursts Type III with its correlated solar flares can be explained through the magnetic reconnection theory. Type III bursts usually involve non-thermal emission process which is emitted through the ejected energetic particles from solar events such as solar flares which in this case through the magnetic reconnection process.

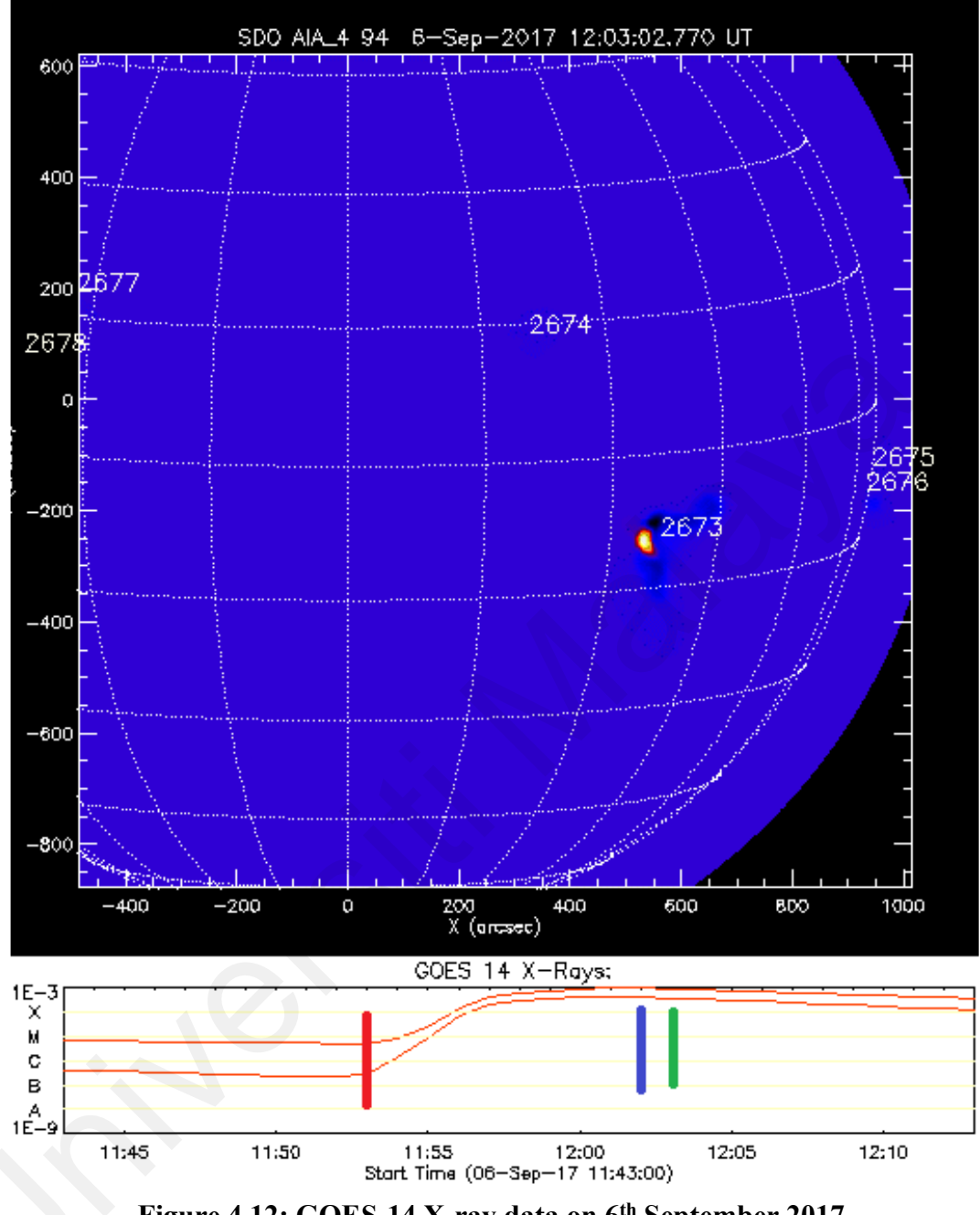


Figure 4.12: GOES-14 X-ray data on 6th September 2017.

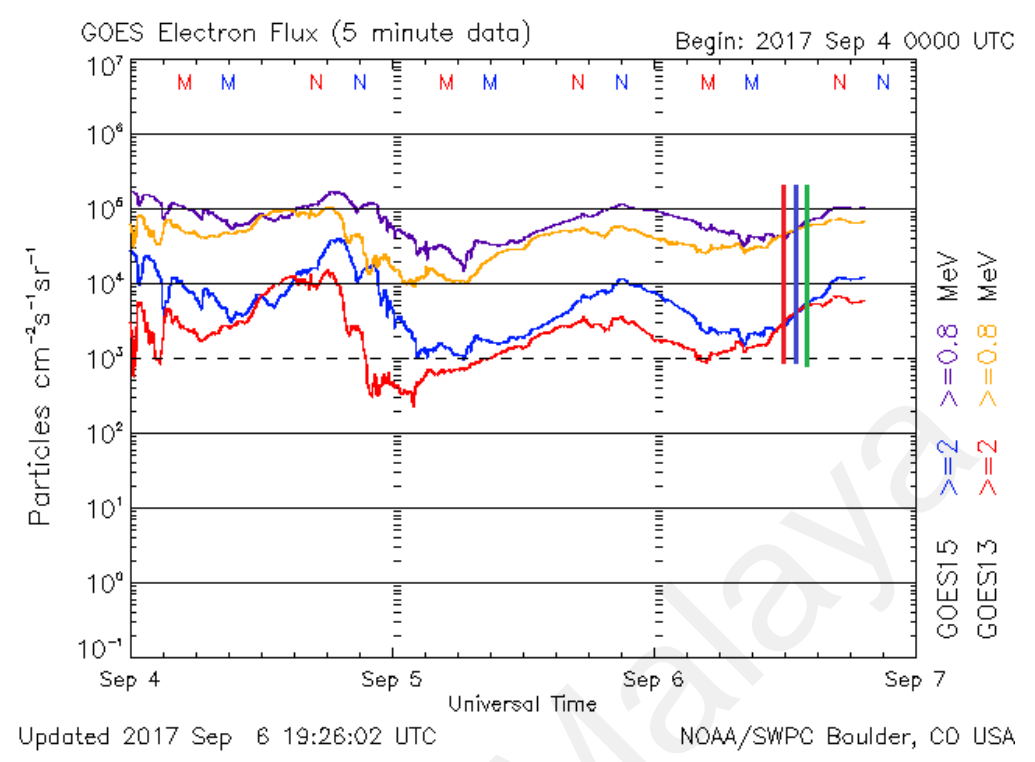


Figure 4.13: GOES-14 electron flux on 6th September 2017.

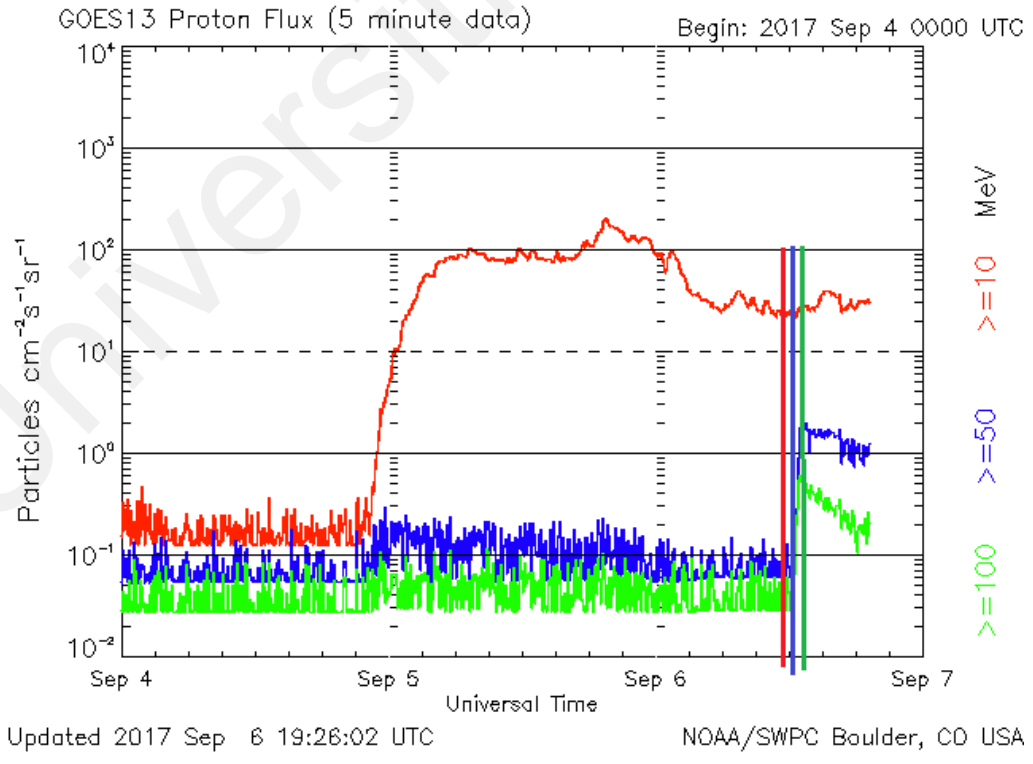


Figure 4.14: GOES-13 proton flux on 6th September 2017.

Figure 4.12 shows the variation of 1-minute X-ray flux in Watts $m^{-2}$  on  $6^{th}$  September 2017. In this figure, it shows that the flux data obtained from GOES-14. In the X-ray variation graph shown in the bottom of the figure, the increment of the X-ray flux was clearly displayed within the solar events interval. The colored 3 vertical lines represent the timeline of occurrence of solar flare (red), occurrence of the series of type III solar radio bursts (blue) and post formation of the series of type III solar radio bursts (green). The Total Electron Content (TEC) in radio waves can be used to determine the electron flux. TEC is an indicator of the total number of electrons that exist along the pathway to reach the ground. Solar radiation and activity which propagates from the lower atmosphere are the primary factors that influence TEC. The velocity changes of the waves passing through the ionosphere result in variations of the electron flux.

Figure 4.13 illustrates the 5-minutes data for electron flux in Particles  $cm^{-2} \ s^{-1} \ sr^{-1}$  for 3 days from 4<sup>th</sup> September 2017 to 6<sup>th</sup> September 2017. It shows the variation of electron flux obtained from GOES-13 and GOES-15 of  $\geq 2$  MeV and  $\geq 8$  MeV respectively for both represented in four different colors. From there, it shows the level of electron flux in GOES-13 presented same trend with electron flux obtained from GOES-15 for  $\geq 8$  MeV reached the highest level. The 3 vertical lines represent the timeline of occurrence of solar flare (red), occurrence of the series of type III solar radio bursts (blue) and post formation of the series of type III solar radio bursts (green). In Figure 4.14, the 5-minutes data of proton flux in Particles  $cm^{-2} \ s^{-1} \ sr^{-1}$  is shown for 3 days from 4<sup>th</sup> September 2017 to 6<sup>th</sup> September 2017. In this figure, the data obtained from GOES-13 and GOES-15 come from ( $\geq 100$  MeV,  $\geq 50$  MeV,  $\geq 10$  MeV) are represented in three colors. The proton flux increased clearly during the event day compared to the other two days. The 3 vertical lines represent the timeline of

occurrence of solar flare (red), occurrence of the series of type III solar radio bursts (blue) and post formation of the series of type III solar radio bursts (green).

Also from Figure 4.14, it shows that the proton flux of this event can reach up to 102 MeV. The high in energetic proton flux (typically >10 MeV) are commonly from a shock caused by an energetic solar eruption which related to Solar Proton Event (SPE). SPE has a close relation with the Solar Energetic Particles (SEP) events that originated from impulsive flares or jets which can be driven out by CMEs. The possibility that both series of Type III and Type II sources may be excited by a common disturbance, or closely related disturbances are analogous. This argument is consistent with the findings by (Stewart & Sheridan, 1970; Robinson & Sheridan, 1982; Shanmugaraju et al., (2005); Cho et al., 2011) and provides strong evidence that both types of bursts in the present case were caused by the same shock wave. The eruption was accompanied by the formation of solar energetic particles, which were spotted through the ERNE, together with the massive propellant, indicating that these particles continue to be accelerated for a long time due to their consistent power supply (Allawi et al., 2020).

## 4.2.5 Solar Radio Bursts and Coronal Mass Ejections Relation

In the event of  $6^{th}$  September 2017, it was found that the Type II solar radio burst was observed to be closely associated with coronal mass ejections (CMEs) originated from the coronal shocks. The CMEs were released at the Southeast section of the Sun which was also found to be within the region of AR 2673. However, due to the condition of its TB (5.0 ×  $10^3$  K < TB <  $2.5 \times 10^6$  K) is out of range as per theorized by (Cairns & Robinson, 1987), there is no presence of herringbone feature for the solar radio burst Type II formed in this event as reported in the first objective of this work. As mentioned before, the solar flare X9.3

class which formed in the same active region might be the main driver of the resulting CMEs. As shown in Figure 4.15, 4.16 and 4.17, all these three different types of images show the associated CMEs with the event. All the three figures are extracted from different sources which are C2 coronagraph, STEREO/SECCHI COR1-A image and C2 AIA image with different temperature and wavelength. Each figure is represented by three different situations which are (a) before the occurrence solar radio burst, (b) during the occurrence of solar radio burst and (c) after the occurrence of solar radio burst.



Figure 4.15: C2 coronagraph image on 6th September 2017.

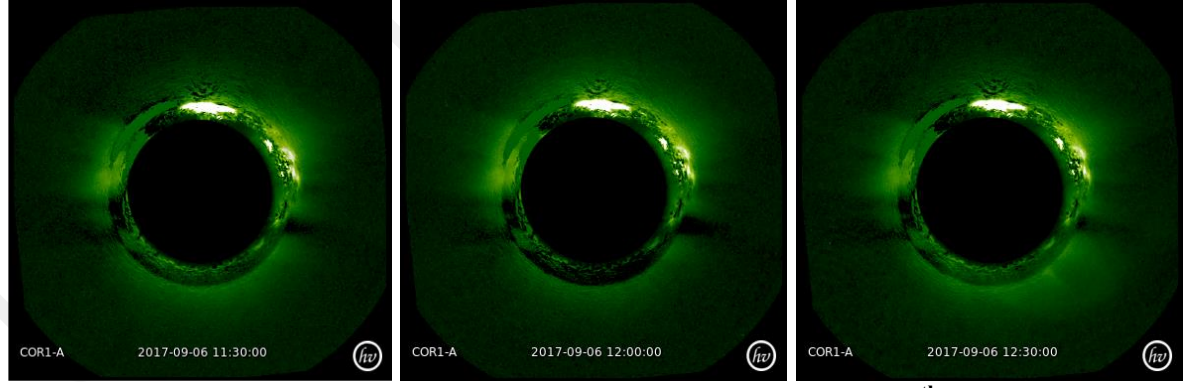


Figure 4.16: STEREO SECCHI COR1 A coronagraph image on 6th September 2017.

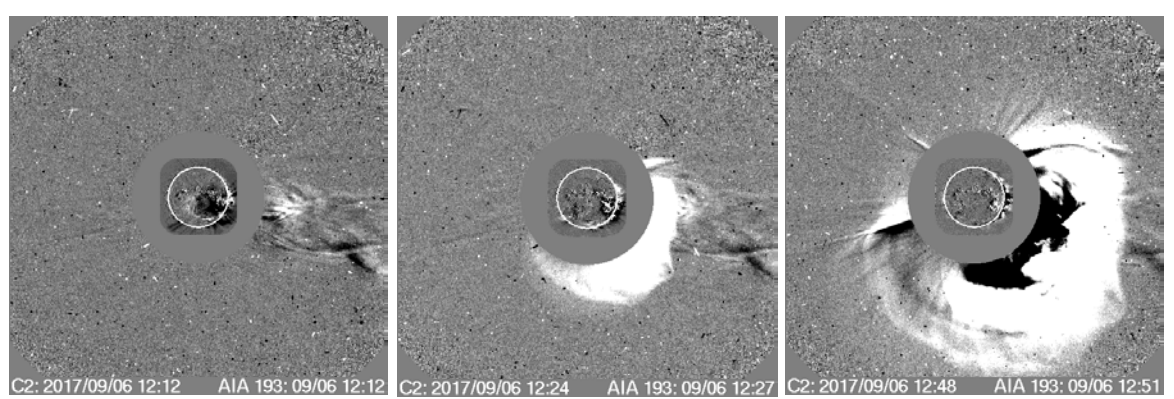


Figure 4.17: C2 AIA image on 6th September 2017.

Table 4.5: CME features information captured on 6th September 2017.

Time	Linear Speed	Acceleration	Kinetic	Flare Start	Flare Peak
(UT)	(kms <sup>-2</sup> )	(ms <sup>-2</sup> )	Energy	Time	Time
12:24:05	1571	-0.3	$3.6 \times 10^{32}$	11:53 UT	12:02 UT

From this event, the CMEs linear speed is measured as a fast CME which travelled at 1571 kms<sup>-2</sup> as shown in Table 4.5. This value indicated that these CMEs formed interplanetary shock. One of the conditions required for a slow drift burst or a Type II burst to occur is that they must be driven by a fast CME (Umuhire et al., 2021). Coronal mass ejection or CME is an impulsive coronal event that is capable of producing Moreton wave (Uchida, 1968). Moreton waves are produced by the evolution of flares or sideways movement through the CME. As shown in Figure 4.15, 4.16 and 4.17, it can be deduced that Moreton waves were closely associated with the CME of the event. Simply said, the Moreton waves also appeared as the Type II solar radio bursts occurred due to the releasing of the CMEs during that event. With the existence of the Moreton waves, coronal fast shock wave produced during the releasing process of CMEs.

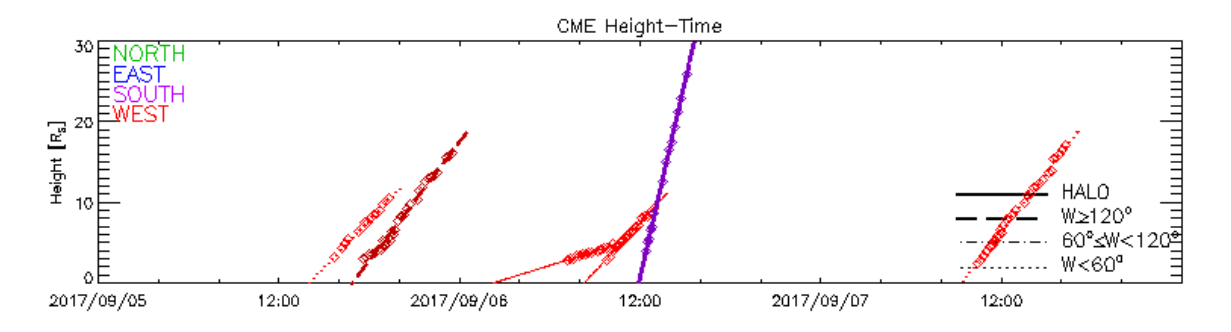


Figure 4.18: CMEs height variation from 5<sup>th</sup> – 7<sup>th</sup> September 2017.

Figure 4.18 shows the variation of CME height from four directions (North, East, South, and West) within 3 days of the event. The height of the CMEs can reach up to 30 Solar Radius (Rs) in the South direction exactly at the same time of the event recorded. As shown in Figure 4.15, 4.16 and 4.17, the CME coronagraph shows the appearances of the CME near the South region of solar disk. The multiple bursts event presented here shows that it might not just have occurred due to strong flare formed around the active region but also closely related with large CMEs. This observation agrees with (Shanmugaraju et al., (2005); Cho et al., (2011); Ma & Chen, 2020) which was similar with the studied case.

**4.3** Identification of Solar Radio Bursts Candidate with Band-splitting to be Detected Using Upgraded Half-wave Dipole Antenna (uHWDA)

## **4.3.1** Solar Radio Bursts Type II

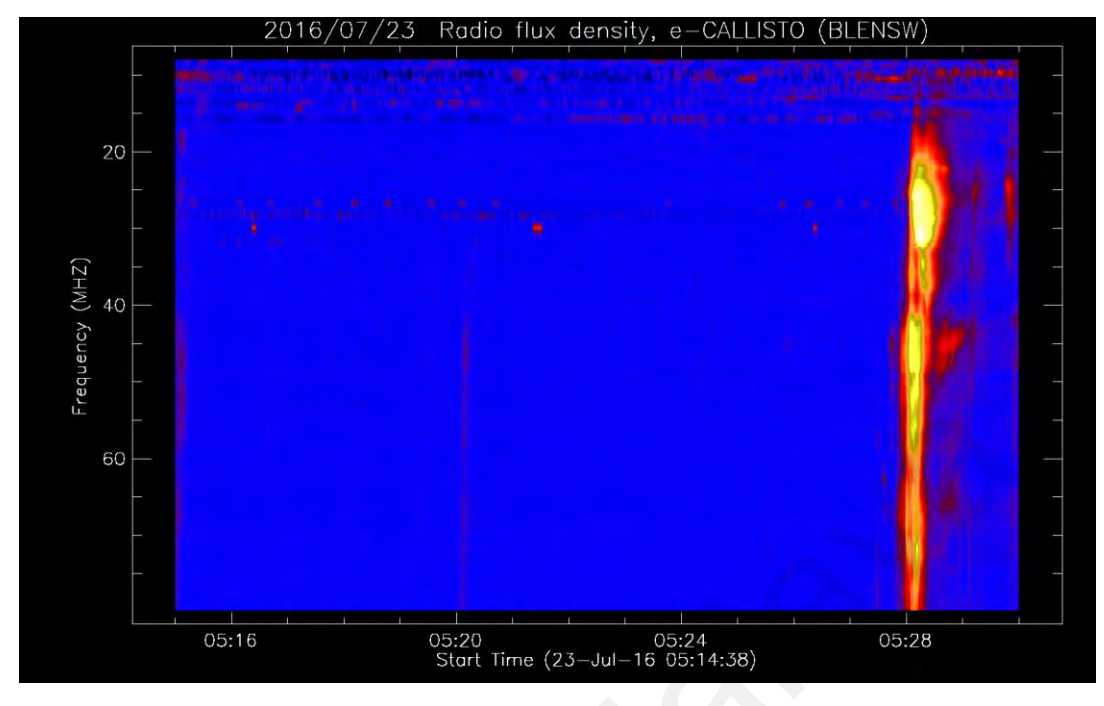
In comparison to other types of bursts, Type II solar radio bursts have distinct band emissions that can be observed on dynamic spectra. These bursts are known for their gradual drift from high to low frequency in a slow manner, making them an interesting event to study. Bursts can also be defined as the displacement of the peak frequency per unit time, (df/dt) (Wijesekera et al., 2018) and showing two separated bands. Type II solar radio bursts are typically associated with Coronal Mass Ejections (CMEs) and, on occasion, solar flares.

These bursts are characterized by their slow drift rates and intense radio emissions. However, interplanetary shocks created during these events are believed to be the underlying cause of this phenomenon. Both CMEs and solar flares are types of solar eruptions activities that release energy and electromagnetic radiation, producing a range of radio signatures linked to non-thermal electrons. (Chrysaphi et al., 2018).

The first detection of Type II solar radio burst event was recorded by Payne-Scott et al., (1947) (Ma and Chen, 2020). Since the first reported activity of the burst, researchers believe that these bursts are excited by magnetohydronamic (MHD) shockwaves originated from CMEs (Monstein, 2012). CMEs have been shown to be a successful means of generating solar radio bursts by generating faint disturbance shock waves at the end of their structure. This process initiates the acceleration of non-thermal electrons, which in turn produce radio bursts (Magdalenic et al., 2021). These phenomena also affect the Type II solar radio bursts to introduce two frequency bands, known as fundamental emission and 2nd harmonic emission. It is also proven that the CMEs that connected with the type II bursts are wide and energetic (Umuhire et al., 2021). The band splitting creates frequency differences between them with approximation of it to be in 1:2 ratio. The split occurs due to the emission originating from the shock regions located upstream and downstream (Majumdar et al., 2021) with the 2<sup>nd</sup> harmonic known lies at 60-90 MHz and the fundamental is 20-60 MHz (Zucca et al., 2012).

## **4.3.2** Investigation on the Solar Radio Burst Event on 23<sup>rd</sup> July 2016

For this work, finding a suitable candidate for the uHWDA detection is made using the e-CALLISTO and NOAA instruments. With the achievement of the uHWDA, comparing e-CALLISTO data with upcoming upgraded HWDA array solar radio burst data will be essential for detecting activities between 45 MHz to 80 MHz as a continuation of this work. A Type II solar radio burst was captured on the date of 23<sup>rd</sup> July 2016 by e-CALLISTO at Bleien observatories from 05:15 UTC until 05:45 UTC spectrographs by both LWA circular polarization 1 and 2 shown in Figure 4.19 and Figure 4.20 respectively. The flux intensity of radio emission can be discerned by observing the color contour that lies between blue and orange (Pauzi et al., 2020). This event occurred with a starting frequency of 55 MHz at 05:29 UTC and it ended at a frequency of 40 MHz at 05:35 UTC. The RAPP FITS Viewer software was used to zoom into the details of the events as shown in Figure 4.21. The frequency was focused into smaller range as the characteristics of burst band-splitting feature need to be observed.



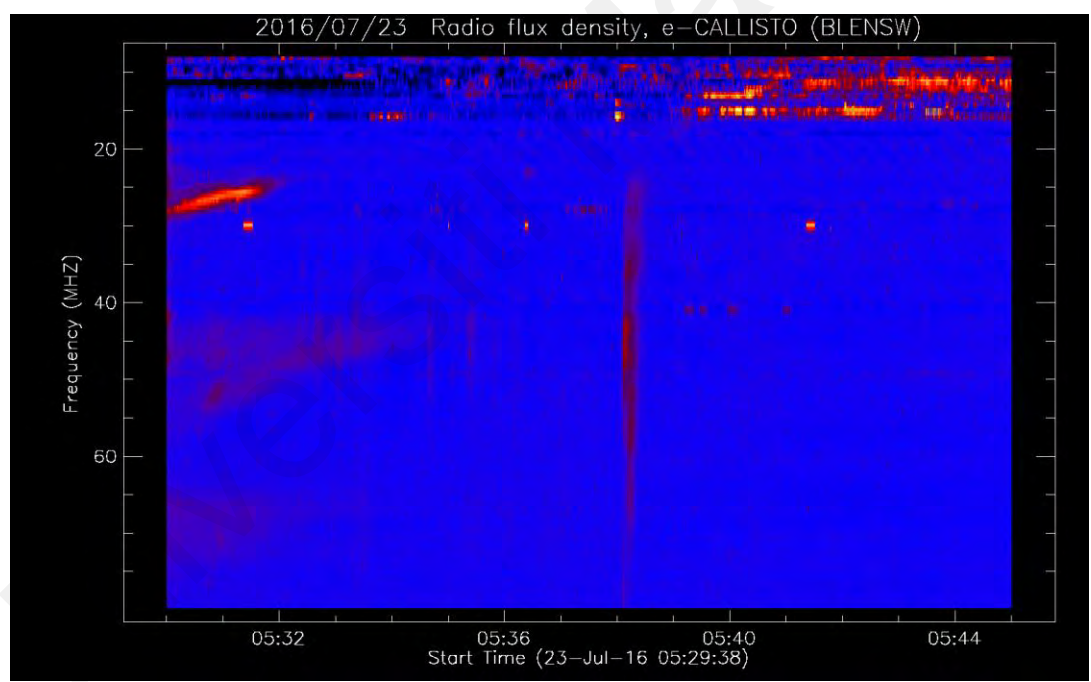
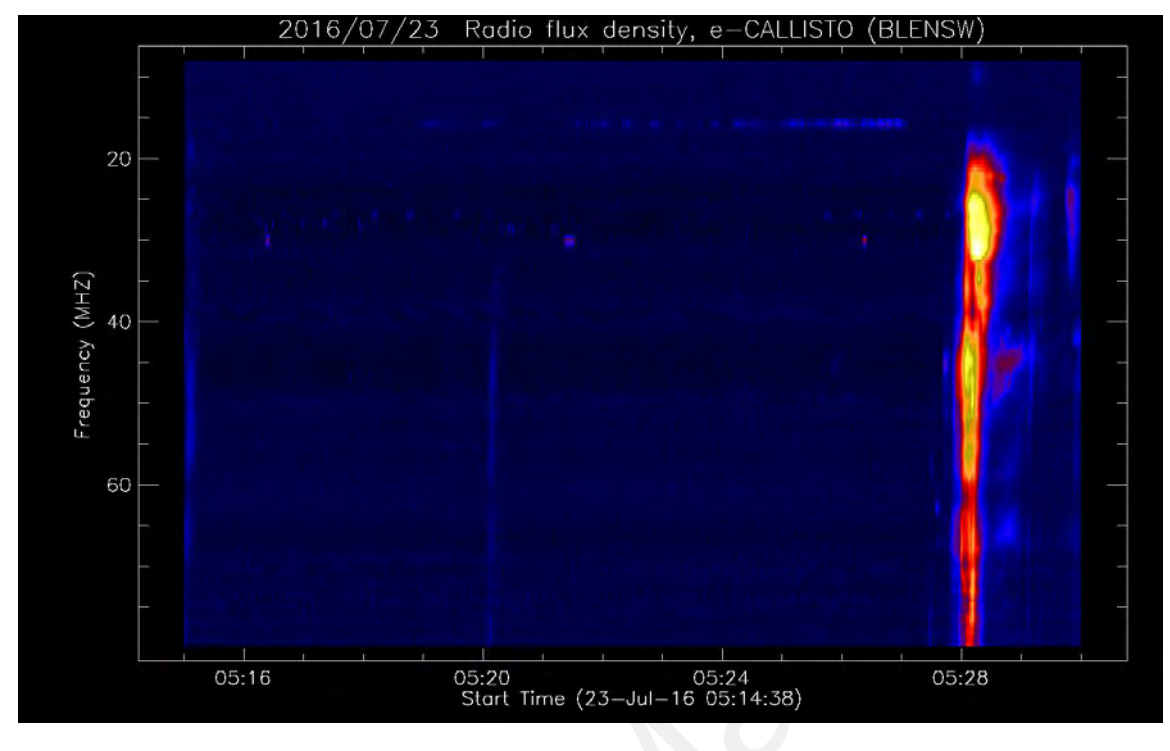


Figure 4.19: e-CALLISTO observations (top and bottom) at 05:15-05:45 UTC from BLENSW 01 Observatory for event  $23^{\rm rd}$  July 2016.



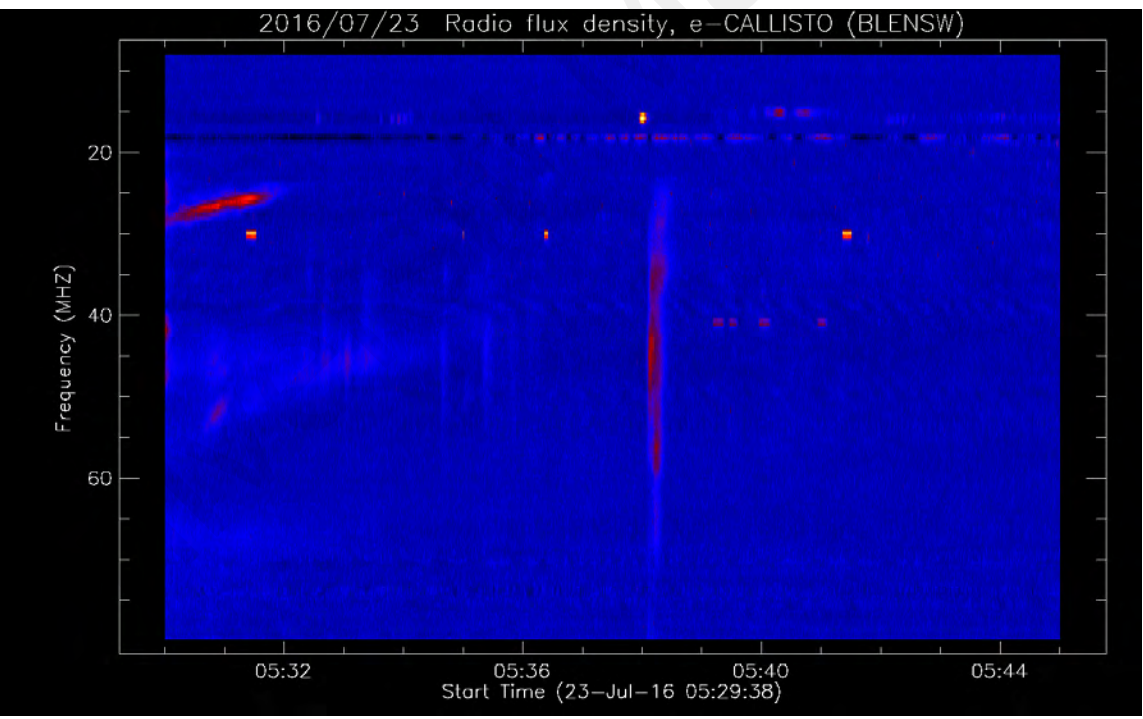


Figure 4.20: e-CALLISTO observations (top and bottom) at 05:15-05:45 UTC from BLENSW 02 Observatory for event  $23^{\rm rd}$  July 2016.

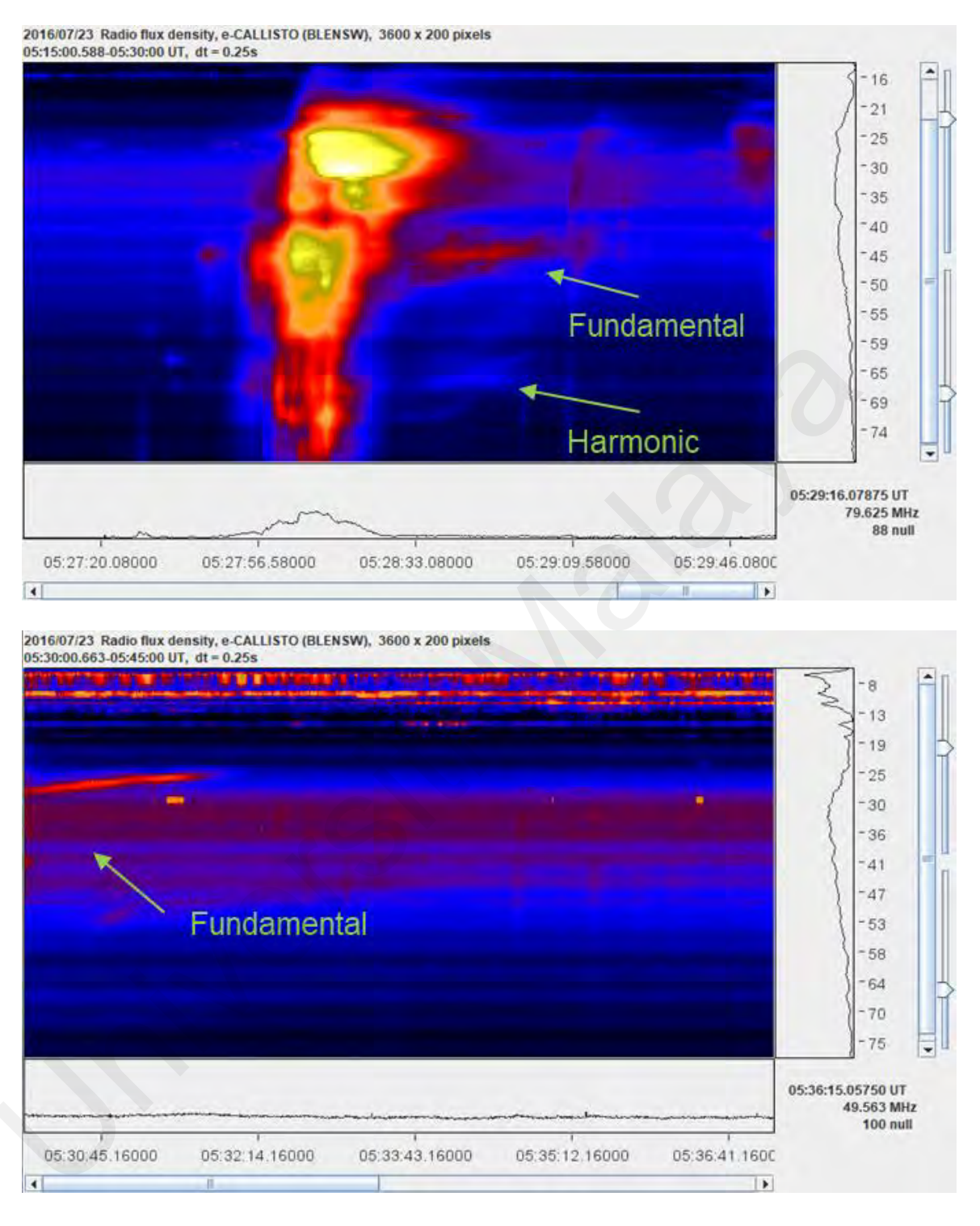


Figure 4.21: Event images (top and bottom) zoomed into smaller frequency range using RAPP FITS Viewer software.

The band splitting of the fundamental and  $2^{nd}$  harmonic emissions from Type II burst was detected during this exact date. The lower band of the fundamental emission is found to be

started around 60 MHz and ended at 25 MHz. For upper band of the 2<sup>nd</sup> harmonic emission started around 75 MHz and ended at 60 MHz. The frequency drift for both emissions happened around 3 minutes which consider as slow frequency drift. From these data, it was confirmed Type II solar radio burst event occurred between 25 MHz to 75 MHz which coincides with the range of the uHWDA array, 55 MHz to 65 MHz.

Using NOAA data, as depicted in Table 4.6 for the event on 23<sup>rd</sup> July 2016 can aid in identifying and verifying the occurrence that was detected from other instruments. Based on data of 23<sup>rd</sup> July 2016 (shown in Table 4.6), a Type II solar radio burst was detected in NOAA databases and observed by e-CALLISTO simultaneously which is from 05:29 UTC until 05:35 UTC. NOAA database is widely recognized as a reliable and impartial source of scientific data in confirming the Type II event and several other observed solar radio burst occurrences.

Table 4.6: Event data of 23<sup>rd</sup> July 2016 adapted from NOAA data archive.

Site	Date	Time	Frequency	Other
1,5		(UTC)	(MHz)	events
				Type IV and VI
San Vito, Italy	23 <sup>rd</sup> July 2016	05:29 – 05:35	25 - 52	solar radio bursts
				oursis

Nonetheless, there existed a significant variance in the occurrence rate of events as detected by e-CALLISTO and NOAA data. The event frequency that read from RAPP viewer data is from 25 MHz to 75 MHz while NOAA is 25 MHz to 52 MHz. To clarify the observed difference, additional investigations are necessary.

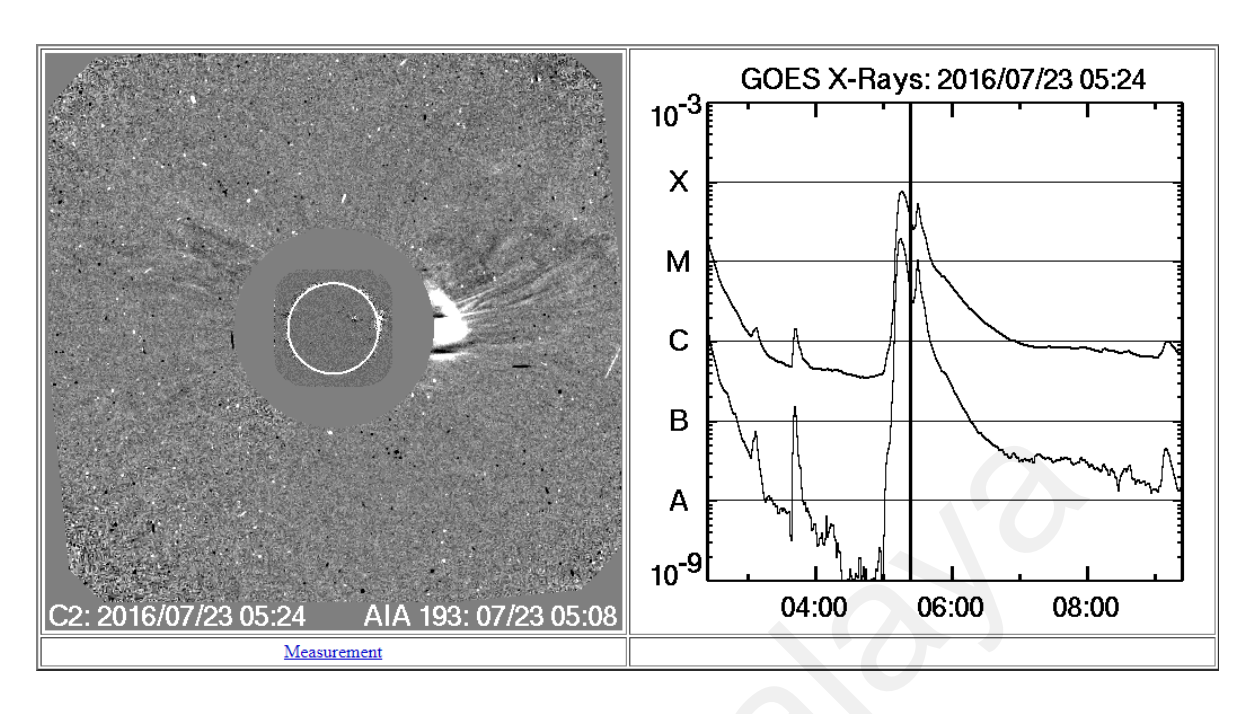


Figure 4.22: C2 Telescope data obtained from CDAW catalog and GOES X-rays data for event 23<sup>rd</sup> July 2016.

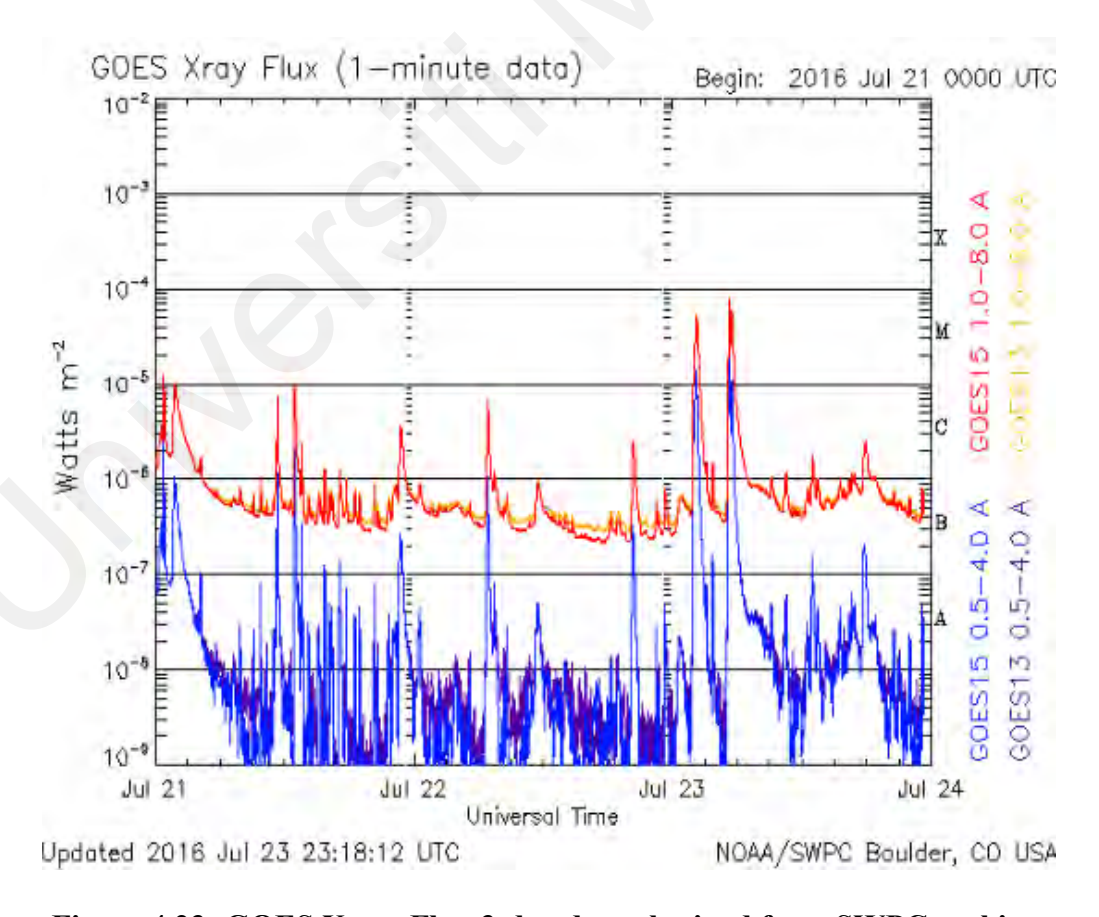


Figure 4.23: GOES X-ray Flux 3-day data obtained from SWPC archive.

Figure 4.22 illustrates the image of the Sun's activity within its coronal and the flares exploded from the same region recorded by GOES Satellite on 23<sup>rd</sup> July 2016 at 05:24 UTC from Coordinated Data Analysis Workshop (CDAW). Figure 4.23 illustrates the GOES X-ray Flux data of solar flares for three days observation starting 21<sup>st</sup> July 2016 until 24<sup>th</sup> July 2016 from the Space Weather Prediction Center (SWPC) data. For these three days data that also organized under NOAA, the solar flare data was recorded on 23<sup>rd</sup> July 2016 after 05:00 UTC peaked twice. A strong M7.6 class detected at 05:16 UTC followed by M5.5 class at 05:31 UTC detected by GOES-15 Satellite with 1.0 Å to 8.0 Å. Both flares are categorized as medium sized flares with power per unit area of 10<sup>-5</sup> Watts<sup>-1</sup> to 10<sup>-4</sup> Watts<sup>-1</sup>. Based on research conducted by (Chen et al., 2019), it is theoretically plausible that an eruptive flare may lead to band splitting. Additionally, through the observed time intervals, it has been determined that these flares are closely associated with the CMEs, hence correlated with the Type II burst.

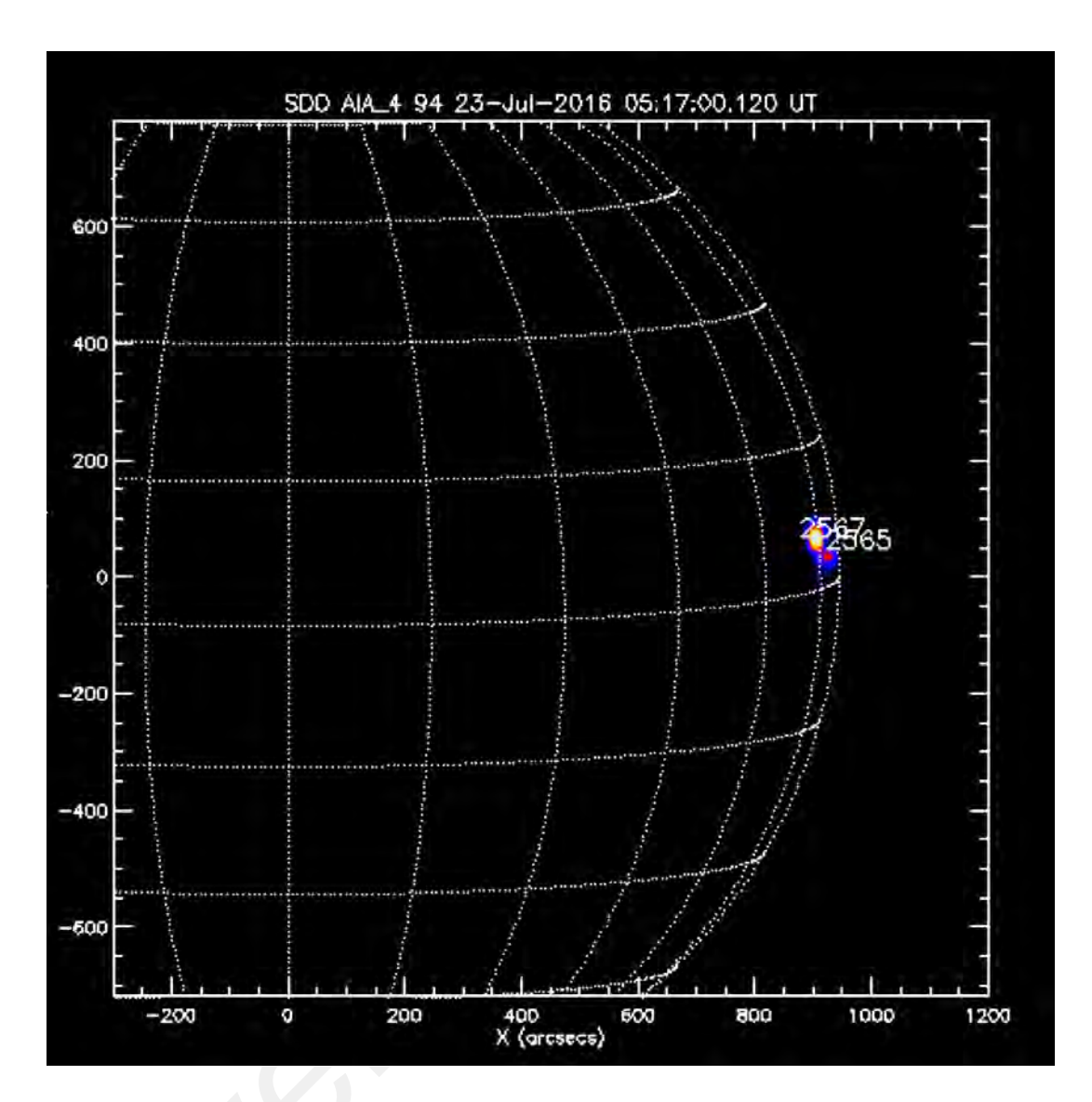


Figure 4.24: Active region of the Sun on 23<sup>rd</sup> July 2016 at 05:17 UTC.

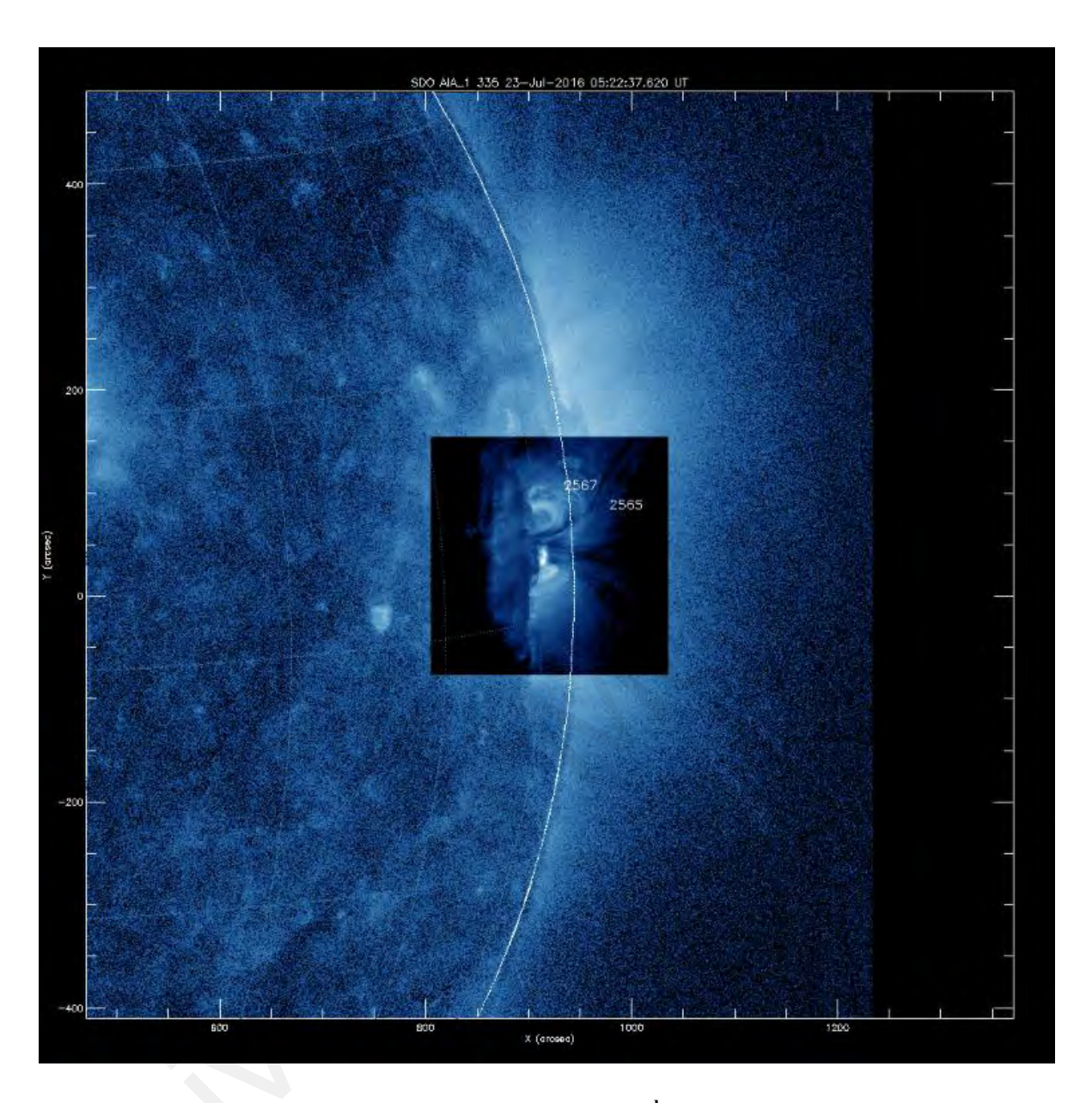


Figure 4.25: Active region of the Sun on 23rd July 2016 at 05:22 UTC.

Based on Figure 4.24 and Figure 4.25 shown, the data achieved from C2 telescope showing the active regions (AR) of the Sun at 05:17 UTC and 05:22 UTC respectively. Observations from Solarsoft and Solar Dynamic Observatory (SDO) websites indicate the presence of two active regions, namely AR2567 and AR2565. However, these solar flares were all confined to the sunspot region AR2567 which hosted CMEs that were not directed towards Earth. The investigation of the relationship of solar flares and CMEs can be made

using this data where it has been proven that the shock front was influenced by these two solar activities (Chrysaphi et al., (2018); Chen et al., (2019)) which resulted in the formation of the band-splitting in solar radio bursts type II. The active region during time of event is important to investigate the origin of Type II solar radio burst as well as studying if the burst is related with the CMEs that explode from the same area and the same time of event. It is highly possible that the investigated band-splitting of the type II solar radio burst from the data collected was caused by exploding CMEs from these two areas, five minutes before the burst event. It is also possible that the eruptive solar flare events caused the CMEs that then excited the band splitting and the slow drift of the Type II burst. The CMEs are manually identified based on these basic parameters shown in Table 4.7 which described the features of the CMEs that correlate with the Type II solar radio burst.

Table 4.7: Information of CMEs occurring on the 23rd July 2016 at 05:24 UTC.

Table 4.7. Information of Civil's occurring on the 25 guly 2010	at 03.24 01C.
Central Position Angle, CPA (deg)	283
Measurement Position Angle, MPA (deg)	271
CME's linear speed (kms <sup>-1</sup> )	835
Angular Width (deg)	117
Acceleration (ms <sup>-2</sup> )	7.9e+30

## **4.3.3** Upgraded vs First Version HWDA Array



Figure 4.26: First version of HWDA antenna array (left); Antenna of uHWDA array obtained from YNAO confidential report (right).

Through the collaboration work of the HWDA array with YNAO, various improvements have been vigorously studied to enhance the capability of this instrument. The HWDA array system has been going through a few major upgrades from the first version of it. The main difference between these two is the design of the antennas. The first version antenna (Figure 4.26 - left) is a rectangular dipole antenna arm blade, while the upgraded version (Figure 4.26 - right) is a grid dipole antenna arm blade. These changes resulted in some improvements to the received data because smaller amount of data will be loss as the upgraded version has the capability to cover wider area resulting from its shape that is being connected to multiple number of parallel wires. The widened bandwidth also applied to the uHWDA array which increases the area of effective radiation of the data received by the antenna. This will give impact to more precise data formed in the spectrograph of the uHWDA array system for the observation study.

Another main change to the upgraded version is instead of having 4 antenna arrays as the first version, it will consist of 16 antenna arrays. This improvement of number of antenna

array creates more effective area of antenna thus succeeding in increasing the instrument gain. This results in more data can be received at one time and elevates the data resolution which is the image of burst formed in the spectrograph. With the achievement of the uHWDA instrument, future observations will be made that will greatly increase the in-depth analysis of the studied solar radio burst band-splitting activity in future publications as a continuation of this work.

### **CHAPTER 5: CONCLUSION**

Within this chapter, each section presents a distinct conclusion based on its objectives accordingly. Firstly, Section 5.1 summarizes the radiation mechanism behind the formation of 'herringbones' features in Solar Radio Bursts Type II. Secondly, Section 5.2 explores the influence of solar activities on the formation of solar radio bursts. Finally, Section 5.3 deduces the last objective of identifying solar radio burst candidates with band-splitting, which will be detected using the upgraded Half-wave Dipole Antenna (uHWDA).

**5.1** Identifying Radiation Mechanism That Contribute to the Formation of Unique Features in Solar Radio Bursts

A Type II solar radio burst with 'herringbone' feature on 3<sup>rd</sup> November 2010 was studied in this work. From the NRH data extracted, the various NRH frequencies line up very well with the time of the formation of the solar radio burst with 'herringbone' feature. The brightness temperatures from all the different NRH frequencies are extremely high. They all exceeded 10<sup>8</sup> K with the maximum brightness temperature at 10<sup>10</sup> K even for 150 MHz. In general, lower frequency has higher TB. The degree of circular polarization is between 1% ~ 27% and was highly left-handed circularly polarized.

A summary of potential radiation mechanisms based on physical parameters was also provided. From the high TB and high |q|, this 'herringbone' pattern of Type II solar radio burst appears to be generated through a Fundamental plasma mechanism. The emission mechanism based on Fundamental plasma is more conducive to the generation of 'herringbones' due to its higher maximum brightness temperature and degree of circular polarization when compared to 2nd harmonic plasma. These qualities correspond to more

intense Type II solar radio bursts. In conclusion, the event studied satisfy the conditions for the formation of the 'herringbone' feature in solar radio burst type II to form through the fundamental plasma mechanism which this able to provide a general idea on the formation of this such unique feature. This proposed mechanism provides a good indicator for studying the radiation mechanism of other solar radio bursts type II specifically that have 'herringbone' unique feature.

# **5.2** Influence of Solar Events with Extreme Eruptions Towards Solar Radio Bursts Activities

Specifically, the event of 6<sup>th</sup> September 2017 was chosen because on that event type II and series of type III occurred simultaneously with the same starting time of the bursts' formation but different end time. For this event, both type II and type III solar radio bursts started at 12:02 UT and ended at 12:21 UT and 12:08 UT, respectively. By referring to SWPC-NOAA details database, both types of solar radio bursts originated from the same active region which is AR2673. In determination of the frequency drift for both types, the simultaneous type II and type III bursts are 0.204 MHzs<sup>-1</sup> and 9.4 MHzs<sup>-1</sup>, respectively. A X9.3 solar flare, which is the highest solar flare detected on that day was found to be associated with the multiple solar radio bursts event. The flare started a few minutes before the burst at 11:53 UT and reached its maximum at 12:02 UT. This solar flare is concluded to be associated with multiple bursts because it occurred within the same active region AR2673.

The X9.3 solar flare was also found to have a strong effect toward the formation of the series of type III. The correlation between solar radio bursts Type III and their corresponding solar flares can be attributed to the magnetic reconnection theory. Typically, Type III bursts are a result of non-thermal emission processes, in this case the magnetic reconnection process

that occurs due to energetic particles ejected from solar events, such as solar flares. The magnetic reconnection process ensues when magnetic lines break and rejoin to form lower-energy configurations, resulting in the conversion of magnetic energy into plasma kinetic energy. This process manifests itself in the form of particles and fast outflows linked to solar phenomena such as solar flares and magnetosphere substorms.

Furthermore, the 1-minute and 5-minute X-ray flux data are provided to show the variation of the X-ray flux before and after the occurrence of the solar radio bursts. The Xray flux data is obtained from the GOES13-15 X-ray databases. Besides that, proton flux from GOES-15 showed the variation between 4<sup>th</sup> September 2017 until 7<sup>th</sup> September 2017. It clearly showed proton flux increment on 6<sup>th</sup> September 2017 as compared to the other days.

In addition, the multiple solar radio bursts captured on 6<sup>th</sup> September 2017 were also found to be clearly associated with CMEs. Three types of coronagraph image are obtained from C2, STEREO SECCHI COR1-A and C2 AIA with different temperature and wavelength. All three coronagraph images showed that CMEs were present during this particular solar radio burst occurrence. Based on this event, the observed CMEs which are classified as fast CMEs are found to be closely related to the solar radio burst type II detected for the event. One of the conditions required for a slow drift burst or a Type II burst to occur is that they must be driven by a fast CME.

To summarize, it can be concluded that solar activities do have strong effects towards the formation of the solar radio bursts causing events such as in this study to observe simultaneous formation of two different types of solar radio bursts. The formation of different

types of solar radio bursts may be caused by the irregular composition of energetic particles that occupies the plasma in the abrupt magnetic field evolution throughout the period of the occurrence of the event.

5.3 Identification of Solar Radio Bursts Features Candidate to be Detected Using UpgradedHalf-wave Dipole Antenna (uHWDA)

On 23<sup>rd</sup> July 2016, a Type II solar radio burst event occurred that was linked to both solar flares and CMEs, resulting in a complex spectrum. The data collected from various instruments corroborates this. GOES X-ray flux data shows that the M7.7 flares had a 13-minute interval between bursts, while the M5.5 flares had a 2-minute interval, indicating a possible correlation. Additionally, SOHO/LASCO data confirmed two active regions displaying CMEs events during the same time frame. The collected data suggests that CMEs and solar flares are the triggers for Type II solar radio bursts, resulting in band splitting and slow drift of the burst. Further analysis which can be done in the future using upgraded HWDA would deepen the understanding of this relation.

The frequency gap that was observed during this event is believed to have started and ended at 60 MHz for both fundamental and 2nd harmonic emission. It is worth noting that this frequency of 60 MHz is situated at the center of the filtered frequency. Because of this small scale of filtered frequency, upgraded HWDA array is highly capable to achieve higher resolution when observing the intensity curves between these two bands. This can lead to more accurate estimation of physical parameters of solar radio burst Type II. Through the bandpass antenna for value of f = 60 MHz and CMEs' height, the density scale height, Ln can be calculated based on power-law relationships which then can be used to estimate other important parameters such as shock speed, v and drift rate, df/dt.

From these parameters, it is possible to elaborate on the intricate characteristics of Type II bursts, CMEs, and the corresponding flares in greater depth. Thus, the concern of the relation between all solar activities and the impact of it on human life can be resolved in the future. Further detection of solar radio bursts using upcoming upgraded HWDA in the future can be investigated and solve the issues arise regarding Type II solar radio bursts.

#### REFERENCES

- Aegerter, T. R. W., Emmons, D. J., & Loper, R. D. (2020). Detection of reconnection signatures in solar flares. Journal of Atmospheric and Solar-Terrestrial Physics, 208, 105375.
- Al Banna, A. (2023). Design a radio receiver for solar activity observation in VLF band. Al-Khwarizmi Engineering Journal, 19(1), 57-69.
- Allawi, H., Alsawad, A., & Mazher, R. (2020). Investigate of 4 Strong Solar Eruptions in September 2017 and their Impacts on the Earth. NeuroQuantology, 18(9), 25.
- Alley, R., & Jentoft-Nilsen, M. (1999). Algorithm theoretical basis document for: Brightness temperature.
- Alpen, E. L. (1997). Radiation biophysics. Academic press.
- Anuar, N. M., Din, A. A., Kasran, F. M., Umar, R., Ab Rahim, S. E., & Jusoh, M. H. (2018). The behavior of solar wind parameters and geomagnetic activity indices for geomagnetically induced current observations. Journal of Fundamental and Applied Sciences, 10(1S), 325-338.
- Batubara, M., Manik, T., Suryana, R., Lathif, M., Sitompul, P., Zamzam, M., & Mumtahana, F. (2017, March). Solar Radio Burst Data Processing of CALLISTO and Frequency Drift Rate Determination of Solar Radio Burst Detected by CALLISTO Network in Indonesia. In IOP Conference Series: Materials Science and Engineering (Vol. 180, No. 1, p. 012049). IOP Publishing.
- Behlke, R. (2001). Solar radio bursts and low frequency radio emissions from space. IRF Scientific Report 275.
- Cairns, I. H., & Robinson, R. D. (1987). Herringbone bursts associated with type II solar radio emission. Solar physics, 111, 365-383.
- Cane, H. V., & White, S. M. (1989). On the source conditions for herringbone structure in type II solar radio bursts. Solar physics, 120, 137-144.
- Chen, B., Shen, C., Reeves, K. K., Guo, F., & Yu, S. (2019). Radio Spectroscopic Imaging of a Solar Flare Termination Shock: Split-band Feature as Evidence for Shock Compression. The Astrophysical Journal, 884(1), 63.

- Chen, C., Wang, Y., Shen, C., Ye, P., Zhang, J., & Wang, S. (2011). Statistical study of coronal mass ejection source locations: 2. Role of active regions in CME production. Journal of Geophysical Research: Space Physics, 116(A12).
- Chen, X., Kontar, E. P., Clarkson, D. L., & Chrysaphi, N. (2023). The frequency ratio and time delay of solar radio emissions with fundamental and harmonic components. Monthly Notices of the Royal Astronomical Society, 520(2), 3117-3126.
- Chernov, G., & Fomichev, V. (2021). On the issue of the origin of type II solar radio bursts. The Astrophysical Journal, 922(1), 82.
- Cho, K. S., Bong, S. C., Moon, Y. J., Shanmugaraju, A., Kwon, R. Y., & Park, Y. D. (2011). Relationship between multiple type II solar radio bursts and CME observed by STEREO/SECCHI. Astronomy & Astrophysics, 530, A16.
- Chrysaphi, N., Kontar, E. P., Holman, G. D., & Temmer, M. (2018). CME-driven shock and type II solar radio burst band splitting. The Astrophysical Journal, 868(2), 79.
- Darnel, J. M., Seaton, D. B., Bethge, C., Rachmeler, L., Jarvis, A., Hill, S. M., ... & Timothy, S. (2022). The GOES-R Solar UltraViolet Imager. Space Weather, 20(4), e2022SW003044.
- De Pontieu, B., McIntosh, S. W., Carlsson, M., Hansteen, V. H., Tarbell, T. D., Boerner, P., ... & Title, A. M. (2011). The origins of hot plasma in the solar corona. Science, 331(6013), 55-58.
- Dulk, G. A. (1985). Radio emission from the sun and stars. Annual review of astronomy and astrophysics, 23(1), 169-224.
- Fainberg, J., & Stone, R. G. (1970). Type III solar radio burst storms observed at low frequencies: II: Average exciter speed. Solar Physics, 15, 433-445.
- Fiorentini, G., Ricci, B., & Villante, F. L. (2004). Nuclear fusion in the sun. Progress of Theoretical Physics Supplement, 154, 309-316.
- Fitzpatrick, R. (2008). Introduction to plasma physics. The University of Texas at Austin: sn, 242.
- Gao, G. N., Wang, M., Lin, J., Wu, N., Tan, C. M., Kliem, B., & Su, Y. (2014). Radio observations of the fine structure inside a post-CME current sheet. Research in Astronomy and Astrophysics, 14(7), 843.

- Gergely, T. E., Kundu, M. R., Erskine, F. T., Sawyer, C., Wagner, W. J., Illing, R., ... & Sheeley, N. (1984). Radio and visible-light observations of a coronal arcade transient. Solar physics, 90, 161-176.
- Gopalswamy, N. (2016, August). Low-frequency radio bursts and space weather. In 2016 URSI Asia-Pacific Radio Science Conference (URSI AP-RASC) (pp. 471-474). IEEE.
- Gulyaeva, T., Haralambous, H., & Stanislawska, I. (2021). Persistent perturbations of ionosphere at diminution of solar and geomagnetic activity during 21–24 solar cycles. Journal of Atmospheric and Solar-Terrestrial Physics, 221, 105706.
- Hamidi, Z. S., Shariff, N. N. M., Ibrahim, Z. A., Monstein, C., Zulkifli, W. W., Ibrahim, M. B., ... & Amran, N. A. (2014, October). Magnetic reconnection of solar flare detected by solar radio burst type III. In Journal of Physics: Conference Series (Vol. 539, No. 1, p. 012006). IOP Publishing.
- Hanslmeier, A., & Messerotti, M. (Eds.). (1999). Motions in the Solar Atmosphere: Proceedings of the Summerschool and Workshop Held at the Solar Observatory Kanzelhöhe Kärnten, Austria, September 1–12, 1997 (Vol. 239). Springer Science & Business Media.
- Huang, J., Yan, Y., & Liu, Y. (2007). An analysis of solar radio burst events on December 1, 2004. Advances in Space Research, 39(9), 1439-1444.
- Ishikawa, R., Bueno, J. T., del Pino Alemán, T., Okamoto, T. J., McKenzie, D. E., Auchère, F., ... & Leenaarts, J. (2021). Mapping solar magnetic fields from the photosphere to the base of the corona. Science Advances, 7(8), Article#eabe8406.
- Karlický, M., & Rybák, J. (2020). The 2017 September 6 Flare: Radio Bursts and Pulsations in the 22–5000 MHz Range and Associated Phenomena. The Astrophysical Journal Supplement Series, 250(2), 31.
- Klein, K. L., Matamoros, C. S., & Zucca, P. (2018). Solar radio bursts as a tool for space weather forecasting. Comptes Rendus Physique, 19(1-2), 36-42.
- Kontar, E. P., Yu, S., Kuznetsov, A. A., Emslie, A. G., Alcock, B., Jeffrey, N. L. S., ... & Subramanian, P. (2017). Imaging spectroscopy of solar radio burst fine structures. Nature communications, 8(1), Article#1515.

- Kolarski, A., Sreckovic, V. A., & Mijic, Z. R. (2022). Monitoring solar activity during 23/24 solar cycle minimum through VLF radio signals. Contrib. Astron. Obs. Skaln. Pleso, 52, 105.
- Kumar, A., & Kumar, S. (2014). Space weather effects on the low latitude D-region ionosphere during solar minimum. Earth, planets and space, 66(1), 1-10.
- Kundu, M. R. (1965). Solar radio astronomy. New York: Interscience Publication.
- Kuphaldt, T. R. (2007). Lessons in Electronic Circuits, Volume II AC, Sixth Edition. Design Science License.
- Lara, A., Gopalswamy, N., Niembro, T., Pérez-Enríquez, R., & Yashiro, S. (2020). Space, time and velocity association of successive coronal mass ejections. Astronomy & Astrophysics, 635, A112.
- Li, T., Priest, E., & Guo, R. (2021). Three-dimensional magnetic reconnection in astrophysical plasmas. Proceedings of the Royal Society A, 477(2249), 20200949.
- Lin, R. P., Potter, D. W., Gurnett, D. A., & Scarf, F. L. (1981). Energetic electrons and plasma waves associated with a solar type III radio burst. Astrophysical Journal, Part 1, vol. 251, Dec. 1, 1981, p. 364-373., 251, 364-373.
- Liu, H., Chen, Y., Cho, K., Feng, S., Vasanth, V., Koval, A., ... & Li, C. (2018). A solar stationary type IV radio burst and its radiation mechanism. Solar Physics, 293, 1-10.
- Ma, S., & Chen, H. (2020). Two successive Type II radio bursts associated with B-class flares and slow CMEs. Frontiers in Astronomy and Space Sciences, 7, 17.
- Magdalenić, J., Marqué, C., Fallows, R. A., Mann, G., Vocks, C., Zucca, P., ... & Melnik, V. (2020). Fine structure of a solar type II radio burst observed by LOFAR. The Astrophysical Journal Letters, 897(1), L15.
- Majumdar, S., Tadepalli, S. P., Maity, S. S., Deshpande, K., Kumari, A., Patel, R., & Gopalswamy, N. (2021). Imaging and Spectral Observations of a Type-II Radio Burst Revealing the Section of the CME-Driven Shock That Accelerates Electrons. Solar Physics, 296(4), 62.
- Marusek, J. A. (2007). Solar storm threat analysis. J. Marusek.
- Melrose, D. B. (1975). Plasma emission due to isotropic fast electrons, and types I, II, and V solar radio bursts. Solar Physics, 43, 211-236.

- Mohd, M. R. S., Johari, J., & Ahmat, F. (2020, November). A review of solar radio burst detection using CALLISTO. In 2020 IEEE 10th International Conference on System Engineering and Technology (ICSET) (pp. 61-66). IEEE.
- Monstein, C. (2011). Catalog of dynamic electromagnetic spectra. Phys Astron Electron Work Bench.
- Monstein, C. (2012). Catalogue of dynamic electromagnetic spectra observed with Callisto and Phoenix-3. Radio Astronomy: Journal of the Society of Amateur Radio Astronomers, 7, 63-78.
- Monstein, C. (2013). Redundant observation and correlation of solar radio bursts. Radio Astronomy: Journal of the Society of Amateur Radio Astronomers,, 8, 31-34.
- Pauzi, F. A. M., Abidin, Z. Z., Guo, S. J., Gao, G. N., Dong, L., & Monstein, C. (2020). Investigation into CME Shock Speed Resulting from Type II Solar Radio Bursts: A Newly Designed Half-Wave Dipole Antenna (HWDA) Array System. Solar Physics, 295, 1-14.
- Pauzi, F. A. M., Abidin, Z. Z., Guo, S. J., Gao, G. N., Dong, L., & Monstein, C. (2020). Investigation into CME Shock Speed Resulting from Type II Solar Radio Bursts: A Newly Designed Half-Wave Dipole Antenna (HWDA) Array System. Solar Physics, 295, 1-14.
- Ramesh, R., Kathiravan, C., & Kumari, A. (2023). Solar coronal density turbulence and magnetic field strength at the source regions of two successive metric type II radio bursts. The Astrophysical Journal, 943(1), 43.
- Rennan Pekünlü, E. (1999). Solar Flares. Turkish Journal of Physics, 23(2), 415-424.
- Robinson, R. D. (1978). The emission of Langmuir waves in the solar corona. The Astrophysical Journal, 222, 696-706.
- Robinson, R. D., & Sheridan, K. V. (1982). A study of multiple type II solar radio events. Publications of the Astronomical Society of Australia, 4(4), 392-396.
- Shanmugaraju, A., Moon, Y. J., Cho, K. S., Kim, Y. H., Dryer, M., & Umapathy, S. (2005). Multiple type II solar radio bursts. Solar Physics, 232, 87-103.

- Srivastava, A. K., Ballester, J. L., Cally, P. S., Carlsson, M., Goossens, M., Jess, D. B., ... & Zaqarashvili, T. V. (2021). Chromospheric heating by magnetohydrodynamic waves and instabilities.
- Stewart, R. T. (1966). The polarization of Herring-Bone features in solar radio bursts of spectral type II. Australian Journal of Physics, 19, 209.
- Stewart, R. T., & Sheridan, K. V. (1970). Evidence of type II and type IV solar radio emission from a common flare-induced shock wave. Solar Physics, 12, 229-239.
- Tassev, Y., Velinov, P. I., Tomova, D., & Mateev, L. (2017). Analysis of extreme solar activity in early September 2017: G4–severe geomagnetic storm (07÷ 08.09) and GLE72 (10.09) in solar minimum. Comptes rendus de l'Acadèmie bulgare des Sciences, 70(10), 1437-1444.
- Thejappa, G., & MacDowall, R. J. (2020). Detection of extreme and exceptional Langmuir wave packets in solar type III radio bursts. Journal of Geophysical Research: Space Physics, 125(6), e2019JA027714.
- Toh, B. Y., Cahill, R., & Fusco, V. F. (2003). Understanding and measuring circular polarization. IEEE Transactions on Education, 46(3), 313-318.
- Uchida, Y. (1968). Propagation of hydromagnetic disturbances in the solar corona and Moreton's wave phenomenon. Solar Physics, 4, 30-44.
- Umuhire, A. C., Gopalswamy, N., Uwamahoro, J., Akiyama, S., Yashiro, S., & Mäkelä, P. (2021). Properties of high-frequency type II radio bursts and their relation to the associated coronal mass ejections. Solar Physics, 296, 1-18.
- Umuhire, A. C., Uwamahoro, J., Raja, K. S., Kumari, A., & Monstein, C. (2021). Trends and characteristics of high-frequency type II bursts detected by CALLISTO spectrometers. Advances in Space Research, 68(8), 3464-3477.
- Van Hoven, G. (1989). Energetics and dynamics of solar activity. Eos, Transactions American Geophysical Union, 70(20), 593-607.
- Vasanth, V., Chen, Y., Feng, S., Ma, S., Du, G., Song, H., ... & Wang, B. (2016). An eruptive hot-channel structure observed at metric wavelength as a moving Type-IV solar radio burst. The Astrophysical Journal Letters, 830(1), L2.

- Vasanth, V., Chen, Y., Lv, M., Ning, H., Li, C., Feng, S., ... & Du, G. (2019). Source imaging of a moving type IV solar radio burst and its role in tracking coronal mass ejection from the inner to the outer corona. The Astrophysical Journal, 870(1), 30.
- Vieira, L. E. A., Kopp, G., de Wit, T. D., da Silva, L. A., Carlesso, F., Barbosa, A. R., ... & Santos, R. (2022). Variability of the Sun's Luminosity Places Constraints on the thermal Equilibrium of the Convection Zone. The Astrophysical Journal Supplement Series, 260(2), 38.
- Vršnak, B., & Lulić, S. (2000). Formation of coronal MHD shock waves–I. The basic mechanism. Solar Physics, 196, 157-180.
- White, S. M. (2007). Solar radio bursts and space weather. Asian Journal of Physics, 16, 189-207.
- White, S., Kassim, N. E., & Erickson, W. C. (2003, February). Solar radioastronomy with the LOFAR (low-frequency array) radio telescope. In Innovative Telescopes and Instrumentation for Solar Astrophysics (Vol. 4853, pp. 111-120). SPIE.
- Wijesekera, J. V., Jayaratne, K. P. S. C., & Adassuriya, J. (2018, April). Analysis of type II and type III solar radio bursts. In Journal of Physics: Conference Series (Vol. 1005, No. 1, p. 012046). IOP Publishing.
- Wild, J. P. (1950). Observations of the spectrum of high-intensity solar radiation at metre wavelengths. III. Isolated bursts. Australian Journal of Chemistry, 3(4), 541-557.
- Winglee, R. M. (1985). Electron-cyclotron maser emission during solar and stellar flares. In Radio Stars: Proceedings of a Workshop on Stellar Continuum Radio Astronomy Held in Boulder, Colorado, USA, 8–10 August 1984 (pp. 49-53). Springer Netherlands.
- Yalim, M. S., Zank, G. P., & Asgari-Targhi, M. (2023). Coronal Loop Heating by Nearly Incompressible Magnetohydrodynamic and Reduced Magnetohydrodynamic Turbulence Models. The Astrophysical Journal, 944(2), 119.
- Yasyukevich, Y., Astafyeva, E., Padokhin, A., Ivanova, V., Syrovatskii, S., & Podlesnyi, A. (2018). The 6 September 2017 X-class solar flares and their impacts on the ionosphere, GNSS, and HF radio wave propagation. Space Weather, 16(8), 1013-1027.
- Zafar, S. S., Hazmin, S. N., Jusoh, M. H., Dagang, A. N., Adzni, M. A. M., & Umar, R. (2021). Behaviour of Geomagnetic storm, horizontal geomagnetic field and solar

- wind parameters during solar flare and CMEs event. In Journal of Physics: Conference Series (Vol. 1768, No. 1, p. 012003). IOP Publishing.
- Zimovets, I., Vilmer, N., Chian, A. L., Sharykin, I., & Struminsky, A. (2012). Spatially resolved observations of a split-band coronal type II radio burst. Astronomy & Astrophysics, 547, A6.
- Zucca, P., Carley, E. P., McCauley, J., Gallagher, P. T., Monstein, C., & McAteer, R. T. J. (2012). Observations of low frequency solar radio bursts from the Rosse solar-terrestrial observatory. Solar Physics, 280, 591-602.